



Measurement of t -channel production of single top quarks and antiquarks in pp collisions at 13 TeV using the full ATLAS Run 2 data sample

The ATLAS Collaboration

The production of single top quarks and top antiquarks via the t -channel exchange of a virtual W boson is measured in proton–proton collisions at a centre-of-mass energy of 13 TeV at the LHC using 140 fb^{-1} of ATLAS data. The total cross-sections are determined to be $\sigma(tq) = 137_{-8}^{+8} \text{ pb}$ and $\sigma(\bar{t}q) = 84_{-5}^{+6} \text{ pb}$ for top-quark and top-antiquark production, respectively. The combined cross-section is found to be $\sigma(tq + \bar{t}q) = 221_{-13}^{+13} \text{ pb}$ and the cross-section ratio is $R_t = \sigma(tq)/\sigma(\bar{t}q) = 1.636_{-0.034}^{+0.036}$. The predictions at next-to-next-to-leading-order in quantum chromodynamics are in good agreement with these measurements. The predicted value of R_t using different sets of parton distribution functions is compared with the measured value, demonstrating the potential to further constrain the functions when using this result in global fits. The measured cross-sections are interpreted in an effective field theory approach, setting limits at the 95% confidence level on the strength of a four-quark operator and an operator coupling the third quark generation to the Higgs boson doublet: $-0.37 < C_{Qq}^{3,1}/\Lambda^2 < 0.06$ and $-0.87 < C_{\phi Q}^3/\Lambda^2 < 1.42$. The constraint $|V_{tb}| > 0.95$ at the 95% confidence level is derived from the measured value of $\sigma(tq + \bar{t}q)$, assuming that the Wtb interaction is a left-handed weak coupling and that $|V_{tb}| \gg |V_{td}|, |V_{ts}|$. In a more general approach, pairs of CKM matrix elements involving top quarks are simultaneously constrained, leading to confidence contours in the corresponding two-dimensional parameter spaces.

Contents

1	Introduction	3
2	The ATLAS detector	4
3	Samples of data and simulated events	5
3.1	Simulation of $t\bar{t}$ and single-top-quark production	6
3.2	Simulation of W +jets, Z +jets and diboson production	7
3.3	Simulation and modelling of multijet production	8
3.4	Samples for the EFT and CKM interpretations	8
4	Object reconstruction and event selection	9
4.1	Object definitions	9
4.2	Modelling of non-prompt and fake leptons	11
4.3	Event selection and definition of signal regions	11
4.4	Control regions for the multijet background	12
5	Separation of signal from background events	12
6	Systematic uncertainties	15
6.1	Experimental uncertainties	18
6.2	Modelling uncertainties	19
7	Measurement results	21
8	Interpretation of the measurements	26
8.1	Sensitivity of R_t to PDF sets	26
8.2	EFT interpretation	26
8.3	Determination of $ V_{tb} $	29
8.4	Generalised CKM interpretation	30
9	Conclusions	31
	Additional plots and interpretations	34
	References	43

1 Introduction

During the 2015–2018 period of operation, known as Run 2, the Large Hadron Collider (LHC) [1] provided proton–proton (pp) collisions at a centre-of-mass energy of $\sqrt{s} = 13$ TeV, giving the collider experiments access to a previously unexplored kinematic range. By measuring top-quark production at this energy scale with high precision, theoretical predictions based on the Standard Model (SM) can be tested and deviations that might result from energy-dependent non-SM couplings can be searched for. Top quarks are produced singly in weak charged-current interactions. The dominant single-top-quark production process at the LHC is characterised by the t -channel exchange of a virtual W boson. Figure 1 depicts example Feynman diagrams of this process at leading order (LO) in perturbation theory. A light quark from one of the colliding protons interacts with a b -quark from another proton by exchanging a virtual W boson. Since the valence u -quark density of the proton is about twice as high as the valence d -quark density, the production cross-section of single top quarks, $\sigma(tq)$, is expected to be higher than the cross-section of top-antiquark production, $\sigma(\bar{t}q)$.

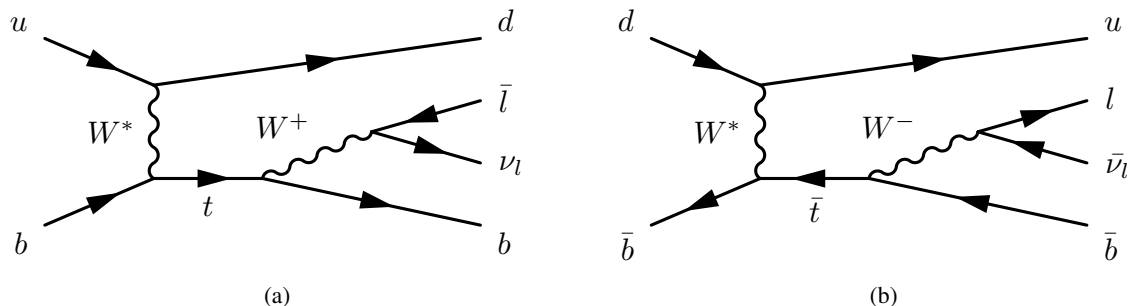


Figure 1: Example Feynman diagrams of (a) single top-quark and (b) single top-antiquark production via the t -channel exchange of a virtual W boson at LO in perturbation theory.

This document presents cross-section measurements of tq and $\bar{t}q$ production using the full data sample recorded with the ATLAS detector [2] during Run 2 of the LHC, corresponding to an integrated luminosity of 140 fb^{-1} . Separate measurements of tq and $\bar{t}q$ production provide sensitivity to the parton distribution functions (PDFs) of u - and d -quarks [3], exploiting the different initial states of the two processes shown in Figure 1. In addition, the combined cross-section $\sigma(tq + \bar{t}q)$ and the cross-section ratio $R_t = \sigma(tq)/\sigma(\bar{t}q)$ are measured. The ratio R_t has better precision than the individual cross-sections because of partial cancellations of common uncertainties. The measurements presented here supersede the results obtained by an ATLAS analysis of early Run 2 data corresponding to an integrated luminosity of 3.2 fb^{-1} [4], significantly improving the precision due to a larger data sample, better detector calibration, the use of more advanced object reconstruction [5, 6], and an improved statistical analysis based on profile maximum-likelihood fits which fully exploit the statistical power of the data sample. This analysis also features an improved treatment of systematic uncertainties related to the modelling of the hard partonic collision and the subsequent hadronisation with event generator programs based on the Monte Carlo (MC) method. The measurements are compared with fixed-order predictions made at next-to-next-to-leading-order (NNLO) in quantum chromodynamics (QCD). The measurement of R_t , in particular, is compared with predictions based on different PDFs.

The measurements are further interpreted in the context of effective field theory (EFT) to constrain the

Wilson coefficients associated with the four-quark operator $O_{Qq}^{3,1}$ and the operator $O_{\phi Q}^3$ that couples the third quark generation to the Higgs boson doublet. Both operators potentially contribute to t -channel single top-quark production in extensions of the SM. Existing limits on the coefficient of $O_{Qq}^{3,1}$ [7–9] are based on the combination of published measurements and do not account for reconstruction effects on EFT signal events, while the analysis presented here employs simulated signal samples and involves template fits to observed distributions. The operator $O_{\phi Q}^3$ features the same Lorentz structure as the Wtb vertex in the SM and limits on this operator are thus obtained from the measured value of $\sigma(tq + \bar{t}q)$. Another interpretation sets limits on the coupling strengths of Wtq vertices, constraining the products of a left-handed form factor f_{LV} and the absolute values of the Cabibbo–Kobayashi–Maskawa (CKM) matrix elements V_{tb} , V_{ts} and V_{td} . The form factor scales the cross-section of tq production with f_{LV}^2 , but leaves the Lorentz structure of the Wtq vertices unchanged; and thus the event kinematics remain unchanged. The SM has $f_{LV} = 1$.

The event selection of the analysis targets tq and $\bar{t}q$ events with leptonically decaying W bosons. Consequently, either one isolated electron or muon and high missing transverse momentum are required. In addition, there must be exactly two hadronic jets with high transverse momentum. Exactly one of these jets must be identified as originating from a b -quark and is hence labelled as a b -tagged jet, while the second jet is preferentially produced in the forward direction at high absolute values of pseudorapidity. The main background processes are top-quark–antiquark ($t\bar{t}$) pair production and $W + b\bar{b}$ production. Two other single top-quark production processes are also relevant backgrounds: the associated production of a W boson and a top quark (tW production) and the production of $t\bar{b}$ or $\bar{t}b$ via the s -channel exchange of a virtual W boson. The selected signal and background events are further separated by constructing discriminants with an artificial neural network (NN). The output distributions of the NN are used in a maximum-likelihood fit to determine the signal yields and measure $\sigma(tq)$, $\sigma(\bar{t}q)$, $\sigma(tq + \bar{t}q)$, and R_t .

The CMS Collaboration measured tq and $\bar{t}q$ production at $\sqrt{s} = 13$ TeV using a partial Run 2 data sample, determining the total cross-sections [10], various differential cross-sections [11], and measuring CKM matrix elements [12].

2 The ATLAS detector

The ATLAS detector covers nearly the entire solid angle around the collision point.¹ It consists of an inner tracking detector surrounded by a thin superconducting solenoid, electromagnetic and hadronic calorimeters, and a muon spectrometer incorporating three large superconducting toroidal magnets.

The inner-detector system (ID) is immersed in a 2 T axial magnetic field and provides charged-particle tracking in the range of $|\eta| < 2.5$. The high-granularity silicon pixel detector covers the vertex region and typically provides four measurements per track, the first hit normally being in the insertable B-layer installed before Run 2 [13, 14]. It is followed by the silicon microstrip tracker, which usually provides eight measurements per track. These silicon detectors are complemented by the transition radiation tracker (TRT), which enables radially extended track reconstruction up to $|\eta| = 2.0$. The TRT also provides electron identification information based on the fraction of hits above a higher energy-deposit threshold corresponding to transition radiation.

¹ ATLAS uses a right-handed coordinate system with its origin at the nominal interaction point (IP) in the centre of the detector and the z -axis along the beam pipe. The x -axis points from the IP to the centre of the LHC ring, and the y -axis points upwards. Cylindrical coordinates (r, ϕ) are used in the transverse plane, ϕ being the azimuthal angle around the z -axis. The pseudorapidity is defined in terms of the polar angle θ as $\eta = -\ln \tan(\theta/2)$. Angular distance is measured in units of $\Delta R \equiv \sqrt{(\Delta\eta)^2 + (\Delta\phi)^2}$.

The calorimeter system covers the pseudorapidity range $|\eta| < 4.9$. Within the region $|\eta| < 3.2$, electromagnetic calorimetry is provided by barrel and endcap high-granularity lead/liquid-argon (LAr) calorimeters, with an additional thin LAr presampler covering $|\eta| < 1.8$ to correct for energy loss in material upstream of the calorimeters. Hadronic calorimetry is provided by the steel/scintillator-tile calorimeter, segmented into three barrel structures within $|\eta| < 1.7$, and two copper/LAr hadronic endcap calorimeters. The solid angle coverage is completed with forward copper/LAr and tungsten/LAr calorimeter modules optimised for electromagnetic and hadronic measurements respectively.

The muon spectrometer (MS) comprises separate trigger and high-precision tracking chambers measuring the deflection of muons in a magnetic field generated by superconducting air-core toroids. The field integral of the toroids ranges between 2.0 and 6.0 Tm across most of the detector. A set of precision chambers covers the region $|\eta| < 2.7$ with three layers of monitored drift tubes, complemented by cathode-strip chambers in the forward region, where the background is highest. The muon trigger system covers the range $|\eta| < 2.4$ with resistive-plate chambers in the barrel, and thin-gap chambers in the endcap regions. Interesting events are selected to be recorded by the first-level trigger system implemented in custom hardware, followed by selections made by algorithms implemented in software in the high-level trigger [15]. The first-level trigger accepts events from the 40 MHz bunch crossings at a rate below 100 kHz, that the high-level trigger further reduces to record events to disk at about 1 kHz.

An extensive software suite [16] is used in the reconstruction and analysis of real and simulated data, in detector operations, and in the trigger and data acquisition systems of the experiment.

3 Samples of data and simulated events

The analysis uses proton–proton (pp) collision data recorded with the ATLAS detector in the years 2015 to 2018 at a centre-of-mass energy of 13 TeV. After applying data-quality requirements [17], the data set corresponds to an integrated luminosity of 140.1 fb^{-1} with a relative uncertainty of 0.83% [18]. The LUCID-2 detector [19] was used for the primary luminosity measurements, complemented by measurements using the inner detector and calorimeters.

Events were selected online during data taking by single-electron or single-muon triggers [20, 21]. Multiple triggers were combined in a logical OR to increase the selection efficiency. The lowest-threshold triggers utilised isolation requirements for reducing the trigger rate. The isolated-lepton triggers had thresholds in transverse momentum (p_T) of 20 GeV for muons and 24 GeV for electrons in 2015 data, and 26 GeV for both lepton types in 2016, 2017 and 2018 data. They were complemented by other triggers with higher p_T thresholds but no isolation requirements to increase the trigger efficiency.

Sets of simulated events from signal and background processes were produced with MC-based event generator programs to model the physics processes. After event generation, the response of the ATLAS detector was simulated using the GEANT4 toolkit [22] with a full detector model [23] or a fast simulation [24, 25] which employed a parameterisation of the calorimeter response. The fast simulation was used for samples that were employed to evaluate systematic uncertainties associated with the event generators and for samples used for the EFT interpretation. To account for additional inelastic pp collisions in the same and neighbouring bunch crossings (pile-up), minimum-bias interactions were overlaid on the hard-scattering events at the level of simulated energy depositions. The minimum-bias events were simulated using PYTHIA 8.186 [26] with the A3 [27] set of tuned parameters and the NNPDF2.3LO PDF set [28]. The

resulting events were weighted to reproduce the observed pile-up distribution. The average number of interactions per bunch crossing during the entire data-taking period from 2015 to 2018 is 33.7.

Finally, the simulated events were reconstructed using the same software as applied to the collision data. The same event selection requirements were applied and the selected events were passed through the same analysis chain. The multijet background is modelled by dedicated samples of events selected with slightly modified requirements (see Section 4.2). Corrections are applied to simulated events such that the lepton trigger and reconstruction efficiencies, jet energy calibration and b -tagging efficiency are in better agreement with the response observed in data. More details of the simulated event samples are provided in the following subsections.

3.1 Simulation of $t\bar{t}$ and single-top-quark production

Samples of simulated events from $t\bar{t}$ and single-top-quark production were generated using the next-to-leading-order (NLO) matrix-element generator POWHEG BOX v2 [29–35], setting the top-quark mass to $m_t = 172.5$ GeV. For $t\bar{t}$ and tW production as well as s -channel single-top-quark production ($t\bar{b}$ production) the NNPDF3.0_{NLO} PDF set [36] was used with the five-flavour scheme. Following a recommendation given in Ref. [35], single top-quark production in the t -channel (tq production) was simulated with the NNPDF3.0_{NLO_NF4} PDF set, which implements the four-flavour scheme. Parton showers, hadronisation, and the underlying event were modelled using PYTHIA 8.230 with the A14 [37] set of tuned parameters and the NNPDF2.3_{LO} PDF set. The POWHEG BOX+PYTHIA generator setup applies a matching scheme to the modelling of hard emissions in the two programs. For $t\bar{t}$ production, the matrix-element-to-parton-shower matching is steered by the h_{damp} parameter, that controls the p_T of the first additional gluon emission beyond the LO Feynman diagram in the parton shower and therefore regulates the high- p_T emission against which the $t\bar{t}$ system recoils. Event generation was run with $h_{\text{damp}} = 1.5 \times m_t$ [38]. The renormalisation and factorisation scales were set dynamically on an event-by-event basis, namely to $\mu_r = \mu_f = \sqrt{m_t^2 + p_T^2(t)}$ for $t\bar{t}$ production and to $\mu_r = \mu_f = 4 \sqrt{m_b^2 + p_T^2(b)}$ for tq production, where $p_T(t)$ is the p_T of the top quark, m_b is the mass of the b -quark, and $p_T(b)$ is the p_T of the b -quark originating from the initial-state gluon that splits into a $b\bar{b}$ pair. The scale choice for tq production follows a recommendation in Ref. [35]. When generating tW events, the scales were set to $\mu_r = \mu_f = m_t$ and the diagram-removal scheme [39] was employed to treat the interference with $t\bar{t}$ production [38].

In the case of tq production, top-quark decays were modelled by MADSPIN [40, 41], while in the case of $t\bar{t}$, $t\bar{b}$ and tW production top-quark decays were handled by POWHEG BOX directly. The decays of bottom and charm hadrons were simulated using the EVTGEN 1.6.0 program [42].

The sample of simulated $t\bar{t}$ events was normalised to a total cross-section of $\sigma(t\bar{t}) = 834 \pm 33$ pb (relative uncertainty: 4.0%), the value obtained from NNLO predictions from the TOP++ 2.0 program (see Ref. [43] and references therein), which includes the resummation of next-to-next-to-leading logarithmic (NNLL) soft-gluon terms. The predicted cross-sections of tq and $\bar{t}q$ production used to normalise the corresponding samples of simulated events are $\sigma(tq) = 134.2 \pm 2.2$ pb and $\sigma(\bar{t}q) = 80.0 \pm 1.6$ pb (relative uncertainties: 1.6% and 2.0%, respectively) and were calculated with the MCFM 10.1 program [44] at NNLO in QCD. The quoted uncertainties include the uncertainties related to a variation of μ_r and μ_f , the uncertainty in the PDFs and in the value of the strong coupling constant α_s . The scale uncertainty is determined by varying μ_r and μ_f independently up and down by a factor of two, whilst never allowing them to differ by a factor greater than two from each other. The combined PDF and α_s uncertainties were determined at the 68%

confidence level (CL) according to the Hessian representation of the PDF4LHC21 PDF set [45]. The total cross-section for $t\bar{b}$ production was computed at NLO in QCD with the HATHOR 2.1 program [46, 47] and the corresponding sample of simulated events was normalised to $\sigma(t\bar{b} + \bar{t}b) = 10.32 \pm 0.38$ pb (relative uncertainty: 3.7%). The cross-section used for normalising the tW sample is $\sigma(tW + \bar{t}W) = 79.3 \pm 2.9$ pb (relative uncertainty: 3.7%) [48]. All cross-section calculations assume $m_t = 172.5$ GeV.

3.2 Simulation of W +jets, Z +jets and diboson production

The production of W and Z bosons in association with jets, including heavy-flavour jets, was simulated with the SHERPA 2.2.1 generator [49]. In this setup, NLO-accurate matrix elements for up to two partons and LO-accurate matrix elements for up to four partons are calculated with the COMIX [50] and OPENLOOPS 1 [51–53] libraries. The default SHERPA parton shower [54] based on Catani–Seymour dipole factorisation and the cluster hadronisation model [55] were used. The generation employed the dedicated set of tuned parameters developed by the SHERPA authors and the NNPDF3.0_{NLO} PDF set.

The NLO matrix elements of a given jet multiplicity are matched to the parton shower using a colour-exact variant of the MC@NLO algorithm [56]. Different jet multiplicities are then merged into an inclusive sample using an improved CKKW matching procedure [57, 58] that is extended to NLO accuracy using the MEPS@NLO prescription [59]. The merging threshold was set to 20 GeV. The W +jets and Z +jets samples are normalised to NNLO predictions [60] of the total cross-sections, obtained with the FEWZ package [61].

After event generation and before detector simulation, the W +jets and Z +jets samples were subjected to hadron-flavour filters. Events in which at least one b -hadron is present were selected and form b -filtered samples. The production of a W boson in association with b -hadrons is dominated by processes in which a radiated high- p_T gluon splits into a $b\bar{b}$ pair. This class of background processes is thus called $W+b\bar{b}$ production. Samples with an applied c -filter were produced by vetoing events that pass the b -filter described above and requiring at least one c -hadron to be present. Two different classes of physics processes contribute to the c -filtered samples, flavour production via gluon splitting leading to $W+c\bar{c}$ and a second class of processes with a down-type quark and a gluon in the initial state, leading to the production of a single c -quark in the final state via $qg \rightarrow W+c$. To represent both classes of processes the associated production of a W boson and c -jets is denoted as $W+c(\bar{c})$ production. Generated events of W +jets production that remain after applying the b -filter and the c -filter as a veto constitute W +light-quark-jet production. The contribution of this process to the expected event yields is much smaller than the contributions of $W+b\bar{b}$ and $W+c(\bar{c})$ production due to the tight b -tagging requirement made, and therefore the W +light-quark-jet contribution is merged with the contribution of the $W+b\bar{b}$ process in the statistical analysis. The Z +jets samples are treated with the same hadron-flavour filtering scheme as the W +jets samples, leading to b -filtered, c -filtered and light-flavour samples. However, Z +jets production is a minor background in the analysis and therefore the flavour split is not used in the statistical analysis.

Samples of on-shell diboson production (WW , WZ and ZZ) were simulated with the same SHERPA setup as described above for W +jets and Z +jets production. The matrix elements considered contain all diagrams with four electroweak vertices and were calculated at NLO accuracy in QCD for up to one additional parton and at LO accuracy for up to three additional parton emissions. The diboson event samples are normalised to the total cross-sections provided by SHERPA.

3.3 Simulation and modelling of multijet production

Events featuring generic high- p_T multijet production may satisfy the event selection if a jet is misidentified as an electron or muon, or if real electrons or muons coming from hadron decays inside the jets satisfy the isolation requirements. The former are called *fake leptons*, the latter *non-prompt leptons*. In addition, non-prompt electrons occur as a result of photon conversions in the detector material. Multijet events with fake electrons or non-prompt electrons are modelled with a sample of simulated dijet events, while events with non-prompt muons are modelled with collision data, described in Section 4.2. The number of events with fake muons is negligible. The dijet event sample was generated using PYTHIA 8.186 with LO matrix elements for dijet production and interfaced to a p_T -ordered parton shower. The scales μ_r and μ_f were set to the square root of the geometric mean of the squared transverse masses of the two outgoing particles in the matrix element, $\mu_r = \mu_f = \sqrt[4]{(p_{T,1}^2 + m_1^2)(p_{T,2}^2 + m_2^2)}$. At generator level, a filter was applied that required the existence of one jet with $p_T > 17$ GeV, which was formed by running a jet clustering algorithm over the stable particles of the generated events. The generation used the NNPDF2.3LO PDF set and the A14 set of tuned parameters. The generated sample of dijet events is used to model the kinematics of electron events of the multijet background when producing template distributions, while the rate of the multijet background is estimated in a data-driven way using dedicated control regions (CRs) described in Section 4.4.

3.4 Samples for the EFT and CKM interpretations

For interpreting the measurement in the framework of EFT, samples of tq (t -channel) and $t\bar{b}$ (s -channel) production were generated with MADGRAPH5_AMC@NLO 2.7.3 using the SMEFTatNLO-NLO model [62] with the five-flavour scheme and the NNPDF3.0NLO PDF set. The operator $O_{Qq}^{3,1}$ was activated, which introduces a four-quark contact interaction. Separate samples of simulated events were generated for each $C_{Qq}^{3,1}/\Lambda^2 \in \{-0.6, -0.2, 0.0, 0.4, 1.0\}$ for single top-quark and top-antiquark production. The setting $C_{Qq}^{3,1}/\Lambda^2 = 0.0$ corresponds to the SM. Each sample includes both tq and $t\bar{b}$ production. The SM production of the two processes is covered as well as the production via the four-quark operator $O_{Qq}^{3,1}$, and the interference of SM and non-SM amplitudes. The generated events were showered with PYTHIA 8.244 using the A14 set of tuned parameters and the NNPDF2.3LO PDF set. In these samples, the top-quark is assumed to decay to W^+b with a branching ratio of 100%.

The generalised CKM interpretation is based on samples of tq and $t\bar{q}$ events generated with MADGRAPH5_AMC@NLO 2.9.9 using the NNPDF3.0NLO PDF set. Eight samples were generated in which all different combinations of Wtq vertices with $q \in \{d, s, b\}$ are considered for the production and the decay vertex, except for the dominant mode that has a Wtb vertex on the production and the decay side. The four-flavour scheme was used for both samples in which the top quark originates from a b -quark. The other six samples were generated based on the five-flavour scheme. Parton showers were simulated with PYTHIA 8.307 using the A14 set of tuned parameters and the NNPDF2.3LO PDF set. The decay of top quarks was simulated with MADSPIN preserving all spin correlations, while W bosons coming from the top-quark decays were forced to decay leptonically. The samples are normalised to cross-sections calculated with MADGRAPH5_AMC@NLO assuming that the CKM matrix elements involved are equal to one, and were simulated with the full detector simulation.

The main background, $t\bar{t}$ production, also involves Wtq vertices when the top quark and antiquark decay. To facilitate a consistent treatment of the $t\bar{t}$ background eight additional samples were generated with POWHEG Box v2, implementing all combinations of Wtq decay vertices, except for the nominal channel that

involves two Wtb vertices. For the alternative samples, the parton shower was simulated with PYTHIA 8.307 using the A14 set of tuned parameters and the NNPDF2.3LO PDF set. The top-quark decay was handled with MADSPIN.

4 Object reconstruction and event selection

The partonic final state of the tq signal process comprises a charged lepton, a neutrino, a b -quark and a light quark (see Figure 1) and is reconstructed by identifying corresponding objects measured in the detector, such as electron and muon candidates, and hadronic jets. The presence of a high- p_T neutrino is indicated by large missing transverse momentum.

4.1 Object definitions

Events are required to have at least one vertex reconstructed from at least two ID tracks with transverse momenta of $p_T > 0.5$ GeV. The primary vertex of an event is defined as the vertex with the highest sum of p_T^2 over all associated ID tracks [63].

Electron candidates are reconstructed by matching a track in the ID to clusters of energy deposits in the electromagnetic calorimeter [64]. The pseudorapidity of clusters, η_{cluster} , is required to be in the range of $|\eta_{\text{cluster}}| < 2.47$. However, clusters are excluded if they are in the transition region $1.37 < |\eta_{\text{cluster}}| < 1.52$ between the barrel and endcap electromagnetic calorimeters. Electron candidates must have $p_T > 10$ GeV. A likelihood-based discriminant is constructed to simultaneously evaluate several properties of electron candidates, including shower shapes in the electromagnetic calorimeter, track quality, and the detection of transition radiation produced in the TRT. By placing a requirement on the discriminant, the selection of true electrons is enhanced, while photon conversions and hadrons misidentified as electrons are largely rejected. Two categories of electrons with different identification quality are defined [64]: the first category implements *Tight* identification criteria and features a high rejection of non-prompt or fake electrons, while the second category with *Loose* identification criteria has higher efficiency at the price of lower purity in prompt electrons. Electrons from decays of weak gauge bosons with $p_T(e) > 15$ GeV satisfy the *Tight* (*Loose*) criteria with an average efficiency of 80% (93%).

Muon candidates are reconstructed by combining tracks in the MS with tracks in the ID [65]. The tracks must be in the range of $|\eta| < 2.5$ and have $p_T > 10$ GeV. Similarly to electrons, two levels of identification criteria are applied, defining *Medium* and *Loose* quality categories of muon candidates [65]. Muons originating from W bosons in $t\bar{t}$ events with $p_T(\mu) > 10$ GeV satisfy the *Medium* (*Loose*) quality criteria with an efficiency of 97% (99%).

The tracks matched to electron and muon candidates must point to the primary vertex, which is ensured by requirements imposed on the transverse impact-parameter significance, $|d_0/\sigma(d_0)| < 5$ for electrons and $|d_0/\sigma(d_0)| < 3$ for muons, and on the longitudinal impact parameter, Δz_0 , for which $|\Delta z_0 \sin(\theta)| < 0.5$ mm must be satisfied for both of the lepton flavours. Non-prompt and fake leptons are efficiently rejected using multivariate discriminants [65] computed with boosted decision trees that combine electromagnetic shower shapes, track information from the ID, and a discriminant used to identify b -jets. Prompt muons with a p_T between 20 and 100 GeV satisfy the imposed isolation requirement with an efficiency of 87%, while the efficiency for muons from semileptonic decays of bottom or charm hadrons is 0.5%. Scale factors are

used to correct the efficiencies in simulation to match the efficiencies measured for the electron [20] and muon [21] triggers, and the reconstruction, identification and isolation criteria [64, 65].

Jets are reconstructed from particle-flow objects [66] with the anti- k_t clustering algorithm [67, 68] using a radius parameter of 0.4. This algorithm matches topological clusters [69] in the calorimeters to selected tracks in the ID. The energy of tracks is subtracted from the matched topological clusters and both the tracks and the energy-subtracted topological clusters are used as input to the clustering. The jet energy is calibrated by applying several simulation-based corrections and techniques correcting for differences between simulation and data [5]. The jets must fulfil $p_T > 30$ GeV and $|\eta| < 4.5$.

To suppress jets originating from pile-up collisions, several track-based variables are combined with a multivariate technique in the jet-vertex-tagger (JVT) discriminant [70]. Jets with $p_T < 60$ GeV and $|\eta| < 2.4$ are required to have a JVT-discriminant above 0.5, which corresponds to an efficiency of 92% for non-pile-up jets, while 98% of jets from pile-up events are rejected. For jets with $p_T < 60$ GeV and $|\eta| > 2.5$, the forward-jet-vertex-tagger (fJVT) [71] is used and an fJVT value below 0.4 is required, resulting in efficiencies of 85% for hard-scattering jets and 50% for pile-up jets. In addition, the jet must satisfy a timing condition. Differences in the efficiencies of the JVT and fJVT requirements between collision data and simulation are corrected by corresponding scale factors.

Jets containing b -hadrons are identified (b -tagged) with the DL1r algorithm, which uses a deep feed-forward neural network with several b -tagging algorithms as inputs [6]. These input algorithms exploit the impact parameters of charged-particle tracks, the properties of reconstructed secondary vertices and the topology of b - and c -hadron decays inside the jets. The requirement on the DL1r discriminant is chosen such that the efficiency of tagging b -jets with $p_T > 20$ GeV produced in simulated dileptonic $t\bar{t}$ events is 60%. Differences in the b -tagging efficiency between collision data and simulation are corrected with simulation-to-data scale factors derived from $t\bar{t}$ events. The scale factors are determined as a function of jet p_T and are found to be consistent with unity within uncertainties. The obtained scale factors depend on the parton-shower generator used to produce the $t\bar{t}$ samples. When using samples produced with a different parton-shower generator, for example SHERPA, to model W +jets events, or when evaluating systematic uncertainties with a setup based on HERWIG, additional correction factors called MC-to-MC scale factors are applied. Since the DL1r algorithm uses measurements from the ID, the identification of b -jets is limited to the region with $|\eta| < 2.5$.

To avoid double-counting objects satisfying more than one selection criterion, a procedure called *overlap removal* is applied. Reconstructed objects defined with *Loose* quality criteria are removed in the following order: electrons sharing an ID track with a muon; jets within $\Delta R = 0.2$ of an electron, thereby avoiding double-counting electron energy deposits as jets; electrons within $\Delta R = 0.4$ of a remaining jet, for reducing the impact of non-prompt electrons; jets within $\Delta R = 0.2$ of a muon if they have two or fewer associated tracks with $p_T > 0.5$ GeV; and muons within $\Delta R = 0.4$ of a remaining jet, reducing the rate of non-prompt muons.

The missing transverse momentum \vec{p}_T^{miss} is reconstructed as the negative vector sum of the p_T of the reconstructed leptons and jets, as well as ID tracks that point to the primary vertex but are not associated with a reconstructed object [72]. The latter contribution to \vec{p}_T^{miss} is named soft-track component. The magnitude of \vec{p}_T^{miss} is denoted by E_T^{miss} .

4.2 Modelling of non-prompt and fake leptons

Events of the multijet background with an identified electron candidate are modelled using the *jet-electron* method [73]. Simulated events from dijet production are selected if they contain a jet depositing a large fraction ($>80\%$) of its energy in the electromagnetic calorimeter. This jet is classified as an electron, labelled as the jet-electron, and is treated in the subsequent steps of the analysis in the same way as a properly identified prompt electron as defined in the previous section. The jet-electrons must satisfy the nominal p_T and $|\eta|$ requirements, but electron identification requirements are not applied.

Multijet events with non-prompt muons are modelled with collision events highly enriched in non-prompt muons [73]. Starting from the same sample of collision events as the nominal selection, a subset of events enriched in non-prompt muons is obtained by inverting or modifying some of the muon isolation requirements, such that the resulting sample does not overlap with the nominal sample. The kinematic requirements on p_T and $|\eta|$ are the same as for the nominal muon selection.

4.3 Event selection and definition of signal regions

Candidate events are required to have exactly one charged lepton (ℓ) with $p_T(\ell) > 28$ GeV, either an electron of *Tight* quality or a muon of *Medium* quality. The charged lepton is required to match the object that caused the event to pass a single-lepton trigger. To reduce contributions from $t\bar{t}$ events in the dilepton decay channel, any event with an additional lepton satisfying the *Loose* quality conditions with $p_T > 10$ GeV is rejected.

Multijet events containing fake or non-prompt leptons tend to have low E_T^{miss} and low W transverse mass, in contrast to events with prompt leptons from W and Z decays. The W transverse mass is defined as

$$m_T(W) = \sqrt{2p_T(\ell)E_T^{\text{miss}}(1 - \cos \Delta\phi(\vec{p}_T^{\text{miss}}, \ell))},$$

using the difference between the azimuthal angles of \vec{p}_T^{miss} and the charged lepton, $\Delta\phi(\vec{p}_T^{\text{miss}}, \ell)$. To reduce the multijet background, $E_T^{\text{miss}} > 30$ GeV and $m_T(W) > 50$ GeV are applied as selection requirements.

Exactly two jets with $p_T > 30$ GeV and $|\eta| < 4.5$ are required. Exactly one of these jets must be b -tagged, while the second jet must fail to meet the b -tagging requirement. The latter jet is therefore called the *untagged* jet. The b -tagged jet is explicitly required to have $|\eta| < 2.5$. Events with forward jets with $2.3 < |\eta| < 4.5$ are removed if at least one of the jets has $30 \text{ GeV} < p_T < 35 \text{ GeV}$, leading to an improved modelling of the $|\eta|$ distribution of untagged jets in the given regime.

To further suppress the multijet background and to remove poorly reconstructed leptons with low p_T , an additional requirement is applied based on the azimuthal angle between the charged lepton and the leading jet (j_1), i.e. the jet with the largest p_T . This quantity is denoted by $\Delta\phi(j_1, \ell)$. The imposed requirement is

$$p_T(\ell) > 40 \text{ GeV} \cdot \frac{|\Delta\phi(j_1, \ell)|}{\pi}, \quad (1)$$

which leads to a tighter p_T requirement on the charged lepton than the baseline definition if the leading jet and the charged lepton have a back-to-back topology, namely if $|\Delta\phi(j_1, \ell)| > 0.7\pi$. For the maximum separation $|\Delta\phi(j_1, \ell)| = \pi$ between the two objects, $p_T(\ell) > 40$ GeV must be satisfied.

Furthermore, an additional selection criterion is imposed on the invariant mass of the charged lepton and the b -tagged jet, $m(\ell b)$. Since the off-shell region for top-quark decays is not included in the calculation

CR name	Requirement
B-e-plus	$q_e/e = +1, \eta(e) < 1.37, E_T^{\text{miss}} < 30 \text{ GeV}$
B-e-minus	$q_e/e = -1, \eta(e) < 1.37, E_T^{\text{miss}} < 30 \text{ GeV}$
EC-e-plus	$q_e/e = +1, \eta(e) > 1.52, E_T^{\text{miss}} < 30 \text{ GeV}$
EC-e-minus	$q_e/e = -1, \eta(e) > 1.52, E_T^{\text{miss}} < 30 \text{ GeV}$
CR μ -plus	$q_\mu/e = +1, 28 \text{ GeV} < p_T(\mu) < 40 \text{ GeV} \cdot \frac{ \Delta\phi(j_1, \ell) }{\pi}$
CR μ -minus	$q_\mu/e = -1, 28 \text{ GeV} < p_T(\mu) < 40 \text{ GeV} \cdot \frac{ \Delta\phi(j_1, \ell) }{\pi}$

Table 1: Summary of the definition of the CRs.

of the matrix element of the event generator, it is not modelled well. Therefore, the tail of the $m(\ell b)$ distribution is removed by requiring $m(\ell b) < 160 \text{ GeV}$; this imposes a threshold that is slightly above the kinematic limit at LO, $m(\ell b)_{\text{limit}}^2 = m_t^2 - m_W^2$.

Two separate signal regions (SRs) are defined for events with a positively or a negatively charged lepton. These regions are denoted SR plus and SR minus, respectively.

4.4 Control regions for the multijet background

Since the misidentification of jets as electrons or muons are not well modelled by the detector simulation, the rate of the multijet background is determined in a data-driven way by including dedicated CRs in the fits of the statistical analysis. The rate of fake and non-prompt electrons is constrained in four CRs that are defined by the same selection criteria as the two SRs but inverting the E_T^{miss} requirement. Since the relative numbers of electrons detected in the barrel ($|\eta| < 1.37$) and endcap ($|\eta| > 1.52$) sections of the electromagnetic calorimeter are not modelled well enough by the sample of simulated dijet events, separate CRs are defined for the barrel and endcap regions and are denoted CR B-e-plus, CR B-e-minus, CR EC-e-plus and CR EC-e-minus. Only the event yields in these regions are included in the maximum-likelihood fit. The rate of non-prompt muons is constrained in two CRs defined by the same selection criteria as used for the two SRs but inverting the requirement on the p_T in Eq. 1. The two CRs are named CR μ -plus and CR μ -minus. The distributions of the difference in the azimuthal angles of \vec{p}_T^{miss} and the muon, $\Delta\phi(\vec{p}_T^{\text{miss}}, \mu)$, are included in the maximum-likelihood fits. Table 1 provides a summary of the definition of the CRs.

5 Separation of signal from background events

An artificial neural network is used to separate signal and background events in the two SRs by combining several kinematic variables into an optimised NN discriminant named D_{nn} . In addition to variables derived from the reconstructed objects, the NN builds on a reconstruction of the W boson and the top quark. The reconstruction of the leptonically decaying W boson requires the determination of the neutrino momentum.

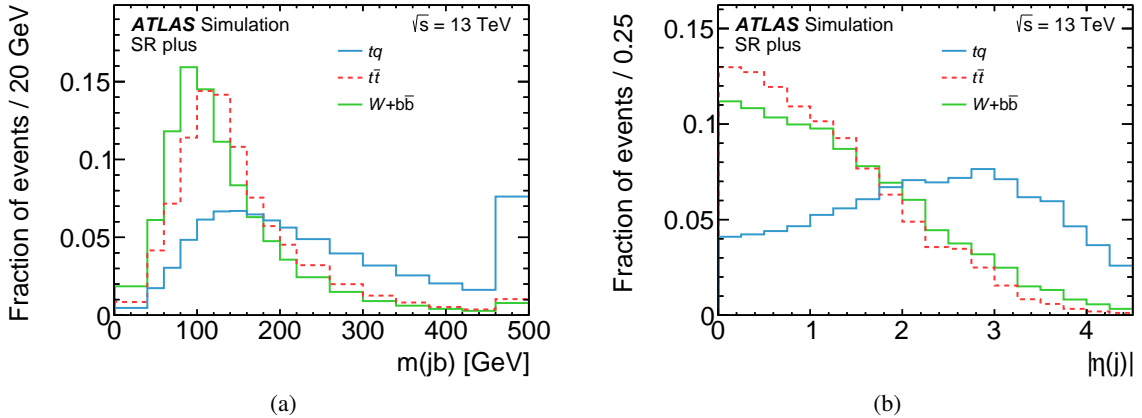


Figure 2: Probability densities of the two most discriminating input variables to the NN in SR plus. (a) The invariant mass $m(jb)$ of the untagged jet and the b -tagged jet and (b) the absolute value of the pseudorapidity of the untagged jet $|\eta(j)|$. The distributions are shown for the tq signal process, and the $t\bar{t}$ and the $W+b\bar{b}$ backgrounds. Events beyond the x -axis range are included in the last bin.

While the x - and y -components of the neutrino momentum, $p_x(\nu)$ and $p_y(\nu)$, are approximated by the components of \vec{p}_T^{miss} , the z -component, $p_z(\nu)$, is determined by constraining the mass of the reconstructed W boson to match the measured world average [74]. If the resulting quadratic equation has two real solutions, the one with the smallest $|p_z(\nu)|$ is chosen. In the case of complex solutions, which occur due to the limited E_T^{miss} resolution, a kinematic fit is performed that rescales the $p_x(\nu)$ and $p_y(\nu)$ such that the imaginary part vanishes and at the same time the distance between the transverse components of the neutrino momentum and \vec{p}_T^{miss} is minimised [75]. The W boson is formed by adding the four-vectors of the reconstructed neutrino and the charged lepton. The top quark is reconstructed by adding the four-vector of the W boson and the b -jet.

The NN is implemented using the NeuroBayes package [76, 77], which combines a three-layer feed-forward NN with a complex and robust preprocessing of the input variables before they are presented to the NN. The preprocessing produces a ranking of the input variables based on an algorithm employing the total correlation of a set of variables to the target function, which assumes the value 1 for signal and 0 for background events [78]. Utilising this ranking, NNs with different numbers of variables are trained, the full analysis is performed and the expected uncertainty of the measurement is determined. Networks using more input variables tend to result in measurements with lower uncertainties in $\sigma(tq)$, $\sigma(t\bar{q})$, $\sigma(tq + t\bar{q})$, and R_t . However, when employing 15–30 variables, only marginal further improvements are found if more variables are added. As a result, the 17 highest-ranking input variables are chosen for training the final NN. These input variables are listed and described in Table 2. The probability densities of the two most discriminating variables, $m(jb)$ and $|\eta(j)|$, are shown for the tq signal process, and the $t\bar{t}$ and the $W+b\bar{b}$ backgrounds in Figure 2 for SR plus. The symbol j represents the untagged jet.

A single NN is trained using a sample of simulated events comprising both the positively and negatively charged leptons, since the event kinematics of tq and $t\bar{q}$ production is very similar. This simple approach gives similar sensitivity as a scenario in which separate NNs are trained in the SR plus and SR minus. The NN is trained against all considered backgrounds with a fraction of 50% signal events and 50% background events. The different background processes are weighted relative to each other according to their expected numbers of events. NeuroBayes uses Bayesian regularisation techniques for the training process to improve

No.	Symbol	Description
1.	$m(jb)$	Invariant mass of the untagged jet (j) and the b -tagged jet (b)
2.	$ \eta(j) $	Absolute value of the pseudorapidity of the untagged jet
3.	$ \Delta p_T(W, jb) $	Absolute value of the difference in transverse momentum between the reconstructed W boson and the jet pair
4.	$ \Delta\phi(W, jb) $	Absolute value of the difference in azimuthal angle between the reconstructed W boson and the jet pair
5.	$m(t)$	Invariant mass of the reconstructed top quark
6.	$ \Delta\eta(\ell, j) $	Absolute value of the difference in pseudorapidity between the charged lepton (ℓ) and the untagged jet
7.	$\Delta R(\ell, j)$	Angular distance of the charged lepton and the untagged jet
8.	$ \Delta\eta(b, \ell) $	Absolute value of the difference in pseudorapidity between the b -tagged jet and the charged lepton
9.	$m_T(W)$	Transverse mass of the W boson
10.	$m(\ell b)$	Invariant mass of the charged lepton and the b -tagged jet
11.	$H_T(\ell, \text{jets}, E_T^{\text{miss}})$	Scalar sum of the transverse momenta of the charged lepton and the jets and E_T^{miss}
12.	$ \Delta\eta(b, j) $	Absolute value of the difference in the pseudorapidity of the two jets
13.	$ \Delta\phi(j, t) $	Absolute value of the difference in the azimuthal angle between the untagged jet and the reconstructed top quark
14.	$\cos\theta^*(\ell, j)$	Cosine of the angle θ^* between the charged lepton and the untagged jet in the rest frame of the reconstructed top quark
15.	$ \eta(\ell) $	Absolute value of the pseudorapidity of the charged lepton
16.	S	Sphericity defined as the sum of the 2nd and 3rd largest eigenvalues of the sphericity tensor multiplied by $3/2$
17.	$ \Delta p_T(\ell, j) $	Absolute value of the difference in transverse momentum of the charged lepton and the untagged jet

Table 2: The 17 variables used for the training of the NN ordered by their discriminating power. The sphericity tensor $S^{\alpha\beta}$ used to define the sphericity S is formed with the three-momenta \vec{p}_i of the reconstructed objects, namely the jets, the charged lepton and the reconstructed neutrino. The tensor is given by $S^{\alpha\beta} = \frac{\sum_i p_i^\alpha p_i^\beta}{\sum_i |\vec{p}_i|^2}$ where α and β correspond to the spatial components x , y and z .

the generalisation performance and to avoid overtraining. The network infrastructure consists of one input node for each input variable plus one bias node, followed by 22 nodes arranged in a single hidden layer, and one output node that gives a continuous output in the interval $(-1, +1)$. As a non-linear activation

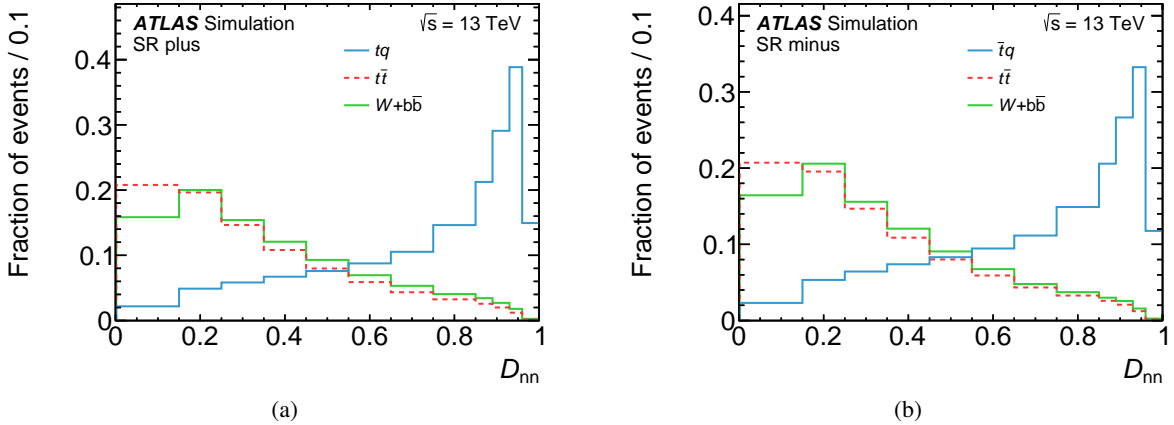


Figure 3: Probability densities of the NN discriminants for the tq and $\bar{t}q$ signal processes, and the $t\bar{t}$ and $W+b\bar{b}$ backgrounds in (a) SR plus and (b) SR minus.

function NeuroBayes uses the symmetric sigmoid function

$$S(x) = \frac{2}{1 + e^{-x}} - 1,$$

which maps the interval $(-\infty, +\infty)$ to the interval $(-1, +1)$. In the region close to zero, the sigmoid function has a linear response. The final discriminant D_{nn} is obtained by linearly scaling the output of the NN to the interval $(0, 1)$.

The probability densities of D_{nn} for the two SRs are shown in Figure 3 for the tq signal process and the main backgrounds, namely the $t\bar{t}$ and $W+b\bar{b}$ processes. Prior to the application of the NN to the observed collision data in the SRs, the modelling of the input variables is checked. For this purpose, a preliminary estimate of the rate of the multijet background is obtained by fitting the full E_T^{miss} distribution for electron events and fitting the $\Delta\phi(E_T^{\text{miss}}, \ell)$ distributions in CR μ -plus and CR μ -minus. Since the resulting estimate of the multijet background is only a preliminary step towards the final results, this fit is performed without using uncertainties other than the statistical data uncertainty and the MC statistical uncertainties. In the validation plots, the rates of all other processes including the signal process are set to their predicted values. The distributions of the eight most discriminating variables before performing the final maximum-likelihood fit (pre-fit) are shown in Figures 4 and 5 for SR plus. In all cases, the model describes the observed distributions within the estimated uncertainties. The pre-fit D_{nn} distributions are shown in Figure 6 for SR plus and SR minus.

6 Systematic uncertainties

Several sources of systematic uncertainty affect the expected event yield from signal and background processes, and the shape of the NN discriminants used in the maximum-likelihood fits. The systematic uncertainties are divided into two major categories. Experimental uncertainties are associated with the reconstruction of the four-momenta of final-state objects: electrons, muons, untagged jets, b -tagged jets, and E_T^{miss} . The second category of uncertainties is related to the modelling of scattering processes. All uncertainties are propagated through the analysis and their effects on the expected event yields and

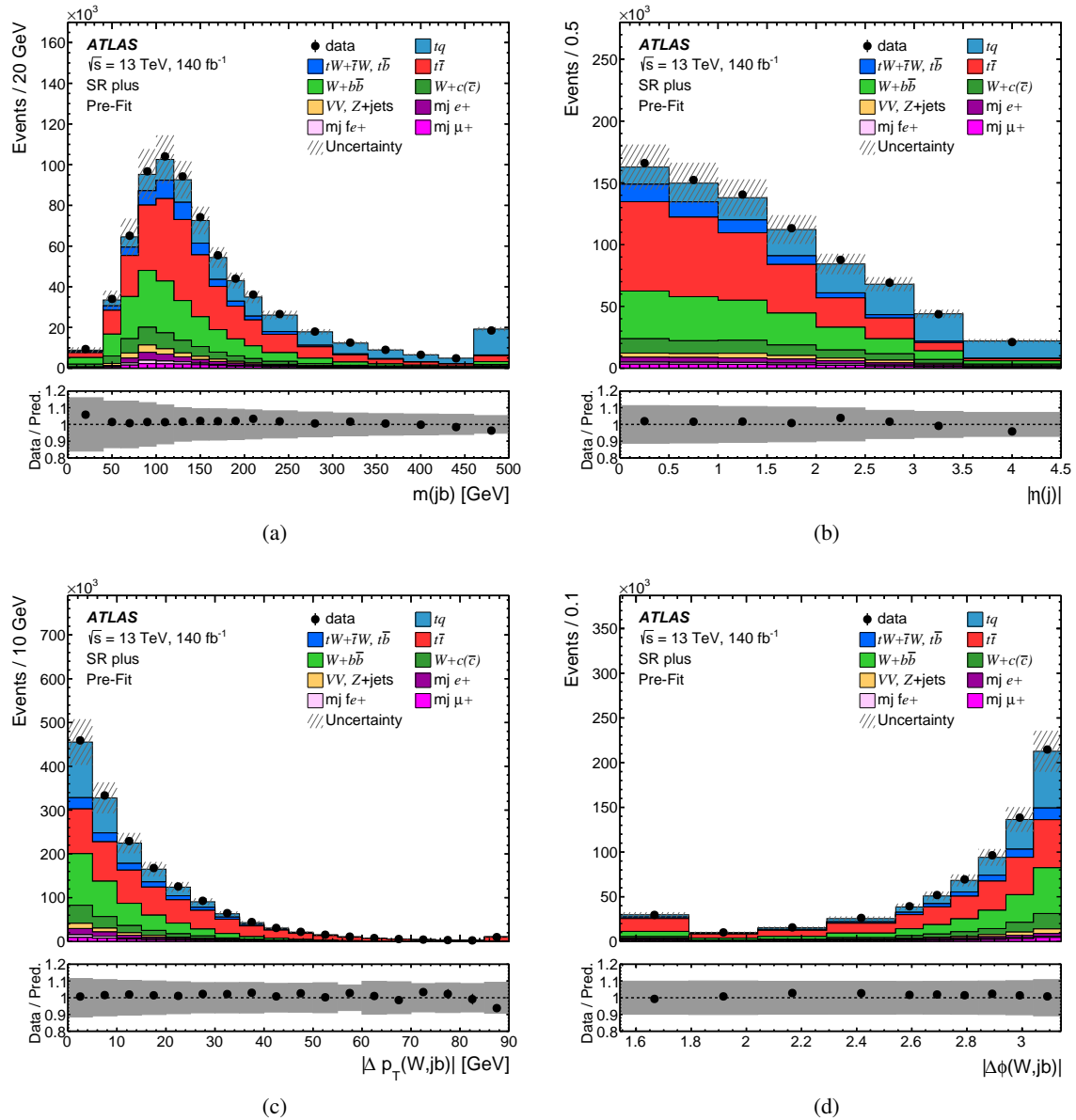


Figure 4: Pre-fit distributions of the four most discriminating input variables to the NN in SR plus: (a) the invariant mass $m(jb)$ of the untagged jet and the b -tagged jet, (b) the absolute value of the pseudorapidity of the untagged jet $|\eta(j)|$, (c) the absolute value of the difference in p_T between the reconstructed W boson and the jet pair, and (d) the difference in azimuth angle between the reconstructed W boson and the jet pair $|\Delta\phi(W, jb)|$. The observed distributions (dots) are compared with the expected distributions (histograms) from simulated events. In these distributions, the signal contribution is shown stacked on top of contributions from all considered background processes. All uncertainties considered in the analysis are included in the hatched uncertainty band. Events beyond the x -axis range are included in the last bin; the same applies to the first bin of the $|\Delta\phi(W, jb)|$ distribution in (d). The lower panel shows the ratio of data and the prediction; in this panel, the uncertainty is displayed as a grey band.

discriminant distributions are accounted for by including corresponding nuisance parameters in the fit. In the following, the estimation of experimental and modelling uncertainties is explained in more detail.

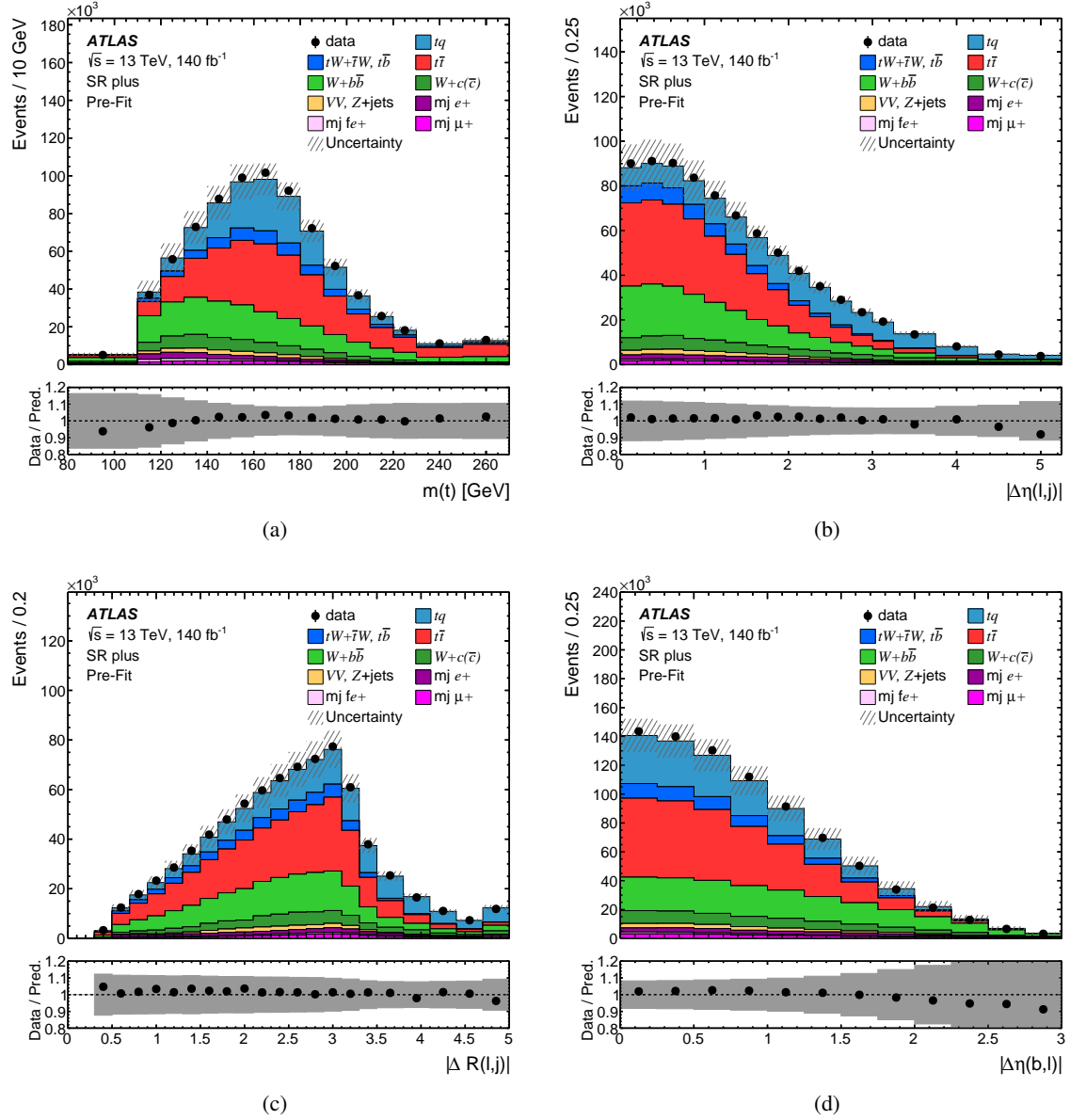


Figure 5: Pre-fit distributions of the four next most discriminating input variables to the NN in SR plus: (a) the invariant mass of the reconstructed top quark $m(t)$, (b) the absolute value of the difference in pseudorapidity between the charged lepton and the untagged jet $|\Delta\eta(\ell, j)|$, (c) the angular distance of the charged lepton and the untagged jet $|\Delta R(\ell, j)|$, and (d) the absolute value of the difference in pseudorapidity between the b -tagged jet and the charged lepton $|\Delta\eta(b, \ell)|$. The observed distributions (dots) are compared with the expected distributions (histograms) from simulated events. In these distributions, the signal contribution is shown stacked on top of contributions from all considered background processes. All uncertainties considered in the analysis are included in the hatched uncertainty band. Events beyond the x -axis range are included in the last bin. The lower panel shows the ratio of data and the prediction; in this panel, the uncertainty is displayed as a grey band.

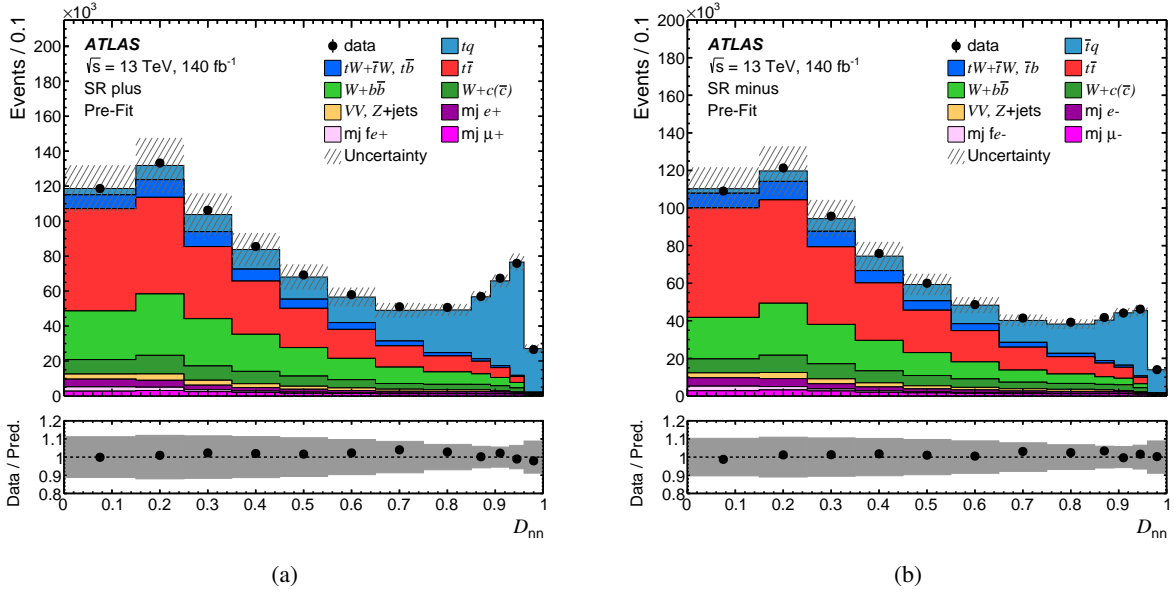


Figure 6: Pre-fit distributions of the D_{nn} in (a) SR plus and (b) SR minus. The observed distributions (dots) are compared with the expected distributions (histograms) from simulated events. In these distributions, the signal contribution is shown stacked on top of contributions from all considered background processes. All uncertainties considered in the analysis are included in the hatched uncertainty band. The lower panel shows the ratio of data and the prediction; in this panel, the uncertainty is displayed as a grey band.

6.1 Experimental uncertainties

The uncertainty in the integrated luminosity of the combined 2015–2018 data set is 0.83% and is based on a calibration of the luminosity scale using x – y beam-separation scans [18]. The luminosity uncertainty is applied to the expected signal and background event yields except for the multijet background, which is estimated in a data-driven way.

Scale factors are applied to simulated events to correct for reconstruction, identification, isolation and trigger performance differences between data and detector simulation for electrons and muons. These scale factors and their systematic uncertainties, as well as the lepton momentum scale and resolution, were assessed using $Z \rightarrow e^+e^-$ and $Z \rightarrow \mu^+\mu^-$ events in simulation and data [64, 65, 79, 80]. The probability of charge misidentification of reconstructed electrons is estimated from simulated events to be 1.9×10^{-3} . The net effect is a migration of events at the level of 6×10^{-4} from the SR plus to the SR minus (see Table 6). An uncertainty of 100% on this rate is applied in the maximum-likelihood fits and is taken to be anticorrelated between the tq and the $\bar{t}q$ processes.

The jet energy scale (JES) was calibrated using a combination of test-beam data, simulation and in situ techniques [5]. The JES is parameterised in bins of jet p_T and η . Its uncertainty is decomposed into a set of 30 uncorrelated components, of which 29 are non-zero in a given event depending on the type of simulation used. Sources of uncertainty contributing to the JES uncertainties computed using the detector position η_{det} include the η intercalibration of forward jets within $0.8 < |\eta_{\text{det}}| < 4.5$ with those in the central barrel region ($|\eta_{\text{det}}| < 0.8$), pile-up modelling, jet flavour composition and response, differences between jets induced by b -quarks and those from gluons or light-quarks, single-particle response, detector modelling, non-closure, and effects of jets not fully contained within the calorimeter.

The uncertainty of the jet energy resolution (JER) is evaluated by smearing jet energies according to a Gaussian function with width σ_{smear} [5]. Thirteen orthogonal components account for jet p_T - and η -dependent differences between simulation and data that were determined using dijet events and noise measurements based on random cones. The smearing is applied to simulated events, used to build the fit model, if the resolution in data is larger than in MC simulation, and to pseudo-data, obtained from simulated events, when the resolution is larger in simulation than in collision data. The JER uncertainties are defined by combining both variations and thereby taking the anticorrelation between different components into account. The nominal data remain unchanged. The uncertainty in the efficiency to satisfy the JVT requirement for pile-up suppression was derived in $Z(\rightarrow \mu^+ \mu^-)$ +jets events and is also considered [70]. The uncertainty in E_T^{miss} due to a possible miscalibration of its soft-track component was derived from data–simulation comparisons of the p_T balance between the hard and soft E_T^{miss} components [72].

The b -tagging requirement made in the measurement requires the consideration of uncertainties in the b -tagging efficiency of true b -jets and in the mistagging rates of light-quark jets and c -jets. The b -tagging efficiency is measured in dileptonic $t\bar{t}$ events. Differences between data and detector simulation are corrected by p_T -dependent scale factors applied to simulated events. The uncertainty in the scale factors is decomposed into 45 orthogonal components [81]. The uncertainties depend on the p_T of the b -jets and are propagated through the analysis as weights. The rate of mistagging c -jets as b -jets was measured in semileptonic $t\bar{t}$ events, where one of the W bosons decays into an electron or a muon and a neutrino and the other decays into a quark–antiquark pair [82]. This event sample allows the measurement to utilise the relatively large and known $W \rightarrow cs$ branching ratio. The mistagging rate of c -jets depends on the jet p_T and has a total uncertainty in the range of 3%-17%. The uncertainties are decomposed into 20 orthogonal components. The misidentification rate of light-quark jets was evaluated based on the techniques described in Ref. [83]. The resulting calibration factors are in the range of about 1.5 to 3 with uncertainties up to 50%. The uncertainties are decomposed into 20 independent eigenvectors.

6.2 Modelling uncertainties

Uncertainties in the theoretical cross-sections are evaluated for the top-quark background processes ($t\bar{t}$, tW and $t\bar{b}$) as quoted in Section 3.1. Due to the tight b -tagging requirement the largest contribution to the W +jets background comes from $W+b\bar{b}$ production in which the b -quarks are produced via gluon splitting ($g \rightarrow b\bar{b}$). An uncertainty of $\pm 40\%$ is assigned to the expected rate of this process, covering differences seen in previous measurements [84] between the SHERPA prediction and ATLAS collision data. The contribution of the associated production of a W boson and light-quark jets to the expected event yield is much smaller and therefore this contribution is merged with the $W+b\bar{b}$ process in the statistical analysis. The same uncertainty of $\pm 40\%$ is assigned to it. Events in which a W boson is produced in association with c -jets are mainly due to the $sg \rightarrow W^- c$ and $\bar{s}g \rightarrow W^+ \bar{c}$ scattering processes. An uncertainty of $\pm 20\%$ is assigned to the rate of $W+c$ -jets production. The same uncertainty is applied to the rate of the combined process of Z +jets and diboson production. The fit result and its uncertainty depend only marginally on the specific assignment of the uncertainties ($\pm 40\%$ and $\pm 20\%$, respectively) in the $W+b\bar{b}$, Z +jets, and diboson cross-sections. In the maximum-likelihood fit, separate nuisance parameters are used for the cross-section uncertainties of $W+b\bar{b}$ production and $W+c$ -jets production in the regions with positive and negative charge.

Uncertainties in modelling parton showers and hadronisation are assigned to the tq signal and the top-quark background processes ($t\bar{t}$, tW and $t\bar{b}$ production) by comparing the nominal samples with alternative samples for which POWHEG Box v2 was interfaced to HERWIG 7.2.1 [85, 86] (for $t\bar{t}$ production) or HERWIG 7.1.6 (for

tq , tW and $t\bar{b}$ production) instead of PYTHIA 8.230. The uncertainties are considered to be uncorrelated for the different scattering processes, namely the tq signal process and the three top-quark background processes. In the statistical analysis, normalisation and shape effects are decorrelated as well.

Uncertainties related to the choice of μ_r and μ_f for the matrix-element calculations are evaluated by varying the scales independently by factors of 2 and 0.5, separately for each of the top-quark production processes and for W +jets production. The scale variations are implemented as generator weights in the nominal sample. These weights are propagated through the entire analysis.

The uncertainty in matching the NLO matrix elements to the parton shower when generating $t\bar{t}$ and tq events is evaluated by comparing the nominal samples of simulated events to samples with an alternative setting of the p_T^{hard} parameter in the matching code. This parameter regulates the definition of the vetoed region of the parton shower and is thus important to avoid overlap in the phase space filled by POWHEG and PYTHIA. The nominal setting of $p_T^{\text{hard}} = 0$ imposes a veto based on the p_T of the gluon emission produced by POWHEG, while the alternative setting $p_T^{\text{hard}} = 1$ leads to a veto defined by the minimal p_T among all final-state partons. This estimate of the uncertainty follows the description in Ref. [87] and was studied by the ATLAS Collaboration in Ref. [88]. The uncertainty in the choice of the h_{damp} parameter for the $t\bar{t}$ event generation is estimated by using an additional $t\bar{t}$ sample produced with the h_{damp} parameter set to $3 \times m_t$, while keeping all other generator settings the same as for the nominal sample of events.

Uncertainties in the amount of initial-state and final-state radiation are assessed for the top-quark production processes by varying the parameter Var3c of the A14 parton-shower tune within the uncertainties of the tune and, for final-state radiation, by varying the renormalisation scale μ_r , at which the strong coupling constant α_s is evaluated, by factors of 0.5 and 2.0. The two variations are handled independently. The uncertainty due to the scheme for removing the overlap of the tW process with $t\bar{t}$ production is evaluated by comparing the nominal sample, using the diagram-removal scheme, with a sample produced with an alternative scheme (diagram subtraction) [39].

In all uncertainty evaluations mentioned above the alternative samples or reweighted samples are normalised to the total cross-section of the nominal samples.

Uncertainties in the PDFs are evaluated for the top-quark production processes using the PDF4LHC15 prescription with 30 eigenvectors [89]. Simulated events are reweighted to the central value and the eigenvectors of the combined PDF set. Systematically varied templates are constructed by taking the differences between the samples reweighted to the central value and those reweighted to the eigenvectors. In the likelihood fit, the PDF uncertainties are treated as correlated across the top-quark production processes.

The uncertainty in the multijet background is evaluated by modifying the selection criteria for jet-electron and non-prompt-muon candidates. Two alternative selections of jet-electron candidates are defined by varying the requirement on the energy fraction measured in the electromagnetic calorimeter, leading to two alternative shapes of the D_{nn} distributions for the multijet background in the SRs. In the statistical analysis, these shapes are used as “up” and “down” variations of a single nuisance parameter. For non-prompt-muon candidates a single variation is defined by varying the isolation criteria.

To account for differences in the pile-up distribution between simulation and data, the pile-up profile in the simulation is corrected to match the one in data. The uncertainty associated with the correction factor is applied in the measurement as a variation of the event weight.

The uncertainties due to the finite number of simulated events, also called the MC statistical uncertainty, is accounted for by adding a nuisance parameter for each bin of the D_{nn} distributions and the distributions in the CRs, implementing the Barlow–Beeston approach [90].

7 Measurement results

The cross-sections $\sigma(tq)$ and $\sigma(\bar{t}q)$ are determined in a simultaneous binned profile maximum-likelihood fit. To properly account for the correlations of systematic uncertainties when forming the sum and the ratio of $\sigma(tq)$ and $\sigma(\bar{t}q)$, $\sigma(tq + \bar{t}q)$ and R_t are measured in a second fit in which the parameterisation of the signal strength parameters is modified accordingly, while all other parameters of the fit setup are kept the same. The fitted distributions are the D_{nn} distributions in SR plus and SR minus, the $\Delta\phi(E_{\text{T}}^{\text{miss}}, \ell)$ distributions in the CR μ -plus and the CR μ -minus, and the event yields in the CR B-e-plus, the CR B-e-minus, the CR EC-e-plus and the CR EC-e-minus. In both fits, the event yields of the multijet background are left floating, while the yields of all other backgrounds are constrained to their predictions within the associated uncertainties.

The likelihood function is constructed as a product of Poisson probability terms over all considered bins. The fitted event yields in the bins depend on nuisance parameters that include the effects of systematic uncertainties. Each nuisance parameter, except those representing the MC statistical uncertainties, is constrained by a Gaussian term in the likelihood function. Some systematically varied discriminant distributions are smoothed and nuisance parameters of systematic uncertainties with negligible impact are entirely removed to reduce spurious effects in the minimisation, improve the convergence of the fit, and reduce the computing time. Normalisation and shape effects of a source of systematic uncertainty are treated separately in this removal process. Single-sided systematic variations are turned into symmetric variations by taking the full difference in event yield and shape between the nominal model and the alternative model and mirroring this difference in the opposite direction. For most sources with two variations, their effects are made symmetric by using the average deviation from the nominal prediction. Exceptions are the uncertainties in the JER and in the jet-electron model, for which the asymmetric variations are kept because the underlying effects are known to be asymmetric. No significant pulls of nuisance parameters are observed.

The total cross-sections for tq and $\bar{t}q$ production are measured to be

$$\sigma(tq) = 137_{-8}^{+8} \text{ pb} \quad \text{and} \quad \sigma(\bar{t}q) = 84_{-5}^{+6} \text{ pb}.$$

The NNLO predictions for these cross-sections (see Section 3.1) agree very well with the measurements. The relative precision reached is +5.9% and –5.5% for $\sigma(tq)$ and +6.6% and –6.2% for $\sigma(\bar{t}q)$. The fits to the observed data for the combined tq and $\bar{t}q$ cross-section and R_t give the following results:

$$\sigma(tq + \bar{t}q) = 221_{-13}^{+13} \text{ pb} \quad \text{and} \quad R_t = 1.636_{-0.034}^{+0.036}$$

with a relative precision of +6.1% and –5.7% for the combined cross-section and +2.2% and –2.1% for R_t . The global goodness of fit is evaluated with the saturated model [74] yielding a p -value of 76%. Table 3 provides a breakdown of the uncertainties categorised in groups according to different sources. The impact of a particular group of uncertainties is evaluated by performing an alternative likelihood fit in which the nuisance parameters related to the sources of uncertainty under investigation are fixed to their best-fit values as obtained from the nominal fit. The squared impact of the considered group of uncertainties is determined

Uncertainty group	$\Delta\sigma(tq)/\sigma(tq)$	$\Delta\sigma(\bar{t}q)/\sigma(\bar{t}q)$	$\Delta\sigma(tq + \bar{t}q)/\sigma(tq + \bar{t}q)$	$\Delta R_t/R_t$
Data statistics	+0.4 / -0.4	+0.5 / -0.5	+0.3 / -0.3	+0.6 / -0.6
Signal modelling	+4.9 / -4.5	+5.2 / -4.8	+5.0 / -4.6	+0.9 / -0.9
Background modelling	+1.8 / -1.6	+2.1 / -1.9	+1.8 / -1.6	+1.5 / -1.4
MC statistics	+1.0 / -1.0	+1.4 / -1.3	+1.1 / -1.0	+0.8 / -0.8
PDFs	+0.4 / -0.4	+1.2 / -1.0	+0.6 / -0.6	+0.9 / -0.8
Jets	+2.2 / -2.0	+3.0 / -2.7	+2.5 / -2.2	+1.0 / -0.9
<i>b</i> -tagging	+1.6 / -1.5	+1.7 / -1.5	+1.6 / -1.5	+0.2 / -0.1
Leptons	+1.1 / -1.0	+1.1 / -1.0	+1.1 / -1.0	+0.1 / -0.1
Luminosity	+0.9 / -0.8	+0.9 / -0.9	+0.9 / -0.8	< 0.1
Total	+5.9 / -5.5	+6.6 / -6.2	+6.1 / -5.7	+2.2 / -2.1

Table 3: The impact of different groups of systematic uncertainties on $\sigma(tq)$, $\sigma(\bar{t}q)$, $\sigma(tq + \bar{t}q)$ and R_t given in %.

as the difference between the square of the nominal total uncertainty and the square of the uncertainty obtained from the alternative fit. For the measured cross-sections, the uncertainties in the signal modelling are the dominating ones, while they largely cancel out for the measurement of R_t . The data statistical uncertainty is very small compared with the systematic uncertainties. Since many uncertainties largely cancel out when forming the ratio, the uncertainty in R_t is much reduced compared with the uncertainties in the cross-sections.

The eight single most important systematic uncertainties in the cross-section measurements are listed in Table 4. The four most important systematic uncertainties are due to the modelling of the tq process with an event generator. The single largest uncertainty is the rate effect due to the definition of the matching scale of the tq process. The eight most important systematic uncertainties in the R_t measurement are listed in Table 5. As a cross-check, the selected sample of events was split according to the lepton flavour into an electron and a muon sample and the measurements were repeated, leading to results compatible with the nominal analysis.

The D_{nn} distributions after performing the fit are shown for both of the SRs in Figure 7. The correlations induced by the maximum-likelihood fit are taken into account and lead to a large reduction in the size of the uncertainty band. The post-fit event yields of the different processes are provided in Table 6.

Dependence on m_t The cross-sections and the ratio R_t are determined at a fixed value of $m_t = 172.5$ GeV. The mass dependence of the measurements is determined by repeating the measurement with samples of simulated events produced with different values of m_t , namely $m_t = 171$ GeV and $m_t = 174$ GeV. The dependence of the resulting cross-sections on m_t is fitted with a first-order polynomial, for which the

Systematic uncertainty	$\Delta\sigma(tq)/\sigma(tq)$	$\Delta\sigma(\bar{t}q)/\sigma(\bar{t}q)$	$\Delta\sigma(tq + \bar{t}q)/\sigma(tq + \bar{t}q)$
tq matching scale definition, rate	+3.1 / -2.9	+2.8 / -2.6	+2.9 / -2.8
tq parton shower, rate	+2.6 / -2.5	+3.3 / -3.2	+2.9 / -2.8
tq final-state radiation	+2.1 / -2.0	+2.2 / -2.1	+2.1 / -2.0
tq matching scale definition, shape	+1.6 / -1.5	+1.2 / -1.2	+1.5 / -1.4
JES η intercalibration modelling	+1.2 / -1.2	+1.6 / -1.5	+1.4 / -1.3
b -tagging NP B1	+1.0 / -0.9	+1.0 / -1.0	+1.0 / -0.9
b -tagging NP B0	+1.0 / -0.9	+1.0 / -1.0	+1.0 / -0.9
Luminosity	+0.9 / -0.8	+0.9 / -0.9	+0.9 / -0.8

Table 4: The impact of the eight most important systematic uncertainties on $\sigma(tq)$, $\sigma(\bar{t}q)$ and $\sigma(tq + \bar{t}q)$ given in %. The sequence of the uncertainties is given by the impact on $\sigma(tq + \bar{t}q)$.

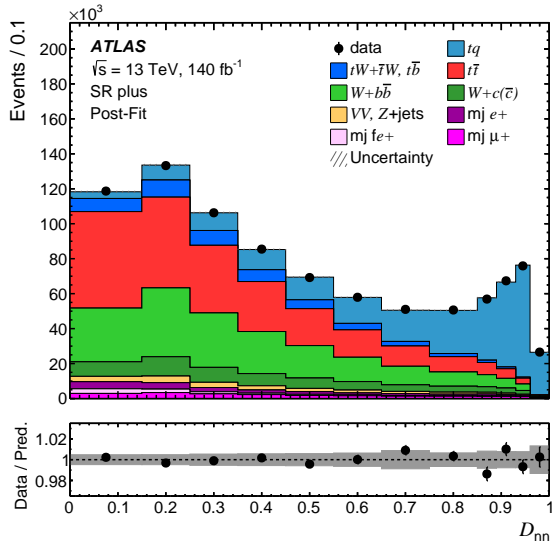
Systematic uncertainty	$\Delta R_t/R_t$
$W^- + c(\bar{c})$ cross-section	+0.8 / -0.8
tq parton shower, rate	+0.7 / -0.7
$W^+ + c(\bar{c})$ cross-section	+0.5 / -0.5
PDF eigenvector 09	+0.5 / -0.5
MC statistical uncertainty in D_{nn} bin 10 of SR minus	+0.4 / -0.4
JES η intercalibration modelling	+0.4 / -0.4
tq matching scale definition, shape	+0.4 / -0.4
PDF eigenvector 05	+0.4 / -0.4

Table 5: The impact of the eight most important systematic uncertainties on R_t in %.

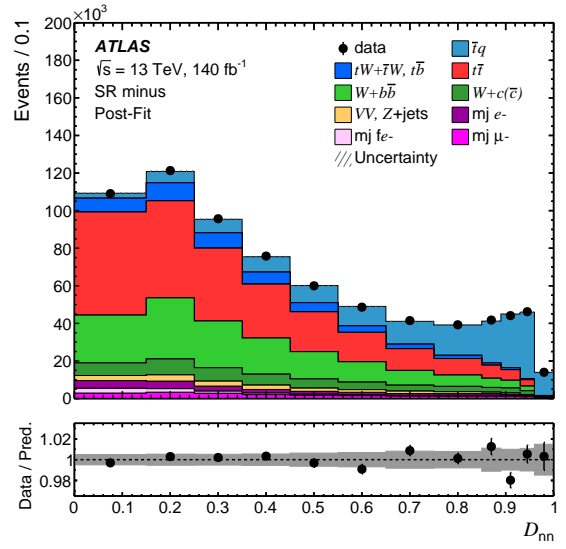
constant term is given by the central value at $m_t = 172.5$ GeV, namely

$$\sigma(m_t) = \sigma(172.5 \text{ GeV}) + a \cdot \Delta m_t [\text{GeV}],$$

where $\Delta m_t = m_t - 172.5$ GeV. The slopes are fitted to be $a = (-1.50 \pm 0.26)$ pb GeV⁻¹ for $\sigma(tq)$, $a = (-0.85 \pm 0.31)$ pb GeV⁻¹ for $\sigma(\bar{t}q)$, and $a = (-2.35 \pm 0.69)$ pb GeV⁻¹ for $\sigma(tq + \bar{t}q)$. For R_t the effect is found to be negligible.



(a)



(b)

Figure 7: The observed D_{nn} distributions (dots) for (a) SR plus and (b) SR minus are compared with the expected distributions (histograms) from simulated events after the fit (post-fit). In these distributions, the signal contribution is shown stacked on top of contributions from all contributing background processes. All uncertainties considered in the analysis are included in the hatched uncertainty band. The correlations induced by the fit are taken into account. The lower panel shows the ratio of data and the prediction; in this panel, the uncertainty is displayed as a grey band.

Process	SR plus	SR minus
tq	$169\,000 \pm 6\,000$	150 ± 150
$\bar{t}q$	90 ± 90	$109\,000 \pm 4\,000$
$tW + \bar{t}W, t\bar{b} + \bar{t}b$	$51\,000 \pm 4\,000$	$49\,000 \pm 4\,000$
$t\bar{t}$	$265\,000 \pm 14\,000$	$265\,000 \pm 14\,000$
$W+b\bar{b}$	$198\,000 \pm 21\,000$	$159\,000 \pm 17\,000$
$W+c(\bar{c})$	$60\,000 \pm 13\,000$	$49\,000 \pm 11\,000$
Z+jets, diboson	$21\,000 \pm 4\,000$	$19\,000 \pm 4\,000$
Multijet	$50\,000 \pm 10\,000$	$50\,000 \pm 10\,000$
Total	$814\,000 \pm 2\,100$	$698\,800 \pm 2\,000$
Observed	814 185	698 845

Table 6: The post-fit event yields in the two SRs. All uncertainties applied in the analysis are included. Correlations, including anticorrelations, among the nuisance parameters related to the uncertainties are taken into account as determined in the maximum-likelihood fit, leading to a reduction in the size of the uncertainties, in particular for the total prediction. The event yields of the different processes as quoted in the table do not add up to the total sum given because of rounding effects.

8 Interpretation of the measurements

The measurements of the tq production cross-sections presented in Section 7 are interpreted in different ways. Predictions based on different PDF sets are compared with the measured R_t value in Section 8.1. A search for a contribution of a four-quark EFT operator to tq production using the D_{nn} distributions in the SRs is presented in Section 8.2. The result of this search yields a confidence interval for the EFT coefficient $C_{Qq}^{3,1}/\Lambda^2$. In addition, the measurement of $\sigma(tq + \bar{t}q)$ is used to derive limits on the EFT coefficient $C_{\phi Q}^3/\Lambda^2$. The corresponding operator $O_{\phi Q}^3$ has the same Lorentz structure as the Wtb vertex in the SM, and thus simply scales the cross-section of tq production, while kinematic distributions are not altered by its presence. The CKM matrix element V_{tb} is extracted from the measurement of $\sigma(tq + \bar{t}q)$ (see Section 8.3). In a more general approach, confidence contours are determined in the $f_{LV}|V_{td}|$ -versus- $f_{LV}|V_{tb}|$, the $f_{LV}|V_{ts}|$ -versus- $f_{LV}|V_{tb}|$, and the $f_{LV}|V_{ts}|$ -versus- $f_{LV}|V_{td}|$ planes; the results are presented in Section 8.4.

8.1 Sensitivity of R_t to PDF sets

With an uncertainty of $+2.2\%$ / -2.1% , the measurement of R_t can potentially distinguish between different PDF sets. Predictions of R_t made with different PDF sets at NNLO, namely ABMP [91], ATLAS [92], CTEQ [93], MSHT [94], NNPDF [36, 95], and PDF4LHC [45], are compared with the measured value in Figure 8. The calculations were performed with the MCFM 10.1 program [44]. The differences between the R_t predictions are driven by differences between the u - and d -quark PDFs. The PDFs provided by the different groups differ in the data used, the value of α_s assumed, the values of quark masses used, and the treatment of heavy quarks. The scale uncertainties for the theoretical predictions are included in Figure 8. The scale uncertainties are determined by varying μ_r and μ_f independently up and down by a factor of two, whilst never allowing them to differ by a factor greater than two from each other. The scale uncertainty is defined as the envelope of the six resulting variations. The uncertainties in the predictions also include the uncertainties provided by the PDF set under investigation and, where possible, uncertainties in α_s .²

The prediction of ABMP is incompatible with the measurement of R_t at the level of approximately three standard deviations. All other predictions are in agreement with the measured value within the experimental and theoretical uncertainties. The predictions of ATLASpdf21 and NNPDF3.0 are the closest to the central value of the measurement, while all other predictions are approximately one standard deviation above. This is comparable to the difference seen between predictions and the ATLAS measurement at a centre-of-mass energy of 8 TeV in Run 1 of the LHC [96]. The slightly higher uncertainty of the ATLASpdf21 prediction compared with those predictions based on other ATLAS PDF sets is attributed to the usage of a wider range of input data samples and, associated to that, a modified uncertainty definition.

8.2 EFT interpretation

The Standard Model Effective Field Theory (SMEFT) provides a model-independent framework for indirect searches for new physics. Within this framework, the SM is regarded as a low-energy approximation of a more fundamental theory involving interactions at an energy scale Λ . The impact of new physics is

² There is no functionality implemented to vary α_s for ATLAS (epWZ16). For MSHT the strong coupling constant is varied simultaneously with the PDF eigenvectors rather than independently.

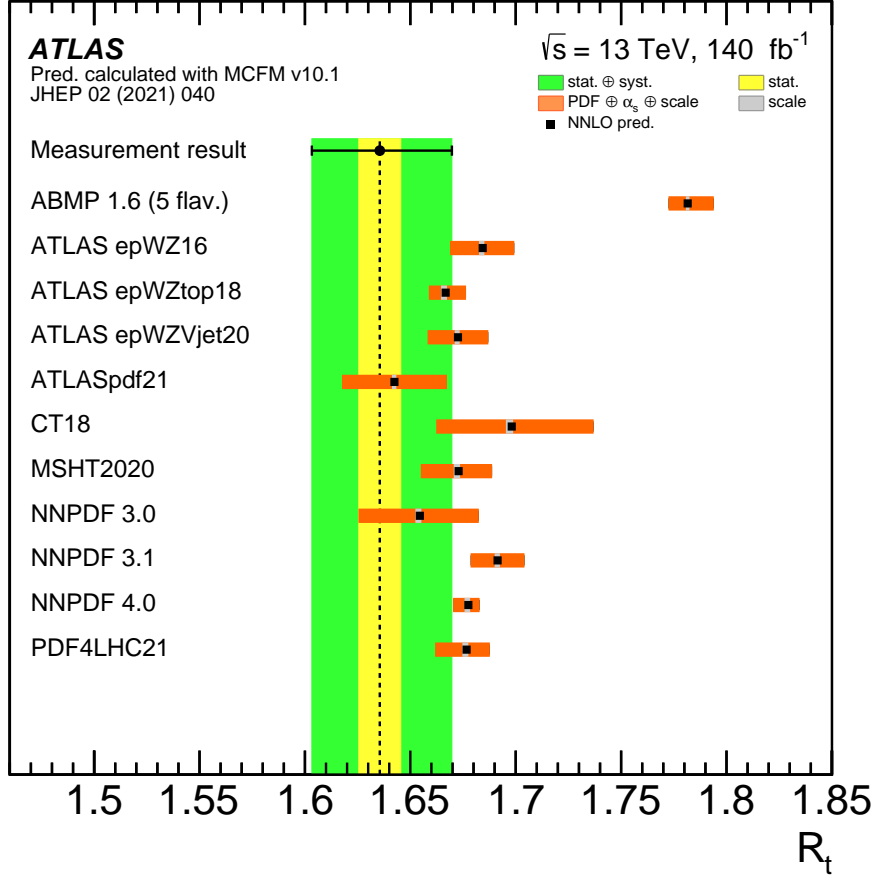


Figure 8: The measured value of R_t (dot). The yellow band represents the statistical uncertainty and the green band represents the total uncertainty of the measurement. For comparison, the NNLO predictions of MCFM based on different PDF sets are included: ABMP [91], ATLAS [92], CTEQ [93], MSHT [94], NNPDF [36, 95], and PDF4LHC [45]. The uncertainties in the theoretical predictions include PDF, scale and α_s uncertainties.

parameterised by higher-dimensional operators maintaining SM symmetries. The effective Lagrangian is given by

$$\mathcal{L}_{\text{eff}} = \mathcal{L}_{\text{SM}} + \sum_i \frac{C_i}{\Lambda^2} O_i + \text{Hermitian conjugate},$$

where \mathcal{L}_{SM} is the SM Lagrangian. The O_i are effective dimension-6 operators and the C_i are the associated Wilson coefficients. In this EFT interpretation, two operators are considered, the four-quark operator $O_{qq}^{3,1}$ and the operator $O_{\phi Q}^3$ coupling the third quark generation to the Higgs boson doublet Φ .

The relevant operators, expressed in the Warsaw basis, are

$$\begin{aligned} O_{qq}^{1(ijkl)} &= (\bar{q}_i \gamma^\mu q_j)(\bar{q}_k \gamma_\mu q_l), \\ O_{qq}^{3(ijkl)} &= (\bar{q}_i \gamma^\mu \tau^I q_j)(\bar{q}_k \gamma_\mu \tau^I q_l) \quad \text{and} \\ O_{\phi Q}^3 &= i(\Phi^\dagger \tau^I D_\mu \Phi)(\bar{Q} \gamma^\mu \tau^I Q). \end{aligned}$$

The q denote weak-isospin doublets with $ijkl \in 1, 2, 3$ as quark generation indices, while Q represents the doublet of the third quark generation. All contributing four-quark processes depend solely on a linear

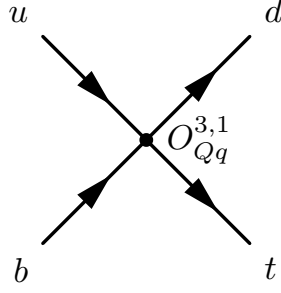


Figure 9: Representative LO Feynman diagram of a four-quark contact interaction leading to the production of a single top quark.

combination of Wilson coefficients

$$C_{Qq}^{3,1} = \sum_{i=1,2} C_{qq}^{3(ii33)} + \frac{1}{6} C_{qq}^{1(i33i)} - \frac{1}{6} C_{qq}^{3(i33i)},$$

therefore the four-quark interaction is fully characterised by $O_{Qq}^{3,1}$ [97].

The operator $O_{Qq}^{3,1}$ leads to non-SM single top-quark production, as illustrated in Figure 9, for example via the process $b + u \rightarrow t + d$. Top quarks produced in this way feature different angular distributions and kinematics than those produced via SM processes. A non-zero contribution from the operator $O_{\phi Q}^3$ does not alter the Lorentz structure of the Wtb vertex, it merely leads to a rescaling of the vertex strength, and thus changes the total cross-section, but it does not alter the shape of any kinematic distributions.

Events with single top quarks produced via SM vertices (tq and $t\bar{b}$ production) and via $O_{Qq}^{3,1}$ vertices were generated with MADGRAPH, as detailed in Section 3.4. These samples are subjected to the regular analysis chain, including the event selection and the processing of the NN analysis. Using the five different EFT samples, the single top-quark event yield ν_j in each bin j of the D_{nn} distributions in SR plus and SR minus is parameterised by a polynomial of second degree in the EFT coefficient $C_{Qq}^{3,1}$.

$$\nu_j = \nu_{0j} + a_{1j} \frac{C_{Qq}^{3,1}}{\Lambda^2} + a_{2j} \frac{(C_{Qq}^{3,1})^2}{\Lambda^4}.$$

The constant term ν_{0j} represents tq and $t\bar{b}$ production in the SM and is normalised to the SM cross-section predictions of both the processes, as reported in Section 3.1. The term linear in $C_{Qq}^{3,1}$ represents the effect of the interference of SM and non-SM amplitudes and the term proportional to $(C_{Qq}^{3,1})^2$ is entirely due to the four-quark operator. Based on a maximum-likelihood scan of the parameter $C_{Qq}^{3,1}/\Lambda^2$ the 95% CL interval is determined to be

$$-0.37 < C_{Qq}^{3,1}/\Lambda^2 < 0.06.$$

All SM processes are modelled in the same way as in the cross-section measurements presented in Section 7. The same systematic uncertainties are applied. The constraints presented improve the limits set by the ATLAS measurement of the charge asymmetry in $t\bar{t}$ production [98], which obtained a confidence interval of $[-0.70, 0.75]$. The interpretation of cross-section measurements of $t\bar{t}Z$ production by ATLAS [99] reaches the constraints $[-0.34, 0.23]$, similar to the ones presented above. Limits on the parameter $C_{Qq}^{3,1}/\Lambda^2$ were also set by global EFT fits that include inputs from measurements by the ATLAS and CMS

Collaborations. The results in Ref. [7] are based on various measurements of Higgs boson, diboson and top-quark production processes and lead to a confidence interval for $C_{Qq}^{3,1}/\Lambda^2$ of $[-0.088, 0.166]$ at the 95% CL when including terms of order Λ^{-4} . A similar approach by a different group of analysers [8] leads to a confidence interval of $[-0.043, 0.16]$. Using only top-quark measurements for the analysis, the authors of Ref. [9] obtain $C_{Qq}^{3,1}/\Lambda^2 \in [-0.39, 0.11]$. The comparison to these results of global EFT analyses demonstrates that the limits on $C_{Qq}^{3,1}/\Lambda^2$ obtained from the tq cross-section measurements presented in this document are quite competitive. An important difference to appreciate is that the results of Refs. [7–9] do not account for reconstruction effects on EFT signal events, while the results presented here are based on simulated samples that include detector effects.

Since the EFT operator $O_{\phi Q}^3$ has the same Lorentz structure as the Wtb vertex in the SM, and kinematic distributions of tq and $\bar{t}q$ events are thus not altered by contributions from $O_{\phi Q}^3$, limits on the corresponding Wilson coefficient $C_{\phi Q}^3/\Lambda^2$ are derived from the measured cross-section $\sigma(tq + \bar{t}q)$. The cross-section $\sigma(tq + \bar{t}q)$ is calculated for different values of $C_{\phi Q}^3/\Lambda^2$ with MADGRAPH5_AMC@NLO 2.7.3 using the SMEFTatNLO-NLO model [62] with the five-flavour scheme and the NNPDF3.0_{NLO} PDF set, and is obtained as the sum of $\sigma(tq)$ and $\sigma(\bar{t}q)$. The contribution of the quadratic term in $C_{\phi Q}^3/\Lambda^2$ is negligible in the relevant parameter range, and thus a linear function is fitted to the relative change in $\sigma(tq + \bar{t}q)$ as a function of $C_{\phi Q}^3/\Lambda^2$ relative to its value at $C_{\phi Q}^3/\Lambda^2 = 0$, resulting in a slope of 0.12 ± 0.02 . Based on this parameterisation, the 95% CL interval of $C_{\phi Q}^3/\Lambda^2$ is determined to be

$$-0.87 < C_{\phi Q}^3/\Lambda^2 < 1.42.$$

These constraints improve limits obtained by the interpretation of cross-section measurements of $t\bar{t}Z$ production that yielded the confidence interval $[-0.95, 2.0]$ [99]. However, the combined interpretation of Higgs boson, diboson, and top-quark measurements yielded a stronger limit of $[-0.375, 0.344]$ [7].

8.3 Determination of $|V_{tb}|$

Single top-quark production in the t -channel proceeds primarily via a Wtb vertex and the cross-section is proportional to $f_{LV}^2 \cdot |V_{tb}|^2$. In the SM, the left-handed form factor f_{LV} is exactly one and the CKM matrix is unitary. Assuming the unitarity relations, the measured values of other CKM matrix elements suggest that $|V_{tb}|$ is very close to one. However, new-physics contributions could alter the value of f_{LV} significantly. The determination of $f_{LV} \cdot |V_{tb}|$ based on single-top-quark cross-section measurements is independent of assumptions about the number of quark generations and the unitarity of the CKM matrix. The only assumptions made are that $|V_{tb}| \gg |V_{td}|, |V_{ts}|$ and that the Wtb interaction is a left-handed weak coupling, as in the SM.

The value of $f_{LV}^2 \cdot |V_{tb}|^2$ is extracted by dividing the measured value of $\sigma(tq + \bar{t}q)$ by the SM expectation of $214.2 \pm 3.4(\text{scale} + \text{PDF}) \pm 0.6(\Delta m_t)$ pb [44]. When calculating $f_{LV}^2 \cdot |V_{tb}|^2$, the experimental and theoretical uncertainties are added in quadrature. The uncertainty in m_t is also considered, assuming $\Delta m_t = \pm 0.33$ GeV based on a combination of Run 1 measurements of m_t by the ATLAS and CMS Collaborations [100]. The result obtained is

$$f_{LV} \cdot |V_{tb}| = 1.015 \pm 0.031,$$

improving the precision by 30% compared with the combination of Run 1 measurements by ATLAS and CMS [101]. The Particle Data Group combined all available measurements performed at the Tevatron and the LHC to 1.014 ± 0.029 [74].

Restricting the range of $|V_{tb}|$ to the interval $[0, 1]$ and setting $f_{LV} = 1$, as required by the SM, a lower limit on $|V_{tb}|$ is extracted: $|V_{tb}| > 0.95$ at the 95% CL. In the Bayesian-style limit computation, it is assumed that the likelihood curve of $|V_{tb}|^2$ is a Gaussian function, centered at the measured value. A flat prior in $|V_{tb}|^2$ is applied, being one in the interval $[0, 1]$ and zero otherwise.

8.4 Generalised CKM interpretation

The interpretation of the tq cross-section measurements presented in Section 8.3 neglects the contributions due to Wts and Wtd vertices. In a more general approach, this caveat is avoided. Nine contributions to tq production are considered, differing in the combination of Wtq vertices for top-quark production and decay with $q \in \{d, s, b\}$. In $t\bar{t}$ production, Wtq vertices occur for the top-quark and top-antiquark decays. Again, nine different combinations of vertices are considered, thus treating the most important background process at the same level of modelling as the tq signal process. Including the effect of Wts and Wtd vertices for $t\bar{t}$ production improves the sensitivity of the measurement to $|V_{ts}|$ and $|V_{td}|$ by approximately 20%. The effects of Wts and Wtd vertices on the event yields of tW and $t\bar{b}$ production are neglected, since the corresponding event yields for these processes are much smaller than the yields for tq and $t\bar{t}$ production. Three different fit scenarios are investigated. In each scenario, two V_{tq} matrix elements are considered to be free parameters, while the third parameter is fixed to be either 0 or 1:

- Scenario 1 $|V_{tb}| \neq 0, |V_{td}| \neq 0$ and $|V_{ts}| = 0$,
- Scenario 2 $|V_{tb}| \neq 0, |V_{ts}| \neq 0$ and $|V_{td}| = 0$,
- Scenario 3 $|V_{td}| \neq 0, |V_{ts}| \neq 0$ and $f_{LV}|V_{tb}| = 1$.

The form factor f_{LV} is non-zero in all scenarios and is also allowed to be greater than one. For each scenario, a maximum-likelihood scan of the two non-zero CKM matrix elements is performed. As a result, confidence contours are determined at the 95% CL in the $f_{LV}|V_{td}|$ -versus- $f_{LV}|V_{tb}|$, the $f_{LV}|V_{ts}|$ -versus- $f_{LV}|V_{tb}|$, and the $f_{LV}|V_{ts}|$ -versus- $f_{LV}|V_{td}|$ planes. These contours are shown in Figure 10. The parameter $f_{LV}|V_{tb}|$ is constrained at the 95% CL to a range between 0.95 and 1.05, and $f_{LV}|V_{td}|$ and $f_{LV}|V_{ts}|$ are constrained to be < 0.23 and < 0.58 , respectively. The constraint on $|V_{td}|$ is stronger compared with the one on $|V_{ts}|$ because the d -quark is a valence quark of the proton, while s -quarks appear as sea-quarks only. The interpretation uses the nominal simulation-to-data corrections for the efficiency of tagging b -quark jets, which was determined with $t\bar{t}$ events in the dilepton channel assuming $|V_{tb}| = 1$ and thus $\mathcal{B}(t \rightarrow Wb) = 100\%$. This assumption is increasingly violated when moving to large values of $|V_{td}|$ and $|V_{ts}|$ and thus constitutes a caveat of the generalised CKM interpretation presented here. A similar model-independent measurement of the modulus of the CKM matrix elements $|V_{tb}|$, $|V_{td}|$, and $|V_{ts}|$ was performed by the CMS Collaboration and yielded $|V_{tb}| = 0.988 \pm 0.024$ and $|V_{td}|^2 + |V_{ts}|^2 = 0.06 \pm 0.06$ [12].

The CKM matrix elements $|V_{td}|$ and $|V_{ts}|$ are determined very precisely using measurements of the mass differences Δm_d and Δm_s of the mass eigenstates of B_d^0 and B_s^0 mesons [74]. However, these determinations are based on $B-\bar{B}$ meson oscillations that are induced by box diagrams with top quarks, use lattice QCD results, and neglect corrections suppressed by $|V_{tb}| - 1$, and thus introduce a certain level of model dependence that is reduced in the studies presented here for tree-level processes, namely single top-quark production and decay. In addition, the top-quark processes give access to a much higher energy scale.

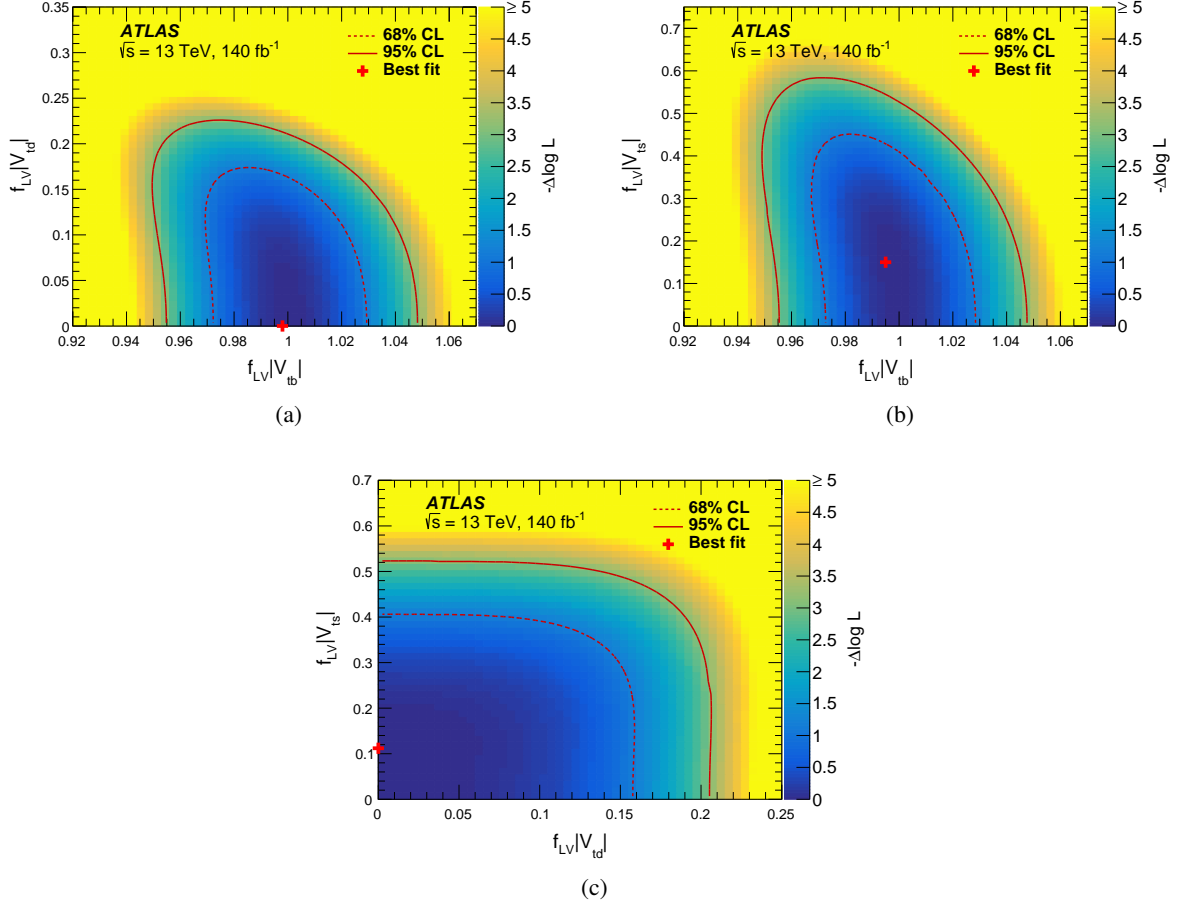


Figure 10: Confidence contours obtained from maximum-likelihood scans in (a) the $f_{LV}|V_{td}|$ -versus- $f_{LV}|V_{tb}|$ plane, (b) the $f_{LV}|V_{ts}|$ -versus- $f_{LV}|V_{tb}|$ plane, and (c) the $f_{LV}|V_{ts}|$ -versus- $f_{LV}|V_{td}|$ plane. Contours at the 68% and 95% confidence levels are shown. The two-dimensional histogram contains the values of the difference of the log-likelihood function at a certain point in the plane to the minimum of the log-likelihood function indicated by the red cross.

9 Conclusions

The production of single top quarks and top antiquarks via the t -channel exchange of a virtual W boson is measured in proton–proton collisions at the LHC at a centre-of-mass energy of 13 TeV, using the full Run 2 data sample of 140 fb^{-1} recorded with the ATLAS detector. Events are selected with either one isolated electron or muon, high E_T^{miss} , and exactly two hadronic jets with high p_T . Exactly one of these jets is required to be b -tagged. An artificial NN is used to construct a discriminant that separates signal and background events. The distributions of the discriminant are used in profile maximum-likelihood fits to determine the signal yields.

The total cross-sections are determined to be $\sigma(tq) = 137^{+8}_{-8} \text{ pb}$ and $\sigma(\bar{t}q) = 84^{+6}_{-5} \text{ pb}$ for top-quark and top-antiquark production, respectively. The combined cross-section is found to be $\sigma(tq + \bar{t}q) = 221^{+13}_{-13} \text{ pb}$ and the cross-section ratio is $R_t = \sigma(tq)/\sigma(\bar{t}q) = 1.636^{+0.036}_{-0.034}$. The predictions made at NNLO in perturbation theory are in good agreement with the measured cross-sections, which reach greater precision than previous measurements by the ATLAS and CMS Collaborations with partial Run 2 data samples at

$\sqrt{s} = 13$ TeV. The relative precision of the measurements presented also surpasses the precision reached in ATLAS Run 1 measurements at $\sqrt{s} = 7$ TeV and $\sqrt{s} = 8$ TeV. The new results are thus the most precise measurements of tq and $\bar{t}q$ production to date.

The predictions using various sets of PDFs are compared with the measured value of R_t , demonstrating the potential of further constraining the functions if the measurement is included into future fits. The measurements of $\sigma(tq)$, $\sigma(\bar{t}q)$, and $\sigma(tq + \bar{t}q)$ are interpreted in an EFT approach, setting limits at the 95% CL on the strength of the four-quark operator $O_{Qq}^{3,1}$ and the operator $C_{\phi Q}^3/\Lambda^2$: $-0.37 < C_{Qq}^{3,1}/\Lambda^2 < 0.06$ and $-0.87 < C_{\phi Q}^3/\Lambda^2 < 1.42$, respectively. The measured value of $\sigma(tq + \bar{t}q)$ is further used to derive the constraint $|V_{tb}| > 0.95$ at the 95% CL and determine $f_{LV} \cdot |V_{tb}| = 1.015 \pm 0.031$, improving by 30% the determination of this quantity based on a combination of Run 1 measurements by ATLAS and CMS. In a more general approach, confidence contours are determined in the $f_{LV}|V_{td}|$ -versus- $f_{LV}|V_{tb}|$, the $f_{LV}|V_{ts}|$ -versus- $f_{LV}|V_{tb}|$, and the $f_{LV}|V_{ts}|$ -versus- $f_{LV}|V_{td}|$ planes. The parameter $f_{LV}|V_{tb}|$ is constrained at the 95% CL to a range between 0.95 and 1.05, and $f_{LV}|V_{td}|$ and $f_{LV}|V_{ts}|$ are constrained to be < 0.23 and < 0.58 , respectively.

Acknowledgements

We thank CERN for the very successful operation of the LHC and its injectors, as well as the support staff at CERN and at our institutions worldwide without whom ATLAS could not be operated efficiently.

The crucial computing support from all WLCG partners is acknowledged gratefully, in particular from CERN, the ATLAS Tier-1 facilities at TRIUMF/SFU (Canada), NDGF (Denmark, Norway, Sweden), CC-IN2P3 (France), KIT/GridKA (Germany), INFN-CNAF (Italy), NL-T1 (Netherlands), PIC (Spain), RAL (UK) and BNL (USA), the Tier-2 facilities worldwide and large non-WLCG resource providers. Major contributors of computing resources are listed in Ref. [102].

We gratefully acknowledge the support of ANPCyT, Argentina; YerPhI, Armenia; ARC, Australia; BMWFW and FWF, Austria; ANAS, Azerbaijan; CNPq and FAPESP, Brazil; NSERC, NRC and CFI, Canada; CERN; ANID, Chile; CAS, MOST and NSFC, China; Minciencias, Colombia; MEYS CR, Czech Republic; DNRF and DNSRC, Denmark; IN2P3-CNRS and CEA-DRF/IRFU, France; SRNSFG, Georgia; BMBF, HGF and MPG, Germany; GSRI, Greece; RGC and Hong Kong SAR, China; ISF and Benoziyo Center, Israel; INFN, Italy; MEXT and JSPS, Japan; CNRST, Morocco; NWO, Netherlands; RCN, Norway; MEiN, Poland; FCT, Portugal; MNE/IFA, Romania; MESTD, Serbia; MSSR, Slovakia; ARRS and MIZŠ, Slovenia; DSI/NRF, South Africa; MICINN, Spain; SRC and Wallenberg Foundation, Sweden; SERI, SNSF and Cantons of Bern and Geneva, Switzerland; MOST, Taipei; TENMAK, Türkiye; STFC, United Kingdom; DOE and NSF, United States of America.

Individual groups and members have received support from BCKDF, CANARIE, CRC and DRAC, Canada; CERN-CZ, PRIMUS 21/SCI/017 and UNCE SCI/013, Czech Republic; COST, ERC, ERDF, Horizon 2020, ICSC-NextGenerationEU and Marie Skłodowska-Curie Actions, European Union; Investissements d’Avenir Labex, Investissements d’Avenir Idex and ANR, France; DFG and AvH Foundation, Germany; Herakleitos, Thales and Aristeia programmes co-financed by EU-ESF and the Greek NSRF, Greece; BSF-NSF and MINERVA, Israel; Norwegian Financial Mechanism 2014-2021, Norway; NCN and NAWA, Poland; La Caixa Banking Foundation, CERCA Programme Generalitat de Catalunya and PROMETEO and GenT Programmes Generalitat Valenciana, Spain; Göran Gustafssons Stiftelse, Sweden; The Royal Society and Leverhulme Trust, United Kingdom.

In addition, individual members wish to acknowledge support from Chile: Agencia Nacional de Investigación y Desarrollo (FONDECYT 1190886, FONDECYT 1210400, FONDECYT 1230812, FONDECYT 1230987); China: National Natural Science Foundation of China (NSFC - 12175119, NSFC 12275265, NSFC-12075060); Czech Republic: PRIMUS Research Programme (PRIMUS/21/SCI/017); European Union: European Research Council (ERC - 948254), Horizon 2020 Framework Programme (MUCCA - CHIST-ERA-19-XAI-00), European Union, Future Artificial Intelligence Research (FAIR-NextGenerationEU PE00000013), Italian Center for High Performance Computing, Big Data and Quantum Computing (ICSC, NextGenerationEU), Marie Skłodowska-Curie Actions (EU H2020 MSC IF GRANT NO 101033496); France: Agence Nationale de la Recherche (ANR-20-CE31-0013, ANR-21-CE31-0013, ANR-21-CE31-0022), Investissements d'Avenir Idex (ANR-11-LABX-0012), Investissements d'Avenir Labex (ANR-11-LABX-0012); Germany: Baden-Württemberg Stiftung (BW Stiftung-Postdoc Eliteprogramme), Deutsche Forschungsgemeinschaft (DFG - CR 312/5-1); Italy: Istituto Nazionale di Fisica Nucleare (FELLINI G.A. n. 754496, ICSC, NextGenerationEU); Japan: Japan Society for the Promotion of Science (JSPS KAKENHI JP21H05085, JSPS KAKENHI JP22H01227, JSPS KAKENHI JP22H04944); Netherlands: Netherlands Organisation for Scientific Research (NWO Veni 2020 - VI.Veni.202.179); Norway: Research Council of Norway (RCN-314472); Poland: Polish National Agency for Academic Exchange (PPN/PPO/2020/1/00002/U/00001), Polish National Science Centre (NCN 2021/42/E/ST2/00350, NCN UMO-2019/34/E/ST2/00393, UMO-2020/37/B/ST2/01043, UMO-2021/40/C/ST2/00187); Slovenia: Slovenian Research Agency (ARIS grant J1-3010); Spain: BBVA Foundation (LEO22-1-603), Generalitat Valenciana (Artemisa, FEDER, IDIFEDER/2018/048), La Caixa Banking Foundation (LCF/BQ/PI20/11760025), Ministry of Science and Innovation (MCIN & NextGenEU -PCI2022-135018-2, MICIN & FEDER -PID2021-125273NB, RYC2019-028510-I, RYC2020-030254-I, RYC2021-031273-I, RYC2022-038164-I), PROMETEO and GenT Programmes Generalitat Valenciana (CIDEAGENT/2019/023, CIDEAGENT/2019/027); Sweden: Swedish Research Council (VR 2018-00482, VR 2022-03845, VR 2022-04683, VR grant 2021-03651), Knut and Alice Wallenberg Foundation (KAW 2017.0100, KAW 2018.0157, KAW 2018.0458, KAW 2019.0447); Switzerland: Swiss National Science Foundation (SNSF - PCEFP2_194658); United Kingdom: Leverhulme Trust (Leverhulme Trust RPG-2020-004); United States of America: Neubauer Family Foundation.

Additional plots and interpretations

Figure 11 illustrates the fractions of selected events in the two SRs for the different scattering processes based on the post-fit event yields reported in Table 6.

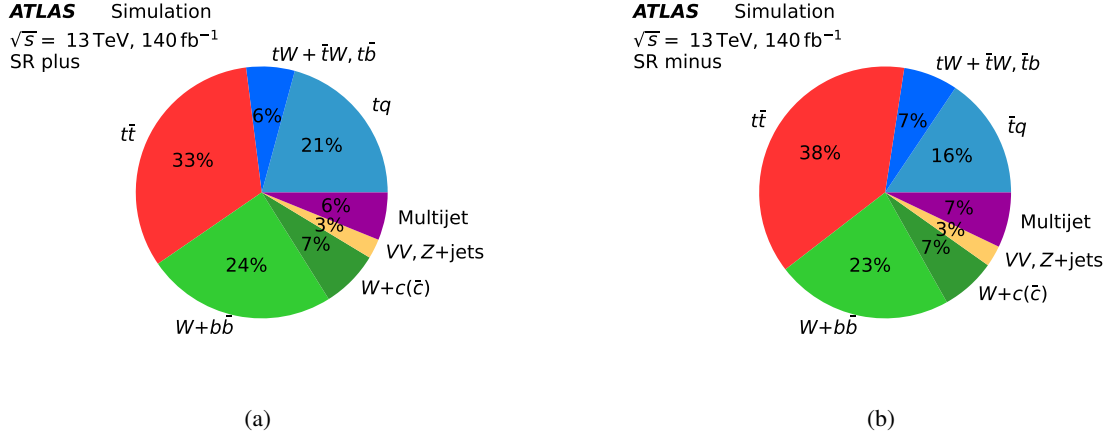


Figure 11: Pie chart of the composition of (a) the SR plus and (b) the SR minus in terms of the different scattering processes. The fractions are based on the post-fit event yields.

The rate of the multijet background is determined by including CRs enriched in this background in the maximum-likelihood fit. Figure 12 shows the post-fit distributions of the variable $\Delta\phi(\vec{p}_T^{\text{miss}}, \mu)$ in the CR μ -plus and CR μ -minus.

Figure 13 compares NNLO predictions obtained with different PDF sets with the measured values of $\sigma(tq)$ and $\sigma(\bar{t}q)$. The PDF sets used are ABMP [91], ATLAS [92], CTEQ [93], MSHT [94], NNPDF [36, 95], and PDF4LHC [45]. All predictions agree with the measurements within the uncertainties.

A 95% CL interval is determined for the EFT coefficient $C_{Qq}^{3,1}/\Lambda^2$ by scanning the likelihood function relative to this parameter. Figure 14 shows the difference between the natural logarithm of the likelihood function relative to its minimum as a function of $C_{Qq}^{3,1}/\Lambda^2$.

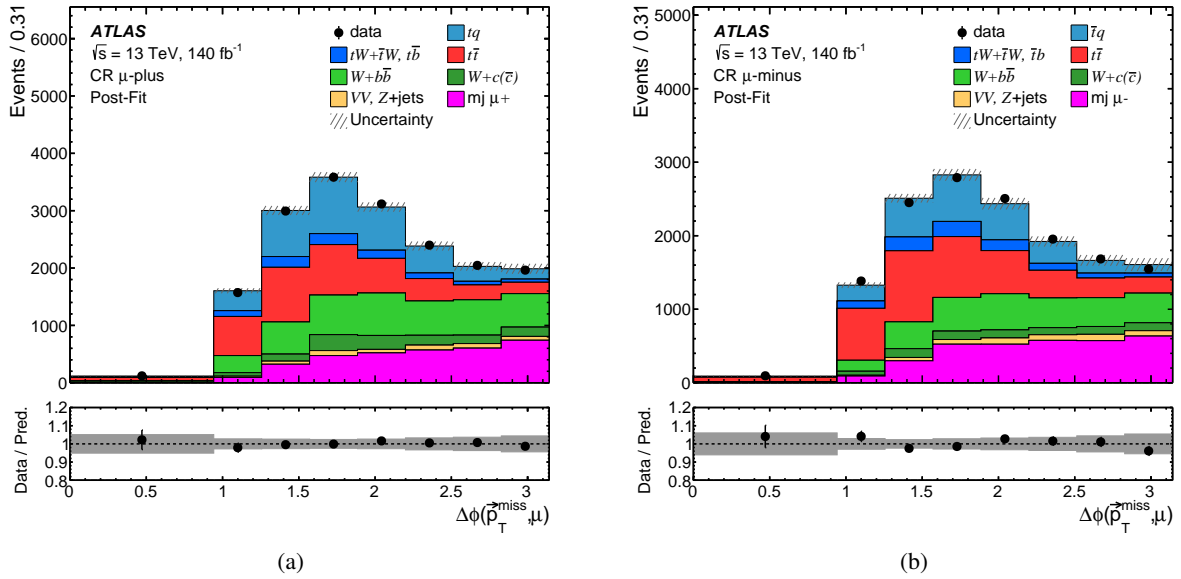


Figure 12: Distributions of the variable $\Delta\phi(\vec{p}_T^{\text{miss}}, \mu)$ in (a) the CR μ -plus and (b) the CR μ -minus after the maximum-likelihood fit is performed (post-fit). In these distributions, the signal contribution is shown stacked on top of contributions from all contributing background processes. All uncertainties considered in the analysis are included in the hatched uncertainty band. The correlations induced by the fit are taken into account. The lower panel shows the ratio of data and the prediction; in this panel, the uncertainty is displayed as a grey band.

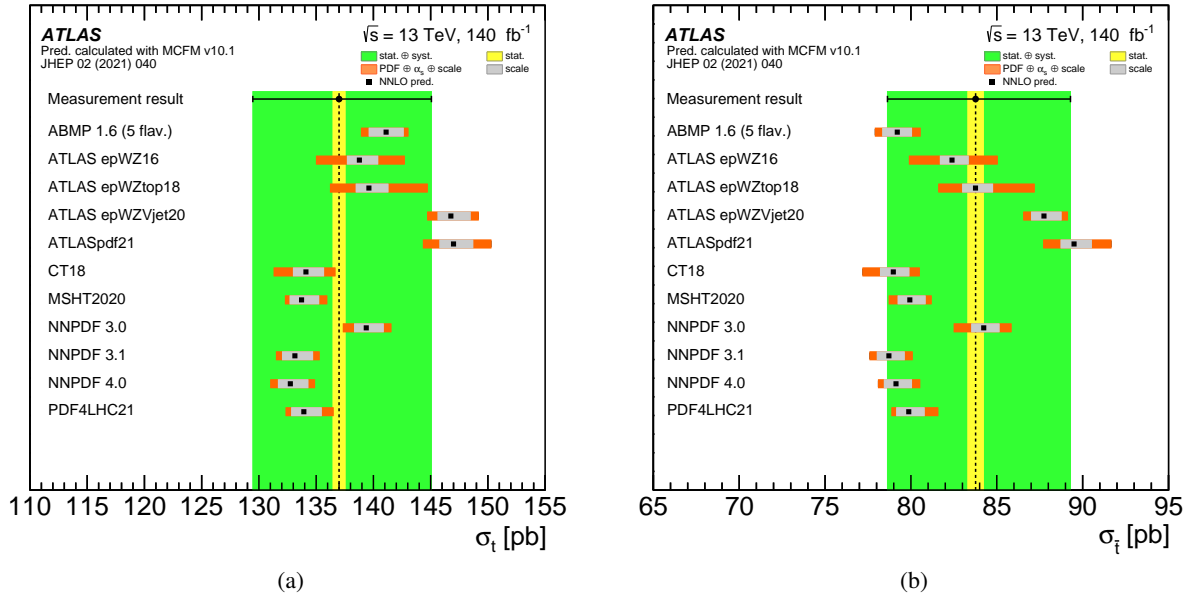


Figure 13: Comparison of NNLO predictions based on several different PDF sets with the measured values (dots) of (a) $\sigma(tq)$ and (b) $\sigma(\bar{t}q)$. The yellow band represents the statistical uncertainty and the green band the total uncertainty. The uncertainties in the theoretical predictions include PDF, scale and α_s uncertainties.

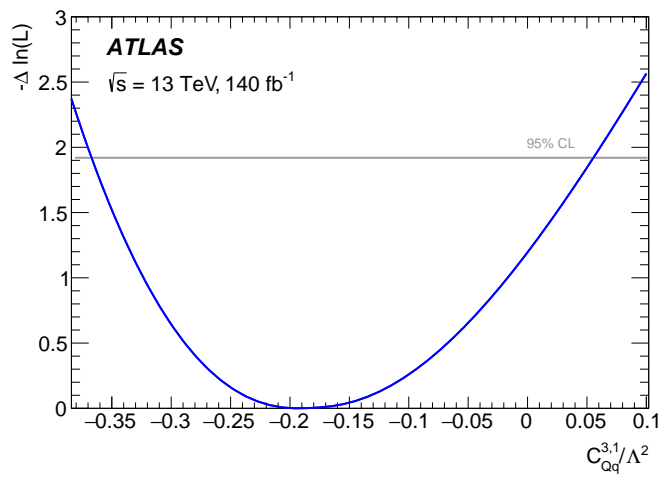


Figure 14: Likelihood scan of the EFT coefficient $C_{Qq}^{3,1}/\Lambda^2$.

References

- [1] L. Evans and P. Bryant, *LHC Machine*, [JINST 3 \(2008\) S08001](#).
- [2] ATLAS Collaboration, *The ATLAS Experiment at the CERN Large Hadron Collider*, [JINST 3 \(2008\) S08003](#).
- [3] E. R. Nocera, M. Ubiali and C. Voisey, *Single top production in PDF fits*, [JHEP 05 \(2020\) 067](#), arXiv: [1912.09543 \[hep-ph\]](#).
- [4] ATLAS Collaboration, *Measurement of the inclusive cross-sections of single top-quark and top-antiquark t -channel production in pp collisions at $\sqrt{s} = 13$ TeV with the ATLAS detector*, [JHEP 04 \(2017\) 086](#), arXiv: [1609.03920 \[hep-ex\]](#).
- [5] ATLAS Collaboration, *Jet energy scale and resolution measured in proton–proton collisions at $\sqrt{s} = 13$ TeV with the ATLAS detector*, [Eur. Phys. J. C 81 \(2021\) 689](#), arXiv: [2007.02645 \[hep-ex\]](#).
- [6] ATLAS Collaboration, *ATLAS flavour-tagging algorithms for the LHC Run 2 pp collision dataset*, [Eur. Phys. J. C 83 \(2023\) 681](#), arXiv: [2211.16345 \[physics.data-an\]](#).
- [7] SMEFiT Collaboration, J. J. Ethier et al., *Combined SMEFT interpretation of Higgs, diboson, and top quark data from the LHC*, [JHEP 11 \(2021\) 089](#), arXiv: [2105.00006 \[hep-ph\]](#).
- [8] J. Ellis, M. Madigan, K. Mimasu, V. Sanz and T. You, *Top, Higgs, diboson and electroweak fit to the Standard Model effective field theory*, [JHEP 04 \(2021\) 279](#), arXiv: [2012.02779 \[hep-ph\]](#).
- [9] I. Brivio et al., *O new physics, where art thou? A global search in the top sector*, [JHEP 02 \(2020\) 131](#), arXiv: [1910.03606 \[hep-ph\]](#).
- [10] CMS Collaboration, *Measurement of the single top quark and antiquark production cross sections in the t channel and their ratio in proton–proton collisions at $\sqrt{s} = 13$ TeV*, [Phys. Lett. B 800 \(2020\) 135042](#), arXiv: [1812.10514 \[hep-ex\]](#).
- [11] CMS Collaboration, *Measurement of differential cross sections and charge ratios for t -channel single top quark production in proton–proton collisions at $\sqrt{s} = 13$ TeV*, [Eur. Phys. J. C 80 \(2020\) 370](#), arXiv: [1907.08330 \[hep-ex\]](#).
- [12] CMS Collaboration, *Measurement of CKM matrix elements in single top quark t -channel production in proton–proton collisions at $\sqrt{s} = 13$ TeV*, [Phys. Lett. B 808 \(2020\) 135609](#), arXiv: [2004.12181 \[hep-ex\]](#).
- [13] ATLAS Collaboration, *ATLAS Insertable B-Layer Technical Design Report*, ATLAS-TDR-19; CERN-LHCC-2010-013, 2010, URL: <https://cds.cern.ch/record/1291633>, Addendum: ATLAS-TDR-19-ADD-1; CERN-LHCC-2012-009, 2012, URL: <https://cds.cern.ch/record/1451888>.
- [14] B. Abbott et al., *Production and integration of the ATLAS Insertable B-Layer*, [JINST 13 \(2018\) T05008](#), arXiv: [1803.00844 \[physics.ins-det\]](#).
- [15] ATLAS Collaboration, *Performance of the ATLAS trigger system in 2015*, [Eur. Phys. J. C 77 \(2017\) 317](#), arXiv: [1611.09661 \[hep-ex\]](#).
- [16] ATLAS Collaboration, *The ATLAS Collaboration Software and Firmware*, ATL-SOFT-PUB-2021-001, 2021, URL: <https://cds.cern.ch/record/2767187>.

- [17] ATLAS Collaboration, *ATLAS data quality operations and performance for 2015–2018 data-taking*, [JINST **15** \(2020\) P04003](#), arXiv: [1911.04632 \[physics.ins-det\]](#).
- [18] ATLAS Collaboration, *Luminosity determination in pp collisions at $\sqrt{s} = 13$ TeV using the ATLAS detector at the LHC*, [Eur. Phys. J. C **83** \(2023\) 982](#), arXiv: [2212.09379 \[hep-ex\]](#).
- [19] G. Avoni et al., *The new LUCID-2 detector for luminosity measurement and monitoring in ATLAS*, [JINST **13** \(2018\) P07017](#).
- [20] ATLAS Collaboration, *Performance of electron and photon triggers in ATLAS during LHC Run 2*, [Eur. Phys. J. C **80** \(2020\) 47](#), arXiv: [1909.00761 \[hep-ex\]](#).
- [21] ATLAS Collaboration, *Performance of the ATLAS muon triggers in Run 2*, [JINST **15** \(2020\) P09015](#), arXiv: [2004.13447 \[physics.ins-det\]](#).
- [22] S. Agostinelli et al., *GEANT4 – a simulation toolkit*, [Nucl. Instrum. Meth. A **506** \(2003\) 250](#).
- [23] ATLAS Collaboration, *The ATLAS Simulation Infrastructure*, [Eur. Phys. J. C **70** \(2010\) 823](#), arXiv: [1005.4568 \[physics.ins-det\]](#).
- [24] ATLAS Collaboration, *The simulation principle and performance of the ATLAS fast calorimeter simulation FastCaloSim*, ATL-PHYS-PUB-2010-013, 2010, URL: <https://cds.cern.ch/record/1300517>.
- [25] ATLAS Collaboration, *Fast Simulation for ATLAS: Atfast-II and ISF*, ATL-SOFT-PROC-2012-065, 2012, URL: <http://cds.cern.ch/record/1458503>.
- [26] T. Sjöstrand, S. Mrenna and P. Skands, *A brief introduction to PYTHIA 8.1*, [Comput. Phys. Commun. **178** \(2008\) 852](#), arXiv: [0710.3820 \[hep-ph\]](#).
- [27] ATLAS Collaboration, *The Pythia 8 A3 tune description of ATLAS minimum bias and inelastic measurements incorporating the Donnachie–Landshoff diffractive model*, ATL-PHYS-PUB-2016-017, 2016, URL: <https://cds.cern.ch/record/2206965>.
- [28] NNPDF Collaboration, R. D. Ball et al., *Parton distributions with LHC data*, [Nucl. Phys. B **867** \(2013\) 244](#), arXiv: [1207.1303 \[hep-ph\]](#).
- [29] P. Nason, *A new method for combining NLO QCD with shower Monte Carlo algorithms*, [JHEP **11** \(2004\) 040](#), arXiv: [hep-ph/0409146](#).
- [30] S. Frixione, G. Ridolfi and P. Nason, *A positive-weight next-to-leading-order Monte Carlo for heavy flavour hadroproduction*, [JHEP **09** \(2007\) 126](#), arXiv: [0707.3088 \[hep-ph\]](#).
- [31] S. Frixione, P. Nason and C. Oleari, *Matching NLO QCD computations with parton shower simulations: the POWHEG method*, [JHEP **11** \(2007\) 070](#), arXiv: [0709.2092 \[hep-ph\]](#).
- [32] S. Alioli, P. Nason, C. Oleari and E. Re, *NLO single-top production matched with shower in POWHEG: s- and t-channel contributions*, [JHEP **09** \(2009\) 111](#), arXiv: [0907.4076 \[hep-ph\]](#), Erratum: [JHEP **02** \(2010\) 011](#).
- [33] S. Alioli, P. Nason, C. Oleari and E. Re, *A general framework for implementing NLO calculations in shower Monte Carlo programs: the POWHEG BOX*, [JHEP **06** \(2010\) 043](#), arXiv: [1002.2581 \[hep-ph\]](#).

- [34] E. Re, *Single-top Wt -channel production matched with parton showers using the POWHEG method*, *Eur. Phys. J. C* **71** (2011) 1547, arXiv: [1009.2450 \[hep-ph\]](#).
- [35] R. Frederix, E. Re and P. Torrielli, *Single-top t -channel hadroproduction in the four-flavour scheme with POWHEG and aMC@NLO*, *JHEP* **09** (2012) 130, arXiv: [1207.5391 \[hep-ph\]](#).
- [36] NNPDF Collaboration, R. D. Ball et al., *Parton distributions for the LHC run II*, *JHEP* **04** (2015) 040, arXiv: [1410.8849 \[hep-ph\]](#).
- [37] ATLAS Collaboration, *ATLAS Pythia 8 tunes to 7 TeV data*, ATL-PHYS-PUB-2014-021, 2014, URL: <https://cds.cern.ch/record/1966419>.
- [38] ATLAS Collaboration, *Studies on top-quark Monte Carlo modelling for Top2016*, ATL-PHYS-PUB-2016-020, 2016, URL: <https://cds.cern.ch/record/2216168>.
- [39] S. Frixione, E. Laenen, P. Motylinski, C. White and B. R. Webber, *Single-top hadroproduction in association with a W boson*, *JHEP* **07** (2008) 029, arXiv: [0805.3067 \[hep-ph\]](#).
- [40] S. Frixione, E. Laenen, P. Motylinski and B. R. Webber, *Angular correlations of lepton pairs from vector boson and top quark decays in Monte Carlo simulations*, *JHEP* **04** (2007) 081, arXiv: [hep-ph/0702198](#).
- [41] P. Artoisenet, R. Frederix, O. Mattelaer and R. Rietkerk, *Automatic spin-entangled decays of heavy resonances in Monte Carlo simulations*, *JHEP* **03** (2013) 015, arXiv: [1212.3460 \[hep-ph\]](#).
- [42] D. J. Lange, *The EvtGen particle decay simulation package*, *Nucl. Instrum. Meth. A* **462** (2001) 152.
- [43] M. Czakon and A. Mitov, *Top++: A program for the calculation of the top-pair cross-section at hadron colliders*, *Comput. Phys. Commun.* **185** (2014) 2930, arXiv: [1112.5675 \[hep-ph\]](#).
- [44] J. Campbell, T. Neumann and Z. Sullivan, *Single-top-quark production in the t -channel at NNLO*, *JHEP* **02** (2021) 040, arXiv: [2012.01574 \[hep-ph\]](#).
- [45] R. D. Ball et al., *The PDF4LHC21 combination of global PDF fits for the LHC Run III*, *J. Phys. G* **49** (2022) 080501, arXiv: [2203.05506 \[hep-ph\]](#).
- [46] M. Aliev et al., *HATHOR – HAdronic Top and Heavy quarks crOss section calculator*, *Comput. Phys. Commun.* **182** (2011) 1034, arXiv: [1007.1327 \[hep-ph\]](#).
- [47] P. Kant et al., *HatHor for single top-quark production: Updated predictions and uncertainty estimates for single top-quark production in hadronic collisions*, *Comput. Phys. Commun.* **191** (2015) 74, arXiv: [1406.4403 \[hep-ph\]](#).
- [48] N. Kidonakis and N. Yamanaka, *Higher-order corrections for tW production at high-energy hadron colliders*, *JHEP* **05** (2021) 278, arXiv: [2102.11300 \[hep-ph\]](#).
- [49] E. Bothmann et al., *Event generation with Sherpa 2.2*, *SciPost Phys.* **7** (2019) 034, arXiv: [1905.09127 \[hep-ph\]](#).
- [50] T. Gleisberg and S. Höche, *Comix, a new matrix element generator*, *JHEP* **12** (2008) 039, arXiv: [0808.3674 \[hep-ph\]](#).

- [51] F. Buccioni et al., *OpenLoops 2*, *Eur. Phys. J. C* **79** (2019) 866, arXiv: [1907.13071 \[hep-ph\]](#).
- [52] F. Cascioli, P. Maierhöfer and S. Pozzorini, *Scattering Amplitudes with Open Loops*, *Phys. Rev. Lett.* **108** (2012) 111601, arXiv: [1111.5206 \[hep-ph\]](#).
- [53] A. Denner, S. Dittmaier and L. Hofer, *COLLIER: A fortran-based complex one-loop library in extended regularizations*, *Comput. Phys. Commun.* **212** (2017) 220, arXiv: [1604.06792 \[hep-ph\]](#).
- [54] S. Schumann and F. Krauss, *A parton shower algorithm based on Catani–Seymour dipole factorisation*, *JHEP* **03** (2008) 038, arXiv: [0709.1027 \[hep-ph\]](#).
- [55] J.-C. Winter, F. Krauss and G. Soff, *A modified cluster-hadronisation model*, *Eur. Phys. J. C* **36** (2004) 381, arXiv: [hep-ph/0311085](#).
- [56] S. Höche, F. Krauss, M. Schönherr and F. Siegert, *A critical appraisal of NLO+PS matching methods*, *JHEP* **09** (2012) 049, arXiv: [1111.1220 \[hep-ph\]](#).
- [57] S. Catani, F. Krauss, B. R. Webber and R. Kuhn, *QCD Matrix Elements + Parton Showers*, *JHEP* **11** (2001) 063, arXiv: [hep-ph/0109231](#).
- [58] S. Höche, F. Krauss, S. Schumann and F. Siegert, *QCD matrix elements and truncated showers*, *JHEP* **05** (2009) 053, arXiv: [0903.1219 \[hep-ph\]](#).
- [59] S. Höche, F. Krauss, M. Schönherr and F. Siegert, *QCD matrix elements + parton showers. The NLO case*, *JHEP* **04** (2013) 027, arXiv: [1207.5030 \[hep-ph\]](#).
- [60] C. Anastasiou, L. Dixon, K. Melnikov and F. Petriello, *High-precision QCD at hadron colliders: Electroweak gauge boson rapidity distributions at next-to-next-to leading order*, *Phys. Rev. D* **69** (2004) 094008, arXiv: [hep-ph/0312266](#).
- [61] R. Gavin, Y. Li, F. Petriello and S. Quackenbush, *FEWZ 2.0: A code for hadronic Z production at next-to-next-to-leading order*, *Comput. Phys. Commun.* **182** (2011) 2388, arXiv: [1011.3540 \[hep-ph\]](#).
- [62] C. Degrande et al., *Automated one-loop computations in the standard model effective field theory*, *Phys. Rev. D* **103** (2021) 096024, arXiv: [2008.11743 \[hep-ph\]](#).
- [63] ATLAS Collaboration, *Vertex Reconstruction Performance of the ATLAS Detector at $\sqrt{s} = 13$ TeV*, ATL-PHYS-PUB-2015-026, 2015, URL: <https://cds.cern.ch/record/2037717>.
- [64] ATLAS Collaboration, *Electron and photon performance measurements with the ATLAS detector using the 2015–2017 LHC proton–proton collision data*, *JINST* **14** (2019) P12006, arXiv: [1908.00005 \[hep-ex\]](#).
- [65] ATLAS Collaboration, *Muon reconstruction and identification efficiency in ATLAS using the full Run 2 pp collision data set at $\sqrt{s} = 13$ TeV*, *Eur. Phys. J. C* **81** (2021) 578, arXiv: [2012.00578 \[hep-ex\]](#).
- [66] ATLAS Collaboration, *Jet reconstruction and performance using particle flow with the ATLAS Detector*, *Eur. Phys. J. C* **77** (2017) 466, arXiv: [1703.10485 \[hep-ex\]](#).
- [67] M. Cacciari, G. P. Salam and G. Soyez, *The anti- k_t jet clustering algorithm*, *JHEP* **04** (2008) 063, arXiv: [0802.1189 \[hep-ph\]](#).

- [68] M. Cacciari, G. P. Salam and G. Soyez, *FastJet user manual*, *Eur. Phys. J. C* **72** (2012) 1896, arXiv: [1111.6097 \[hep-ph\]](#).
- [69] ATLAS Collaboration, *Topological cell clustering in the ATLAS calorimeters and its performance in LHC Run 1*, *Eur. Phys. J. C* **77** (2017) 490, arXiv: [1603.02934 \[hep-ex\]](#).
- [70] ATLAS Collaboration, *Performance of pile-up mitigation techniques for jets in pp collisions at $\sqrt{s} = 8$ TeV using the ATLAS detector*, *Eur. Phys. J. C* **76** (2016) 581, arXiv: [1510.03823 \[hep-ex\]](#).
- [71] ATLAS Collaboration, *Identification and rejection of pile-up jets at high pseudorapidity with the ATLAS detector*, *Eur. Phys. J. C* **77** (2017) 580, arXiv: [1705.02211 \[hep-ex\]](#),
Erratum: *Eur. Phys. J. C* **77** (2017) 712.
- [72] ATLAS Collaboration, *Performance of missing transverse momentum reconstruction with the ATLAS detector using proton–proton collisions at $\sqrt{s} = 13$ TeV*, *Eur. Phys. J. C* **78** (2018) 903, arXiv: [1802.08168 \[hep-ex\]](#).
- [73] ATLAS Collaboration, *Estimation of non-prompt and fake lepton backgrounds in final states with top quarks produced in proton–proton collisions at $\sqrt{s} = 8$ TeV with the ATLAS Detector*, ATLAS-CONF-2014-058, 2014, URL: <https://cds.cern.ch/record/1951336>.
- [74] Particle Data Group, R. L. Workman et al., *Review of Particle Physics*, *PTEP* **2022** (2022) 083C01.
- [75] T. Chwalek, *Measurement of W-Boson Helicity-Fractions in Top-Quark Decays with the CDF II Experiment and Prospects for an Early $t\bar{t}$ Cross-Section Measurement with the CMS Experiment*, Ph.D. Thesis, Karlsruhe U., IEKP-KA-2010-05, FERMILAB-THESIS-2010-74, CERN-THESIS-2010-255, 2010, URL: <https://cds.cern.ch/record/1416031>.
- [76] M. Feindt, *A Neural Bayesian Estimator for Conditional Probability Densities*, IEKP-KA/04-05, 2004, arXiv: [physics/0402093 \[physics.data-an\]](#).
- [77] M. Feindt and U. Kerzel, *The NeuroBayes neural network package*, *Nucl. Instrum. Meth. A* **559** (2006) 190.
- [78] ATLAS Collaboration, *Measurement of the t-channel single top-quark production cross section in pp collisions at $\sqrt{s} = 7$ TeV with the ATLAS detector*, *Phys. Lett. B* **717** (2012) 330, arXiv: [1205.3130 \[hep-ex\]](#).
- [79] ATLAS Collaboration, *Electron and photon energy calibration with the ATLAS detector using LHC Run 2 data*, (2023), arXiv: [2309.05471 \[hep-ex\]](#).
- [80] ATLAS Collaboration, *Studies of the muon momentum calibration and performance of the ATLAS detector with pp collisions at $\sqrt{s} = 13$ TeV*, *Eur. Phys. J. C* **83** (2023) 686, arXiv: [2212.07338 \[hep-ex\]](#).
- [81] ATLAS Collaboration, *ATLAS b-jet identification performance and efficiency measurement with $t\bar{t}$ events in pp collisions at $\sqrt{s} = 13$ TeV*, *Eur. Phys. J. C* **79** (2019) 970, arXiv: [1907.05120 \[hep-ex\]](#).
- [82] ATLAS Collaboration, *Measurement of the c-jet mistagging efficiency in $t\bar{t}$ events using pp collision data at $\sqrt{s} = 13$ TeV collected with the ATLAS detector*, *Eur. Phys. J. C* **82** (2022) 95, arXiv: [2109.10627 \[hep-ex\]](#).

- [83] ATLAS Collaboration, *Calibration of the light-flavour jet mistagging efficiency of the b-tagging algorithms with Z+jets events using 139 fb⁻¹ of ATLAS proton-proton collision data at $\sqrt{s} = 13$ TeV*, (2023), arXiv: [2301.06319 \[hep-ex\]](#).
- [84] ATLAS Collaboration, *Search for flavour-changing neutral-current interactions of a top quark and a gluon in pp collisions at $\sqrt{s} = 13$ TeV with the ATLAS detector*, *Eur. Phys. J. C* **82** (2022) 334, arXiv: [2112.01302 \[hep-ex\]](#).
- [85] M. Bähr et al., *Herwig++ physics and manual*, *Eur. Phys. J. C* **58** (2008) 639, arXiv: [0803.0883 \[hep-ph\]](#).
- [86] J. Bellm et al., *Herwig 7.0/Herwig++ 3.0 release note*, *Eur. Phys. J. C* **76** (2016) 196, arXiv: [1512.01178 \[hep-ph\]](#).
- [87] S. Höche, S. Mrenna, S. Payne, C. T. Preuss and P. Skands, *A Study of QCD Radiation in VBF Higgs Production with Vincia and Pythia*, *SciPost Phys.* **12** (2022) 010, arXiv: [2106.10987 \[hep-ph\]](#).
- [88] ATLAS Collaboration, *Studies on the improvement of the matching uncertainty definition in top-quark processes simulated with POWHEG+PYTHIA8*, ATL-PHYS-PUB-2023-029, 2013, URL: <https://cds.cern.ch/record/2872787>.
- [89] J. Butterworth et al., *PDF4LHC recommendations for LHC Run II*, *J. Phys. G* **43** (2016) 023001, arXiv: [1510.03865 \[hep-ph\]](#).
- [90] R. Barlow and C. Beeston, *Fitting using finite Monte Carlo samples*, *Comput. Phys. Commun.* **77** (1993) 219.
- [91] S. Alekhin, J. Blümlein and S. Moch, *NLO PDFs from the ABMP16 fit*, *Eur. Phys. J. C* **78** (2018) 477, arXiv: [1803.07537 \[hep-ph\]](#).
- [92] ATLAS Collaboration, *Determination of the parton distribution functions of the proton using diverse ATLAS data from pp collisions at $\sqrt{s} = 7, 8$ and 13 TeV*, *Eur. Phys. J. C* **82** (2022) 438, arXiv: [2112.11266 \[hep-ex\]](#).
- [93] T.-J. Hou et al., *New CTEQ global analysis of quantum chromodynamics with high-precision data from the LHC*, *Phys. Rev. D* **103** (2021) 014013, arXiv: [1912.10053 \[hep-ph\]](#).
- [94] S. Bailey, T. Cridge, L. A. Harland-Lang, A. D. Martin and R. S. Thorne, *Parton distributions from LHC, HERA, Tevatron and fixed target data: MSHT20 PDFs*, *Eur. Phys. J. C* **81** (2021) 341, arXiv: [2012.04684 \[hep-ph\]](#).
- [95] NNPDF Collaboration, R. D. Ball et al., *The path to proton structure at 1% accuracy*, *Eur. Phys. J. C* **82** (2022) 428, arXiv: [2109.02653 \[hep-ph\]](#).
- [96] ATLAS Collaboration, *Fiducial, total and differential cross-section measurements of t-channel single top-quark production in pp collisions at 8 TeV using data collected by the ATLAS detector*, *Eur. Phys. J. C* **77** (2017) 531, arXiv: [1702.02859 \[hep-ex\]](#).
- [97] TopFitter Collaboration, A. Buckley et al., *Constraining top quark effective theory in the LHC Run II era*, *JHEP* **04** (2016) 015, arXiv: [1512.03360 \[hep-ph\]](#).
- [98] ATLAS Collaboration, *Evidence for the charge asymmetry in $pp \rightarrow t\bar{t}$ production at $\sqrt{s} = 13$ TeV with the ATLAS detector*, *JHEP* **08** (2023) 077, arXiv: [2208.12095 \[hep-ex\]](#).

- [99] ATLAS Collaboration, *Inclusive and differential cross-section measurements of $t\bar{t}Z$ production in pp collisions at $\sqrt{s} = 13$ TeV with the ATLAS detector, including EFT and spin-correlation interpretations*, 2023, arXiv: [2312.04450](https://arxiv.org/abs/2312.04450) [hep-ex].
- [100] ATLAS and CMS Collaborations, *Combination of measurements of the top quark mass from data collected by the ATLAS and CMS experiments at $\sqrt{s} = 7$ and 8 TeV*, 2023, arXiv: [2402.08713](https://arxiv.org/abs/2402.08713) [hep-ex].
- [101] ATLAS and CMS Collaborations, *Combinations of single-top-quark production cross-section measurements and $|f_{LV}V_{tb}|$ determinations at $\sqrt{s} = 7$ and 8 TeV with the ATLAS and CMS experiments*, *JHEP* **05** (2019) 088, arXiv: [1902.07158](https://arxiv.org/abs/1902.07158) [hep-ex].
- [102] ATLAS Collaboration, *ATLAS Computing Acknowledgements*, ATL-SOFT-PUB-2023-001, 2023, URL: <https://cds.cern.ch/record/2869272>.

The ATLAS Collaboration

G. Aad ¹⁰², B. Abbott ¹²⁰, K. Abeling ⁵⁵, N.J. Abicht ⁴⁹, S.H. Abidi ²⁹, A. Aboulhorma ^{35e}, H. Abramowicz ¹⁵¹, H. Abreu ¹⁵⁰, Y. Abulaiti ¹¹⁷, A.C. Abusleme Hoffman ^{137a}, B.S. Acharya ^{69a,69b,n}, C. Adam Bourdarios ⁴, L. Adamczyk ^{86a}, L. Adamek ¹⁵⁵, S.V. Addepalli ²⁶, M.J. Addison ¹⁰¹, J. Adelman ¹¹⁵, A. Adiguzel ^{21c}, T. Adaye ¹³⁴, A.A. Affolder ¹³⁶, Y. Afik ³⁶, M.N. Agaras ¹³, J. Agarwala ^{73a,73b}, A. Aggarwal ¹⁰⁰, C. Agheorghiesei ^{27c}, A. Ahmad ³⁶, F. Ahmadov ^{38,z}, W.S. Ahmed ¹⁰⁴, S. Ahuja ⁹⁵, X. Ai ^{62a}, G. Aielli ^{76a,76b}, A. Aikot ¹⁶³, M. Ait Tamlihat ^{35e}, B. Aitbenchikh ^{35a}, I. Aizenberg ¹⁶⁹, M. Akbiyik ¹⁰⁰, T.P.A. Åkesson ⁹⁸, A.V. Akimov ³⁷, D. Akiyama ¹⁶⁸, N.N. Akolkar ²⁴, K. Al Khoury ⁴¹, G.L. Alberghi ^{23b}, J. Albert ¹⁶⁵, P. Albicocco ⁵³, G.L. Albouy ⁶⁰, S. Alderweireldt ⁵², M. Aleksa ³⁶, I.N. Aleksandrov ³⁸, C. Alexa ^{27b}, T. Alexopoulos ¹⁰, F. Alfonsi ^{23b}, M. Algren ⁵⁶, M. Alhroob ¹²⁰, B. Ali ¹³², H.M.J. Ali ⁹¹, S. Ali ¹⁴⁸, S.W. Alibocus ⁹², M. Aliev ¹⁴⁵, G. Alimonti ^{71a}, W. Alkakhri ⁵⁵, C. Allaire ⁶⁶, B.M.M. Allbrooke ¹⁴⁶, J.F. Allen ⁵², C.A. Allendes Flores ^{137f}, P.P. Allport ²⁰, A. Aloisio ^{72a,72b}, F. Alonso ⁹⁰, C. Alpigiani ¹³⁸, M. Alvarez Estevez ⁹⁹, A. Alvarez Fernandez ¹⁰⁰, M. Alves Cardoso ⁵⁶, M.G. Alviggi ^{72a,72b}, M. Aly ¹⁰¹, Y. Amaral Coutinho ^{83b}, A. Ambler ¹⁰⁴, C. Amelung ³⁶, M. Amerl ¹⁰¹, C.G. Ames ¹⁰⁹, D. Amidei ¹⁰⁶, S.P. Amor Dos Santos ^{130a}, K.R. Amos ¹⁶³, V. Ananiev ¹²⁵, C. Anastopoulos ¹³⁹, T. Andeen ¹¹, J.K. Anders ³⁶, S.Y. Andreev ^{47a,47b}, A. Andreatta ^{71a,71b}, S. Angelidakis ⁹, A. Angerami ^{41,ac}, A.V. Anisenkov ³⁷, A. Annovi ^{74a}, C. Antel ⁵⁶, M.T. Anthony ¹³⁹, E. Antipov ¹⁴⁵, M. Antonelli ⁵³, F. Anulli ^{75a}, M. Aoki ⁸⁴, T. Aoki ¹⁵³, J.A. Aparisi Pozo ¹⁶³, M.A. Aparo ¹⁴⁶, L. Aperio Bella ⁴⁸, C. Appelt ¹⁸, A. Apyan ²⁶, N. Aranzabal ³⁶, C. Arcangeletti ⁵³, A.T.H. Arce ⁵¹, E. Arena ⁹², J-F. Arguin ¹⁰⁸, S. Argyropoulos ⁵⁴, J.-H. Arling ⁴⁸, O. Arnaez ⁴, H. Arnold ¹¹⁴, G. Artoni ^{75a,75b}, H. Asada ¹¹¹, K. Asai ¹¹⁸, S. Asai ¹⁵³, N.A. Asbah ⁶¹, K. Assamagan ²⁹, R. Astalos ^{28a}, S. Atashi ¹⁶⁰, R.J. Atkin ^{33a}, M. Atkinson ¹⁶², H. Atmani ^{35f}, P.A. Atmasiddha ¹⁰⁶, K. Augsten ¹³², S. Auricchio ^{72a,72b}, A.D. Auriol ²⁰, V.A. Austrup ¹⁰¹, G. Avolio ³⁶, K. Axiotis ⁵⁶, G. Azuelos ^{108,ah}, D. Babal ^{28b}, H. Bachacou ¹³⁵, K. Bachas ^{152,q}, A. Bachi ³⁴, F. Backman ^{47a,47b}, A. Badea ⁶¹, P. Bagnaia ^{75a,75b}, M. Bahmani ¹⁸, A.J. Bailey ¹⁶³, V.R. Bailey ¹⁶², J.T. Baines ¹³⁴, L. Baines ⁹⁴, C. Bakalis ¹⁰, O.K. Baker ¹⁷², E. Bakos ¹⁵, D. Bakshi Gupta ⁸, V. Balakrishnan ¹²⁰, R. Balasubramanian ¹¹⁴, E.M. Baldin ³⁷, P. Balek ^{86a}, E. Ballabene ^{23b,23a}, F. Balli ¹³⁵, L.M. Baltes ^{63a}, W.K. Balunas ³², J. Balz ¹⁰⁰, E. Banas ⁸⁷, M. Bandieramonte ¹²⁹, A. Bandyopadhyay ²⁴, S. Bansal ²⁴, L. Barak ¹⁵¹, M. Barakat ⁴⁸, E.L. Barberio ¹⁰⁵, D. Barberis ^{57b,57a}, M. Barbero ¹⁰², K.N. Barends ^{33a}, T. Barillari ¹¹⁰, M-S. Barisits ³⁶, T. Barklow ¹⁴³, P. Baron ¹²², D.A. Baron Moreno ¹⁰¹, A. Baroncelli ^{62a}, G. Barone ²⁹, A.J. Barr ¹²⁶, J.D. Barr ⁹⁶, L. Barranco Navarro ^{47a,47b}, F. Barreiro ⁹⁹, J. Barreiro Guimarães da Costa ^{14a}, U. Barron ¹⁵¹, M.G. Barros Teixeira ^{130a}, S. Barsov ³⁷, F. Bartels ^{63a}, R. Bartoldus ¹⁴³, A.E. Barton ⁹¹, P. Bartos ^{28a}, A. Basan ¹⁰⁰, M. Baselga ⁴⁹, A. Bassalat ^{66,b}, M.J. Basso ^{156a}, C.R. Basson ¹⁰¹, R.L. Bates ⁵⁹, S. Batlamous ^{35e}, J.R. Batley ³², B. Batool ¹⁴¹, M. Battaglia ¹³⁶, D. Battulga ¹⁸, M. Baucé ^{75a,75b}, M. Bauer ³⁶, P. Bauer ²⁴, L.T. Bazzano Hurrell ³⁰, J.B. Beacham ⁵¹, T. Beau ¹²⁷, P.H. Beauchemin ¹⁵⁸, F. Becherer ⁵⁴, P. Bechtel ²⁴, H.P. Beck ^{19,p}, K. Becker ¹⁶⁷, A.J. Beddall ⁸², V.A. Bednyakov ³⁸, C.P. Bee ¹⁴⁵, L.J. Beamster ¹⁵, T.A. Beermann ³⁶, M. Begalli ^{83d}, M. Begel ²⁹, A. Behera ¹⁴⁵, J.K. Behr ⁴⁸, J.F. Beirer ⁵⁵, F. Beisiegel ²⁴, M. Belfkir ¹⁵⁹, G. Bella ¹⁵¹, L. Bellagamba ^{23b}, A. Bellerive ³⁴, P. Bellos ²⁰, K. Beloborodov ³⁷, N.L. Belyaev ³⁷, D. Bencheikroun ^{35a}, F. Bendebba ^{35a}, Y. Benhammou ¹⁵¹, M. Benoit ²⁹, J.R. Bensinger ²⁶, S. Bentvelsen ¹¹⁴,

L. Beresford ⁴⁸, M. Beretta ⁵³, E. Bergeaas Kuutmann ¹⁶¹, N. Berger ⁴, B. Bergmann ¹³²,
 J. Beringer ^{17a}, G. Bernardi ⁵, C. Bernius ¹⁴³, F.U. Bernlochner ²⁴, F. Bernon ^{36,102}, T. Berry ⁹⁵,
 P. Berta ¹³³, A. Berthold ⁵⁰, I.A. Bertram ⁹¹, O. Bessidskaia Bylund ¹⁷¹, S. Bethke ¹¹⁰,
 A. Betti ^{75a,75b}, A.J. Bevan ⁹⁴, M. Bhamjee ^{33c}, S. Bhatta ¹⁴⁵, D.S. Bhattacharya ¹⁶⁶,
 P. Bhattarai ¹⁴³, V.S. Bhopatkar ¹²¹, R. Bi ^{29,aj}, R.M. Bianchi ¹²⁹, G. Bianco ^{23b,23a}, O. Biebel ¹⁰⁹,
 R. Bielski ¹²³, M. Biglietti ^{77a}, T.R.V. Billoud ¹³², M. Bindi ⁵⁵, A. Bingul ^{21b}, C. Bini ^{75a,75b},
 A. Biondini ⁹², C.J. Birch-sykes ¹⁰¹, G.A. Bird ^{20,134}, M. Birman ¹⁶⁹, M. Biroš ¹³³,
 S. Biryukov ¹⁴⁶, T. Bisanz ⁴⁹, E. Bisceglie ^{43b,43a}, J.P. Biswal ¹³⁴, D. Biswas ¹⁴¹, A. Bitadze ¹⁰¹,
 K. Bjørke ¹²⁵, I. Bloch ⁴⁸, C. Blocker ²⁶, A. Blue ⁵⁹, U. Blumenschein ⁹⁴, J. Blumenthal ¹⁰⁰,
 G.J. Bobbink ¹¹⁴, V.S. Bobrovnikov ³⁷, M. Boehler ⁵⁴, B. Boehm ¹⁶⁶, D. Bogavac ³⁶,
 A.G. Bogdanchikov ³⁷, C. Bohm ^{47a}, V. Boisvert ⁹⁵, P. Bokan ⁴⁸, T. Bold ^{86a}, M. Bomben ⁵,
 M. Bona ⁹⁴, M. Boonekamp ¹³⁵, C.D. Booth ⁹⁵, A.G. Borbély ⁵⁹, I.S. Bordulev ³⁷,
 H.M. Borecka-Bielska ¹⁰⁸, L.S. Borgna ⁹⁶, G. Borissov ⁹¹, D. Bortoletto ¹²⁶, D. Boscherini ^{23b},
 M. Bosman ¹³, J.D. Bossio Sola ³⁶, K. Bouaouda ^{35a}, N. Bouchhar ¹⁶³, J. Boudreau ¹²⁹,
 E.V. Bouhova-Thacker ⁹¹, D. Boumediene ⁴⁰, R. Bouquet ⁵, A. Boveia ¹¹⁹, J. Boyd ³⁶,
 D. Boye ²⁹, I.R. Boyko ³⁸, J. Bracik ²⁰, N. Brahimi ^{62d}, G. Brandt ¹⁷¹, O. Brandt ³²,
 F. Braren ⁴⁸, B. Brau ¹⁰³, J.E. Brau ¹²³, R. Brenner ¹⁶⁹, L. Brenner ¹¹⁴, R. Brenner ¹⁶¹,
 S. Bressler ¹⁶⁹, D. Britton ⁵⁹, D. Britzger ¹¹⁰, I. Brock ²⁴, G. Brooijmans ⁴¹, W.K. Brooks ^{137f},
 E. Brost ²⁹, L.M. Brown ¹⁶⁵, L.E. Bruce ⁶¹, T.L. Bruckler ¹²⁶, P.A. Bruckman de Renstrom ⁸⁷,
 B. Brüers ⁴⁸, A. Bruni ^{23b}, G. Bruni ^{23b}, M. Bruschi ^{23b}, N. Bruscinò ^{75a,75b}, T. Buanes ¹⁶,
 Q. Buat ¹³⁸, D. Buchin ¹¹⁰, A.G. Buckley ⁵⁹, O. Bulekov ³⁷, B.A. Bullard ¹⁴³, S. Burdin ⁹²,
 C.D. Burgard ⁴⁹, A.M. Burger ⁴⁰, B. Burghgrave ⁸, O. Burlayenko ⁵⁴, J.T.P. Burr ³²,
 C.D. Burton ¹¹, J.C. Burzynski ¹⁴², E.L. Busch ⁴¹, V. Büscher ¹⁰⁰, P.J. Bussey ⁵⁹,
 J.M. Butler ²⁵, C.M. Buttar ⁵⁹, J.M. Butterworth ⁹⁶, W. Buttinger ¹³⁴, C.J. Buxo Vazquez ¹⁰⁷,
 A.R. Buzykaev ³⁷, S. Cabrera Urbán ¹⁶³, L. Cadamuro ⁶⁶, D. Caforio ⁵⁸, H. Cai ¹²⁹,
 Y. Cai ^{14a,14e}, V.M.M. Cairo ³⁶, O. Cakir ^{3a}, N. Calace ³⁶, P. Calafiura ^{17a}, G. Calderini ¹²⁷,
 P. Calfayan ⁶⁸, G. Callea ⁵⁹, L.P. Caloba ^{83b}, D. Calvet ⁴⁰, S. Calvet ⁴⁰, T.P. Calvet ¹⁰²,
 M. Calvetti ^{74a,74b}, R. Camacho Toro ¹²⁷, S. Camarda ³⁶, D. Camarero Munoz ²⁶,
 P. Camarri ^{76a,76b}, M.T. Camerlingo ^{72a,72b}, D. Cameron ³⁶, C. Camincher ¹⁶⁵, M. Campanelli ⁹⁶,
 A. Camplani ⁴², V. Canale ^{72a,72b}, A. Canesse ¹⁰⁴, J. Cantero ¹⁶³, Y. Cao ¹⁶², F. Capocasa ²⁶,
 M. Capua ^{43b,43a}, A. Carbone ^{71a,71b}, R. Cardarelli ^{76a}, J.C.J. Cardenas ⁸, F. Cardillo ¹⁶³,
 T. Carli ³⁶, G. Carlino ^{72a}, J.I. Carlotto ¹³, B.T. Carlson ^{129,r}, E.M. Carlson ^{165,156a},
 L. Carminati ^{71a,71b}, A. Carnelli ¹³⁵, M. Carnesale ^{75a,75b}, S. Caron ¹¹³, E. Carquin ^{137f},
 S. Carrá ^{71a}, G. Carratta ^{23b,23a}, F. Carrio Argos ^{33g}, J.W.S. Carter ¹⁵⁵, T.M. Carter ⁵²,
 M.P. Casado ^{13,i}, M. Caspar ⁴⁸, E.G. Castiglia ¹⁷², F.L. Castillo ⁴, L. Castillo Garcia ¹³,
 V. Castillo Gimenez ¹⁶³, N.F. Castro ^{130a,130e}, A. Catinaccio ³⁶, J.R. Catmore ¹²⁵, V. Cavaliere ²⁹,
 N. Cavalli ^{23b,23a}, V. Cavalinini ^{74a,74b}, Y.C. Cekmecelioglu ⁴⁸, E. Celebi ^{21a}, F. Celli ¹²⁶,
 M.S. Centonze ^{70a,70b}, V. Cepaitis ⁵⁶, K. Cerny ¹²², A.S. Cerqueira ^{83a}, A. Cerri ¹⁴⁶,
 L. Cerrito ^{76a,76b}, F. Cerutti ^{17a}, B. Cervato ¹⁴¹, A. Cervelli ^{23b}, G. Cesarini ⁵³, S.A. Cetin ⁸²,
 Z. Chadi ^{35a}, D. Chakraborty ¹¹⁵, J. Chan ¹⁷⁰, W.Y. Chan ¹⁵³, J.D. Chapman ³², E. Chapon ¹³⁵,
 B. Chargeishvili ^{149b}, D.G. Charlton ²⁰, T.P. Charman ⁹⁴, M. Chatterjee ¹⁹, C. Chauhan ¹³³,
 S. Chekanov ⁶, S.V. Chekulaev ^{156a}, G.A. Chelkov ^{38,a}, A. Chen ¹⁰⁶, B. Chen ¹⁵¹, B. Chen ¹⁶⁵,
 H. Chen ^{14c}, H. Chen ²⁹, J. Chen ^{62c}, J. Chen ¹⁴², M. Chen ¹²⁶, S. Chen ¹⁵³, S.J. Chen ^{14c},
 X. Chen ^{62c,135}, X. Chen ^{14b,ag}, Y. Chen ^{62a}, C.L. Cheng ¹⁷⁰, H.C. Cheng ^{64a}, S. Cheong ¹⁴³,
 A. Cheplakov ³⁸, E. Cheremushkina ⁴⁸, E. Cherepanova ¹¹⁴, R. Cherkaoui El Moursli ^{35e},
 E. Cheu ⁷, K. Cheung ⁶⁵, L. Chevalier ¹³⁵, V. Chiarella ⁵³, G. Chiarelli ^{74a}, N. Chiedde ¹⁰²,
 G. Chiodini ^{70a}, A.S. Chisholm ²⁰, A. Chitan ^{27b}, M. Chitishvili ¹⁶³, M.V. Chizhov ³⁸,

K. Choi ¹¹, A.R. Chomont ^{75a,75b}, Y. Chou ¹⁰³, E.Y.S. Chow ¹¹⁴, T. Chowdhury ^{33g},
 K.L. Chu ¹⁶⁹, M.C. Chu ^{64a}, X. Chu ^{14a,14e}, J. Chudoba ¹³¹, J.J. Chwastowski ⁸⁷, D. Cieri ¹¹⁰,
 K.M. Ciesla ^{86a}, V. Cindro ⁹³, A. Ciocio ^{17a}, F. Cirotto ^{72a,72b}, Z.H. Citron ^{169,1}, M. Citterio ^{71a},
 D.A. Ciubotaru ^{27b}, B.M. Ciungu ¹⁵⁵, A. Clark ⁵⁶, P.J. Clark ⁵², J.M. Clavijo Columbie ⁴⁸,
 S.E. Clawson ⁴⁸, C. Clement ^{47a,47b}, J. Clercx ⁴⁸, Y. Coadou ¹⁰², M. Cobal ^{69a,69c},
 A. Coccaro ^{57b}, R.F. Coelho Barrue ^{130a}, R. Coelho Lopes De Sa ¹⁰³, S. Coelli ^{71a}, H. Cohen ¹⁵¹,
 A.E.C. Coimbra ^{71a,71b}, B. Cole ⁴¹, J. Collot ⁶⁰, P. Conde Muiño ^{130a,130g}, M.P. Connell ^{33c},
 S.H. Connell ^{33c}, I.A. Connelly ⁵⁹, E.I. Conroy ¹²⁶, F. Conventi ^{72a,ai}, H.G. Cooke ²⁰,
 A.M. Cooper-Sarkar ¹²⁶, A. Cordeiro Oudot Choi ¹²⁷, F. Cormier ¹⁶⁴, L.D. Corpe ⁴⁰,
 M. Corradi ^{75a,75b}, F. Corriveau ^{104,x}, A. Cortes-Gonzalez ¹⁸, M.J. Costa ¹⁶³, F. Costanza ⁴,
 D. Costanzo ¹³⁹, B.M. Cote ¹¹⁹, G. Cowan ⁹⁵, K. Cranmer ¹⁷⁰, D. Cremonini ^{23b,23a},
 S. Crépe-Renaudin ⁶⁰, F. Crescioli ¹²⁷, M. Cristinziani ¹⁴¹, M. Cristoforetti ^{78a,78b}, V. Croft ¹¹⁴,
 J.E. Crosby ¹²¹, G. Crosetti ^{43b,43a}, A. Cueto ⁹⁹, T. Cuhadar Donszelmann ¹⁶⁰, H. Cui ^{14a,14e},
 Z. Cui ⁷, W.R. Cunningham ⁵⁹, F. Curcio ^{43b,43a}, P. Czodrowski ³⁶, M.M. Czurylo ^{63b},
 M.J. Da Cunha Sargedas De Sousa ^{57b,57a}, J.V. Da Fonseca Pinto ^{83b}, C. Da Via ¹⁰¹,
 W. Dabrowski ^{86a}, T. Dado ⁴⁹, S. Dahbi ^{33g}, T. Dai ¹⁰⁶, D. Dal Santo ¹⁹, C. Dallapiccola ¹⁰³,
 M. Dam ⁴², G. D'amen ²⁹, V. D'Amico ¹⁰⁹, J. Damp ¹⁰⁰, J.R. Dandoy ¹²⁸, M.F. Daneri ³⁰,
 M. Danninger ¹⁴², V. Dao ³⁶, G. Darbo ^{57b}, S. Darmora ⁶, S.J. Das ^{29,aj}, S. D'Auria ^{71a,71b},
 C. David ^{156b}, T. Davidek ¹³³, B. Davis-Purcell ³⁴, I. Dawson ⁹⁴, H.A. Day-hall ¹³², K. De ⁸,
 R. De Asmundis ^{72a}, N. De Biase ⁴⁸, S. De Castro ^{23b,23a}, N. De Groot ¹¹³, P. de Jong ¹¹⁴,
 H. De la Torre ¹¹⁵, A. De Maria ^{14c}, A. De Salvo ^{75a}, U. De Sanctis ^{76a,76b}, A. De Santo ¹⁴⁶,
 J.B. De Vivie De Regie ⁶⁰, D.V. Dedovich ³⁸, J. Degens ¹¹⁴, A.M. Deiana ⁴⁴, F. Del Corso ^{23b,23a},
 J. Del Peso ⁹⁹, F. Del Rio ^{63a}, F. Deliot ¹³⁵, C.M. Delitzsch ⁴⁹, M. Della Pietra ^{72a,72b},
 D. Della Volpe ⁵⁶, A. Dell'Acqua ³⁶, L. Dell'Asta ^{71a,71b}, M. Delmastro ⁴, P.A. Delsart ⁶⁰,
 S. Demers ¹⁷², M. Demichev ³⁸, S.P. Denisov ³⁷, L. D'Eramo ⁴⁰, D. Derendarz ⁸⁷, F. Derue ¹²⁷,
 P. Dervan ⁹², K. Desch ²⁴, C. Deutsch ²⁴, F.A. Di Bello ^{57b,57a}, A. Di Ciaccio ^{76a,76b},
 L. Di Ciaccio ⁴, A. Di Domenico ^{75a,75b}, C. Di Donato ^{72a,72b}, A. Di Girolamo ³⁶,
 G. Di Gregorio ⁵, A. Di Luca ^{78a,78b}, B. Di Micco ^{77a,77b}, R. Di Nardo ^{77a,77b}, C. Diaconu ¹⁰²,
 M. Diamantopoulou ³⁴, F.A. Dias ¹¹⁴, T. Dias Do Vale ¹⁴², M.A. Diaz ^{137a,137b},
 F.G. Diaz Capriles ²⁴, M. Didenko ¹⁶³, E.B. Diehl ¹⁰⁶, L. Diehl ⁵⁴, S. Díez Cornell ⁴⁸,
 C. Díez Pardos ¹⁴¹, C. Dimitriadi ^{161,24,161}, A. Dimitrievska ^{17a}, J. Dingfelder ²⁴, I-M. Dinu ^{27b},
 S.J. Dittmeier ^{63b}, F. Dittus ³⁶, F. Djama ¹⁰², T. Djobava ^{149b}, J.I. Djuvsland ¹⁶,
 C. Doglioni ^{101,98}, A. Dohnalova ^{28a}, J. Dolejsi ¹³³, Z. Dolezal ¹³³, K.M. Dona ³⁹,
 M. Donadelli ^{83c}, B. Dong ¹⁰⁷, J. Donini ⁴⁰, A. D'Onofrio ^{77a,77b}, M. D'Onofrio ⁹²,
 J. Dopke ¹³⁴, A. Doria ^{72a}, N. Dos Santos Fernandes ^{130a}, P. Dougan ¹⁰¹, M.T. Dova ⁹⁰,
 A.T. Doyle ⁵⁹, M.A. Draguet ¹²⁶, E. Dreyer ¹⁶⁹, I. Drivas-koulouris ¹⁰, A.S. Drobac ¹⁵⁸,
 M. Drozdova ⁵⁶, D. Du ^{62a}, T.A. du Pree ¹¹⁴, F. Dubinin ³⁷, M. Dubovsky ^{28a}, E. Duchovni ¹⁶⁹,
 G. Duckeck ¹⁰⁹, O.A. Ducu ^{27b}, D. Duda ⁵², A. Dudarev ³⁶, E.R. Duden ²⁶, M. D'uffizi ¹⁰¹,
 L. Duflot ⁶⁶, M. Dührssen ³⁶, C. Dülsen ¹⁷¹, A.E. Dumitriu ^{27b}, M. Dunford ^{63a}, S. Dungs ⁴⁹,
 K. Dunne ^{47a,47b}, A. Duperrin ¹⁰², H. Duran Yildiz ^{3a}, M. Düren ⁵⁸, A. Durglishvili ^{149b},
 B.L. Dwyer ¹¹⁵, G.I. Dyckes ^{17a}, M. Dyndal ^{86a}, S. Dysch ¹⁰¹, B.S. Dziejczak ⁸⁷,
 Z.O. Earnshaw ¹⁴⁶, G.H. Eberwein ¹²⁶, B. Eckerova ^{28a}, S. Eggebrecht ⁵⁵,
 E. Egidio Purcino De Souza ¹²⁷, L.F. Ehrke ⁵⁶, G. Eigen ¹⁶, K. Einsweiler ^{17a}, T. Ekelof ¹⁶¹,
 P.A. Ekman ⁹⁸, S. El Farkh ^{35b}, Y. El Ghazali ^{35b}, H. El Jarrari ^{35e,148}, A. El Moussaouy ^{35a},
 V. Ellajosyula ¹⁶¹, M. Ellert ¹⁶¹, F. Ellinghaus ¹⁷¹, A.A. Elliot ⁹⁴, N. Ellis ³⁶, J. Elmsheuser ²⁹,
 M. Elsing ³⁶, D. Emelianov ¹³⁴, Y. Enari ¹⁵³, I. Ene ^{17a}, S. Epari ¹³, J. Erdmann ⁴⁹,
 P.A. Erland ⁸⁷, M. Errenst ¹⁷¹, M. Escalier ⁶⁶, C. Escobar ¹⁶³, E. Etzion ¹⁵¹, G. Evans ^{130a},

H. Evans [id](#)⁶⁸, L.S. Evans [id](#)⁹⁵, M.O. Evans [id](#)¹⁴⁶, A. Ezhilov [id](#)³⁷, S. Ezzarqtouni [id](#)^{35a}, F. Fabbri [id](#)⁵⁹,
 L. Fabbri [id](#)^{23b,23a}, G. Facini [id](#)⁹⁶, V. Fadeyev [id](#)¹³⁶, R.M. Fakhruddinov [id](#)³⁷, S. Falciano [id](#)^{75a},
 L.F. Falda Ulhoa Coelho [id](#)³⁶, P.J. Falke [id](#)²⁴, J. Faltova [id](#)¹³³, C. Fan [id](#)¹⁶², Y. Fan [id](#)^{14a}, Y. Fang [id](#)^{14a,14e},
 M. Fanti [id](#)^{71a,71b}, M. Faraj [id](#)^{69a,69b}, Z. Farazpay [id](#)⁹⁷, A. Farbin [id](#)⁸, A. Farilla [id](#)^{77a}, T. Farooque [id](#)¹⁰⁷,
 S.M. Farrington [id](#)⁵², F. Fassi [id](#)^{35e}, D. Fassouliotis [id](#)⁹, M. Faucci Giannelli [id](#)^{76a,76b}, W.J. Fawcett [id](#)³²,
 L. Fayard [id](#)⁶⁶, P. Federic [id](#)¹³³, P. Federicova [id](#)¹³¹, O.L. Fedin [id](#)^{37,a}, G. Fedotov [id](#)³⁷, M. Feickert [id](#)¹⁷⁰,
 L. Feligioni [id](#)¹⁰², D.E. Fellers [id](#)¹²³, C. Feng [id](#)^{62b}, M. Feng [id](#)^{14b}, Z. Feng [id](#)¹¹⁴, M.J. Fenton [id](#)¹⁶⁰,
 A.B. Fenyuk [id](#)³⁷, L. Ferencz [id](#)⁴⁸, R.A.M. Ferguson [id](#)⁹¹, S.I. Fernandez Luengo [id](#)^{137f}, M.J.V. Fernoux [id](#)¹⁰²,
 J. Ferrando [id](#)⁴⁸, A. Ferrari [id](#)¹⁶¹, P. Ferrari [id](#)^{114,113}, R. Ferrari [id](#)^{73a}, D. Ferrere [id](#)⁵⁶, C. Ferretti [id](#)¹⁰⁶,
 F. Fiedler [id](#)¹⁰⁰, A. Filipčić [id](#)⁹³, E.K. Filmer [id](#)¹, F. Filthaut [id](#)¹¹³, M.C.N. Fiolhais [id](#)^{130a,130c,c},
 L. Fiorini [id](#)¹⁶³, W.C. Fisher [id](#)¹⁰⁷, T. Fitschen [id](#)¹⁰¹, P.M. Fitzhugh [id](#)¹³⁵, I. Fleck [id](#)¹⁴¹, P. Fleischmann [id](#)¹⁰⁶,
 T. Flick [id](#)¹⁷¹, M. Flores [id](#)^{33d,ad}, L.R. Flores Castillo [id](#)^{64a}, L. Flores Sanz De Acedo [id](#)³⁶,
 F.M. Follega [id](#)^{78a,78b}, N. Fomin [id](#)¹⁶, J.H. Foo [id](#)¹⁵⁵, B.C. Forland [id](#)⁶⁸, A. Formica [id](#)¹³⁵, A.C. Forti [id](#)¹⁰¹,
 E. Fortin [id](#)³⁶, A.W. Fortman [id](#)⁶¹, M.G. Foti [id](#)^{17a}, L. Fountas [id](#)^{9j}, D. Fournier [id](#)⁶⁶, H. Fox [id](#)⁹¹,
 P. Francavilla [id](#)^{74a,74b}, S. Francescato [id](#)⁶¹, S. Franchellucci [id](#)⁵⁶, M. Franchini [id](#)^{23b,23a},
 S. Franchino [id](#)^{63a}, D. Francis [id](#)³⁶, L. Franco [id](#)¹¹³, L. Franconi [id](#)⁴⁸, M. Franklin [id](#)⁶¹, G. Frattari [id](#)²⁶,
 A.C. Freegard [id](#)⁹⁴, W.S. Freund [id](#)^{83b}, Y.Y. Frid [id](#)¹⁵¹, J. Friend [id](#)⁵⁹, N. Fritzsche [id](#)⁵⁰, A. Froch [id](#)⁵⁴,
 D. Froidevaux [id](#)³⁶, J.A. Frost [id](#)¹²⁶, Y. Fu [id](#)^{62a}, M. Fujimoto [id](#)^{118,ae}, E. Fullana Torregrosa [id](#)^{163,*},
 K.Y. Fung [id](#)^{64a}, E. Furtado De Simas Filho [id](#)^{83b}, M. Furukawa [id](#)¹⁵³, J. Fuster [id](#)¹⁶³, A. Gabrielli [id](#)^{23b,23a},
 A. Gabrielli [id](#)¹⁵⁵, P. Gadow [id](#)³⁶, G. Gagliardi [id](#)^{57b,57a}, L.G. Gagnon [id](#)^{17a}, E.J. Gallas [id](#)¹²⁶,
 B.J. Gallop [id](#)¹³⁴, K.K. Gan [id](#)¹¹⁹, S. Ganguly [id](#)¹⁵³, J. Gao [id](#)^{62a}, Y. Gao [id](#)⁵², F.M. Garay Walls [id](#)^{137a,137b},
 B. Garcia [id](#)²⁹, C. García [id](#)¹⁶³, A. Garcia Alonso [id](#)¹⁴, A.G. Garcia Caffaro [id](#)¹⁷², J.E. García Navarro [id](#)¹⁶³,
 M. Garcia-Sciveres [id](#)^{17a}, G.L. Gardner [id](#)¹²⁸, R.W. Gardner [id](#)³⁹, N. Garelli [id](#)¹⁵⁸, D. Garg [id](#)⁸⁰,
 R.B. Garg [id](#)^{143,o}, J.M. Gargan [id](#)⁵², C.A. Garner [id](#)¹⁵⁵, S.J. Gasiorowski [id](#)¹³⁸, P. Gaspar [id](#)^{83b}, G. Gaudio [id](#)^{73a},
 V. Gautam [id](#)¹³, P. Gauzzi [id](#)^{75a,75b}, I.L. Gavrilenko [id](#)³⁷, A. Gavrilyuk [id](#)³⁷, C. Gay [id](#)¹⁶⁴, G. Gaycken [id](#)⁴⁸,
 E.N. Gazis [id](#)¹⁰, A.A. Geanta [id](#)^{27b}, C.M. Gee [id](#)¹³⁶, C. Gemme [id](#)^{57b}, M.H. Genest [id](#)⁶⁰,
 S. Gentile [id](#)^{75a,75b}, A.D. Gentry [id](#)¹¹², S. George [id](#)⁹⁵, W.F. George [id](#)²⁰, T. Gerialis [id](#)⁴⁶,
 P. Gessinger-Befurt [id](#)³⁶, M.E. Geyik [id](#)¹⁷¹, M. Ghani [id](#)¹⁶⁷, M. Ghneimat [id](#)¹⁴¹, K. Ghorbanian [id](#)⁹⁴,
 A. Ghosal [id](#)¹⁴¹, A. Ghosh [id](#)¹⁶⁰, A. Ghosh [id](#)⁷, B. Giacobbe [id](#)^{23b}, S. Giagu [id](#)^{75a,75b}, T. Giani [id](#)¹¹⁴,
 P. Giannetti [id](#)^{74a}, A. Giannini [id](#)^{62a}, S.M. Gibson [id](#)⁹⁵, M. Gignac [id](#)¹³⁶, D.T. Gil [id](#)^{86b}, A.K. Gilbert [id](#)^{86a},
 B.J. Gilbert [id](#)⁴¹, D. Gillberg [id](#)³⁴, G. Gilles [id](#)¹¹⁴, N.E.K. Gillwald [id](#)⁴⁸, L. Ginabat [id](#)¹²⁷,
 D.M. Gingrich [id](#)^{2,ah}, M.P. Giordani [id](#)^{69a,69c}, P.F. Giraud [id](#)¹³⁵, G. Giugliarelli [id](#)^{69a,69c}, D. Giugni [id](#)^{71a},
 F. Giuli [id](#)³⁶, I. Gkialas [id](#)^{9j}, L.K. Gladilin [id](#)³⁷, C. Glasman [id](#)⁹⁹, G.R. Gledhill [id](#)¹²³, G. Glemža [id](#)⁴⁸,
 M. Glisic [id](#)¹²³, I. Gnesi [id](#)^{43b,f}, Y. Go [id](#)^{29,aj}, M. Goblirsch-Kolb [id](#)³⁶, B. Gocke [id](#)⁴⁹, D. Godin [id](#)¹⁰⁸,
 B. Gokturk [id](#)^{21a}, S. Goldfarb [id](#)¹⁰⁵, T. Golling [id](#)⁵⁶, M.G.D. Gololo [id](#)^{33g}, D. Golubkov [id](#)³⁷,
 J.P. Gombas [id](#)¹⁰⁷, A. Gomes [id](#)^{130a,130b}, G. Gomes Da Silva [id](#)¹⁴¹, A.J. Gomez Delegido [id](#)¹⁶³,
 R. Gonçalves [id](#)^{130a,130c}, G. Gonella [id](#)¹²³, L. Gonella [id](#)²⁰, A. Gongadze [id](#)^{149c}, F. Gonnella [id](#)²⁰,
 J.L. Gonski [id](#)⁴¹, R.Y. González Andana [id](#)⁵², S. González de la Hoz [id](#)¹⁶³, S. Gonzalez Fernandez [id](#)¹³,
 R. Gonzalez Lopez [id](#)⁹², C. Gonzalez Renteria [id](#)^{17a}, M.V. Gonzalez Rodrigues [id](#)⁴⁸,
 R. Gonzalez Suarez [id](#)¹⁶¹, S. Gonzalez-Sevilla [id](#)⁵⁶, G.R. Gonzalvo Rodriguez [id](#)¹⁶³, L. Goossens [id](#)³⁶,
 B. Gorini [id](#)³⁶, E. Gorini [id](#)^{70a,70b}, A. Gorišek [id](#)⁹³, T.C. Gosart [id](#)¹²⁸, A.T. Goshaw [id](#)⁵¹, M.I. Gostkin [id](#)³⁸,
 S. Goswami [id](#)¹²¹, C.A. Gottardo [id](#)³⁶, S.A. Gotz [id](#)¹⁰⁹, M. Goughri [id](#)^{35b}, V. Goumarre [id](#)⁴⁸,
 A.G. Goussiou [id](#)¹³⁸, N. Govender [id](#)^{33c}, I. Grabowska-Bold [id](#)^{86a}, K. Graham [id](#)³⁴, E. Gramstad [id](#)¹²⁵,
 S. Grancagnolo [id](#)^{70a,70b}, M. Grandi [id](#)¹⁴⁶, C.M. Grant [id](#)^{1,135}, P.M. Gravila [id](#)^{27f}, F.G. Gravili [id](#)^{70a,70b},
 H.M. Gray [id](#)^{17a}, M. Greco [id](#)^{70a,70b}, C. Grefe [id](#)²⁴, I.M. Gregor [id](#)⁴⁸, P. Grenier [id](#)¹⁴³, C. Grieco [id](#)¹³,
 A.A. Grillo [id](#)¹³⁶, K. Grimm [id](#)³¹, S. Grinstein [id](#)^{13,t}, J.-F. Grivaz [id](#)⁶⁶, E. Gross [id](#)¹⁶⁹,
 J. Grosse-Knetter [id](#)⁵⁵, C. Grud [id](#)¹⁰⁶, J.C. Grundy [id](#)¹²⁶, L. Guan [id](#)¹⁰⁶, W. Guan [id](#)²⁹, C. Gubbels [id](#)¹⁶⁴,

J.G.R. Guerrero Rojas ¹⁶³, G. Guerrieri ^{69a,69c}, F. Guescini ¹¹⁰, R. Gugel ¹⁰⁰, J.A.M. Guhit ¹⁰⁶, A. Guida ¹⁸, T. Guillemain ⁴, E. Guilloton ^{167,134}, S. Guindon ³⁶, F. Guo ^{14a,14e}, J. Guo ^{62c}, L. Guo ⁴⁸, Y. Guo ¹⁰⁶, R. Gupta ⁴⁸, S. Gurbuz ²⁴, S.S. Gurdasani ⁵⁴, G. Gustavino ³⁶, M. Guth ⁵⁶, P. Gutierrez ¹²⁰, L.F. Gutierrez Zagazeta ¹²⁸, C. Gutschow ⁹⁶, C. Gwenlan ¹²⁶, C.B. Gwilliam ⁹², E.S. Haaland ¹²⁵, A. Haas ¹¹⁷, M. Habedank ⁴⁸, C. Haber ^{17a}, H.K. Hadavand ⁸, A. Hadeef ¹⁰⁰, S. Hadzic ¹¹⁰, J.J. Hahn ¹⁴¹, E.H. Haines ⁹⁶, M. Haleem ¹⁶⁶, J. Haley ¹²¹, J.J. Hall ¹³⁹, G.D. Hallewell ¹⁰², L. Halser ¹⁹, K. Hamano ¹⁶⁵, M. Hamer ²⁴, G.N. Hamity ⁵², E.J. Hampshire ⁹⁵, J. Han ^{62b}, K. Han ^{62a}, L. Han ^{14c}, L. Han ^{62a}, S. Han ^{17a}, Y.F. Han ¹⁵⁵, K. Hanagaki ⁸⁴, M. Hance ¹³⁶, D.A. Hangal ^{41,ac}, H. Hanif ¹⁴², M.D. Hank ¹²⁸, R. Hankache ¹⁰¹, J.B. Hansen ⁴², J.D. Hansen ⁴², P.H. Hansen ⁴², K. Hara ¹⁵⁷, D. Harada ⁵⁶, T. Harenberg ¹⁷¹, S. Harkusha ³⁷, M.L. Harris ¹⁰³, Y.T. Harris ¹²⁶, J. Harrison ¹³, N.M. Harrison ¹¹⁹, P.F. Harrison ¹⁶⁷, N.M. Hartman ¹¹⁰, N.M. Hartmann ¹⁰⁹, Y. Hasegawa ¹⁴⁰, A. Hasib ⁵², S. Haug ¹⁹, R. Hauser ¹⁰⁷, C.M. Hawkes ²⁰, R.J. Hawkings ³⁶, Y. Hayashi ¹⁵³, S. Hayashida ¹¹¹, D. Hayden ¹⁰⁷, C. Hayes ¹⁰⁶, R.L. Hayes ¹¹⁴, C.P. Hays ¹²⁶, J.M. Hays ⁹⁴, H.S. Hayward ⁹², F. He ^{62a}, M. He ^{14a,14e}, Y. He ¹⁵⁴, Y. He ⁴⁸, N.B. Heatley ⁹⁴, V. Hedberg ⁹⁸, A.L. Heggelund ¹²⁵, N.D. Hehir ^{94,*}, C. Heidegger ⁵⁴, K.K. Heidegger ⁵⁴, W.D. Heidorn ⁸¹, J. Heilman ³⁴, S. Heim ⁴⁸, T. Heim ^{17a}, J.G. Heinlein ¹²⁸, J.J. Heinrich ¹²³, L. Heinrich ^{110,af}, J. Hejbal ¹³¹, L. Helary ⁴⁸, A. Held ¹⁷⁰, S. Hellesund ¹⁶, C.M. Helling ¹⁶⁴, S. Hellman ^{47a,47b}, R.C.W. Henderson ⁹¹, L. Henkelmann ³², A.M. Henriques Correia ³⁶, H. Herde ⁹⁸, Y. Hernández Jiménez ¹⁴⁵, L.M. Herrmann ²⁴, T. Herrmann ⁵⁰, G. Herten ⁵⁴, R. Hertenberger ¹⁰⁹, L. Hervas ³⁶, M.E. Hespings ¹⁰⁰, N.P. Hessey ^{156a}, H. Hibi ⁸⁵, S.J. Hillier ²⁰, J.R. Hinds ¹⁰⁷, F. Hinterkeuser ²⁴, M. Hirose ¹²⁴, S. Hirose ¹⁵⁷, D. Hirschbuehl ¹⁷¹, T.G. Hitchings ¹⁰¹, B. Hiti ⁹³, J. Hobbs ¹⁴⁵, R. Hobincu ^{27e}, N. Hod ¹⁶⁹, M.C. Hodgkinson ¹³⁹, B.H. Hodgkinson ³², A. Hoecker ³⁶, J. Hofer ⁴⁸, T. Holm ²⁴, M. Holzbock ¹¹⁰, L.B.A.H. Hommels ³², B.P. Honan ¹⁰¹, J. Hong ^{62c}, T.M. Hong ¹²⁹, B.H. Hooberman ¹⁶², W.H. Hopkins ⁶, Y. Horii ¹¹¹, S. Hou ¹⁴⁸, A.S. Howard ⁹³, J. Howarth ⁵⁹, J. Hoya ⁶, M. Hrabovsky ¹²², A. Hrynevich ⁴⁸, T. Hryn'ova ⁴, P.J. Hsu ⁶⁵, S.-C. Hsu ¹³⁸, Q. Hu ^{62a}, Y.F. Hu ^{14a,14e}, S. Huang ^{64b}, X. Huang ^{14c}, Y. Huang ¹³⁹, Y. Huang ^{14a}, Z. Huang ¹⁰¹, Z. Hubacek ¹³², M. Huebner ²⁴, F. Huegging ²⁴, T.B. Huffman ¹²⁶, C.A. Hugli ⁴⁸, M. Huhtinen ³⁶, S.K. Huiberts ¹⁶, R. Hulsken ¹⁰⁴, N. Huseynov ¹², J. Huston ¹⁰⁷, J. Huth ⁶¹, R. Hyneman ¹⁴³, G. Iacobucci ⁵⁶, G. Iakovidis ²⁹, I. Ibragimov ¹⁴¹, L. Iconomidou-Fayard ⁶⁶, P. Iengo ^{72a,72b}, R. Iguchi ¹⁵³, T. Iizawa ¹²⁶, Y. Ikegami ⁸⁴, N. Ilic ¹⁵⁵, H. Imam ^{35a}, M. Ince Lezki ⁵⁶, T. Ingebretsen Carlson ^{47a,47b}, G. Introzzi ^{73a,73b}, M. Iodice ^{77a}, V. Ippolito ^{75a,75b}, R.K. Irwin ⁹², M. Ishino ¹⁵³, W. Islam ¹⁷⁰, C. Issever ^{18,48}, S. Istin ^{21a,al}, H. Ito ¹⁶⁸, J.M. Iturbe Ponce ^{64a}, R. Iuppa ^{78a,78b}, A. Ivina ¹⁶⁹, J.M. Izen ⁴⁵, V. Izzo ^{72a}, P. Jacka ^{131,132}, P. Jackson ¹, R.M. Jacobs ⁴⁸, B.P. Jaeger ¹⁴², C.S. Jagfeld ¹⁰⁹, G. Jain ^{156a}, P. Jain ⁵⁴, G. Jäkel ¹⁷¹, K. Jakobs ⁵⁴, T. Jakoubek ¹⁶⁹, J. Jamieson ⁵⁹, K.W. Janas ^{86a}, M. Javurkova ¹⁰³, F. Jeanneau ¹³⁵, L. Jeanty ¹²³, J. Jejelava ^{149a,aa}, P. Jenni ^{54,g}, C.E. Jessiman ³⁴, S. Jézéquel ⁴, C. Jia ^{62b}, J. Jia ¹⁴⁵, X. Jia ⁶¹, X. Jia ^{14a,14e}, Z. Jia ^{14c}, Y. Jiang ^{62a}, S. Jiggins ⁴⁸, J. Jimenez Pena ¹³, S. Jin ^{14c}, A. Jinaru ^{27b}, O. Jinnouchi ¹⁵⁴, P. Johansson ¹³⁹, K.A. Johns ⁷, J.W. Johnson ¹³⁶, D.M. Jones ³², E. Jones ⁴⁸, P. Jones ³², R.W.L. Jones ⁹¹, T.J. Jones ⁹², H.L. Joos ^{55,36}, R. Joshi ¹¹⁹, J. Jovicevic ¹⁵, X. Ju ^{17a}, J.J. Junggeburth ¹⁰³, T. Junkermann ^{63a}, A. Juste Rozas ^{13,t}, M.K. Juzek ⁸⁷, S. Kabana ^{137e}, A. Kaczmarska ⁸⁷, M. Kado ¹¹⁰, H. Kagan ¹¹⁹, M. Kagan ¹⁴³, A. Kahn ⁴¹, A. Kahn ¹²⁸, C. Kahra ¹⁰⁰, T. Kaji ¹⁵³, E. Kajomovitz ¹⁵⁰, N. Kakati ¹⁶⁹, I. Kalaitzidou ⁵⁴, C.W. Kalderon ²⁹, A. Kamenshchikov ¹⁵⁵, N.J. Kang ¹³⁶, D. Kar ^{33g}, K. Karava ¹²⁶, M.J. Kareem ^{156b}, E. Karentzos ⁵⁴, I. Karkaniyas ¹⁵², O. Karkout ¹¹⁴, S.N. Karpov ³⁸, Z.M. Karpova ³⁸, V. Kartvelishvili ⁹¹, A.N. Karyukhin ³⁷,

E. Kasimi ¹⁵², J. Katzy ⁴⁸, S. Kaur ³⁴, K. Kawade ¹⁴⁰, M.P. Kawale ¹²⁰, T. Kawamoto ¹³⁵,
 E.F. Kay ³⁶, F.I. Kaya ¹⁵⁸, S. Kazakos ¹⁰⁷, V.F. Kazanin ³⁷, Y. Ke ¹⁴⁵, J.M. Keaveney ^{33a},
 R. Keeler ¹⁶⁵, G.V. Kehris ⁶¹, J.S. Keller ³⁴, A.S. Kelly ⁹⁶, J.J. Kempster ¹⁴⁶, K.E. Kennedy ⁴¹,
 P.D. Kennedy ¹⁰⁰, O. Kepka ¹³¹, B.P. Kerridge ¹⁶⁷, S. Kersten ¹⁷¹, B.P. Kerševan ⁹³,
 S. Keshri ⁶⁶, L. Keszezhova ^{28a}, S. Ketabchi Haghghat ¹⁵⁵, M. Khandoga ¹²⁷, A. Khanov ¹²¹,
 A.G. Kharlamov ³⁷, T. Kharlamova ³⁷, E.E. Khoda ¹³⁸, T.J. Khoo ¹⁸, G. Khorauli ¹⁶⁶,
 J. Khubua ^{149b}, Y.A.R. Khwaira ⁶⁶, A. Kilgallon ¹²³, D.W. Kim ^{47a,47b}, Y.K. Kim ³⁹,
 N. Kimura ⁹⁶, M.K. Kingston ⁵⁵, A. Kirchhoff ⁵⁵, C. Kirfel ²⁴, F. Kirfel ²⁴, J. Kirk ¹³⁴,
 A.E. Kiryunin ¹¹⁰, C. Kitsaki ¹⁰, O. Kivernyk ²⁴, M. Klassen ^{63a}, C. Klein ³⁴, L. Klein ¹⁶⁶,
 M.H. Klein ¹⁰⁶, M. Klein ⁹², S.B. Klein ⁵⁶, U. Klein ⁹², P. Klimek ³⁶, A. Klimentov ²⁹,
 T. Klioutchnikova ³⁶, P. Kluit ¹¹⁴, S. Kluth ¹¹⁰, E. Kneringer ⁷⁹, T.M. Knight ¹⁵⁵, A. Knue ⁴⁹,
 R. Kobayashi ⁸⁸, D. Kobylanski ¹⁶⁹, S.F. Koch ¹²⁶, M. Kocian ¹⁴³, P. Kodyš ¹³³,
 D.M. Koeck ¹²³, P.T. Koenig ²⁴, T. Koffas ³⁴, M. Kolb ¹³⁵, I. Koletsou ⁴, T. Komarek ¹²²,
 K. Köneke ⁵⁴, A.X.Y. Kong ¹, T. Kono ¹¹⁸, N. Konstantinidis ⁹⁶, B. Konya ⁹⁸,
 R. Kopeliansky ⁶⁸, S. Koperny ^{86a}, K. Korcyl ⁸⁷, K. Kordas ^{152,e}, G. Koren ¹⁵¹, A. Korn ⁹⁶,
 S. Korn ⁵⁵, I. Korolkov ¹³, N. Korotkova ³⁷, B. Kortman ¹¹⁴, O. Kortner ¹¹⁰, S. Kortner ¹¹⁰,
 W.H. Kostecka ¹¹⁵, V.V. Kostyukhin ¹⁴¹, A. Kotsokechagia ¹³⁵, A. Kotwal ⁵¹, A. Koulouris ³⁶,
 A. Kourkoumeli-Charalampidi ^{73a,73b}, C. Kourkoumelis ⁹, E. Kourlitis ^{110,af}, O. Kovanda ¹⁴⁶,
 R. Kowalewski ¹⁶⁵, W. Kozanecki ¹³⁵, A.S. Kozhin ³⁷, V.A. Kramarenko ³⁷, G. Kramberger ⁹³,
 P. Kramer ¹⁰⁰, M.W. Krasny ¹²⁷, A. Krasznahorkay ³⁶, J.W. Kraus ¹⁷¹, J.A. Kremer ¹⁰⁰,
 T. Kresse ⁵⁰, L. Kretschmann ¹⁷¹, J. Kretzschmar ⁹², K. Kreul ¹⁸, P. Krieger ¹⁵⁵,
 S. Krishnamurthy ¹⁰³, M. Krivos ¹³³, K. Krizka ²⁰, K. Kroeninger ⁴⁹, H. Kroha ¹¹⁰, J. Kroll ¹³¹,
 J. Kroll ¹²⁸, K.S. Krowpman ¹⁰⁷, U. Kruchonak ³⁸, H. Krüger ²⁴, N. Krumnack ⁸¹, M.C. Kruse ⁵¹,
 J.A. Krzysiak ⁸⁷, O. Kuchinskaia ³⁷, S. Kuday ^{3a}, S. Kuehn ³⁶, R. Kuesters ⁵⁴, T. Kuhl ⁴⁸,
 V. Kukhtin ³⁸, Y. Kulchitsky ^{37,a}, S. Kuleshov ^{137d,137b}, M. Kumar ^{33g}, N. Kumari ⁴⁸,
 A. Kupco ¹³¹, T. Kupfer ⁴⁹, A. Kupich ³⁷, O. Kuprash ⁵⁴, H. Kurashige ⁸⁵, L.L. Kurchaninov ^{156a},
 O. Kurdysh ⁶⁶, Y.A. Kurochkin ³⁷, A. Kurova ³⁷, M. Kuze ¹⁵⁴, A.K. Kvam ¹⁰³, J. Kvitá ¹²²,
 T. Kwan ¹⁰⁴, N.G. Kyriacou ¹⁰⁶, L.A.O. Laatu ¹⁰², C. Lacasta ¹⁶³, F. Lacava ^{75a,75b},
 H. Lacker ¹⁸, D. Lacour ¹²⁷, N.N. Lad ⁹⁶, E. Ladygin ³⁸, B. Laforge ¹²⁷, T. Lagouri ^{137e},
 F.Z. Lahbabi ^{35a}, S. Lai ⁵⁵, I.K. Lakomic ^{86a}, N. Lalloue ⁶⁰, J.E. Lambert ¹⁶⁵, S. Lammers ⁶⁸,
 W. Lampl ⁷, C. Lampoudis ^{152,e}, A.N. Lancaster ¹¹⁵, E. Lançon ²⁹, U. Landgraf ⁵⁴,
 M.P.J. Landon ⁹⁴, V.S. Lang ⁵⁴, R.J. Langenberg ¹⁰³, O.K.B. Langrekken ¹²⁵, A.J. Lankford ¹⁶⁰,
 F. Lanni ³⁶, K. Lantzsch ²⁴, A. Lanza ^{73a}, A. Lapertosa ^{57b,57a}, J.F. Laporte ¹³⁵, T. Lari ^{71a},
 F. Lasagni Manghi ^{23b}, M. Lassnig ³⁶, V. Latonova ¹³¹, A. Laudrain ¹⁰⁰, A. Laurier ¹⁵⁰,
 S.D. Lawlor ⁹⁵, Z. Lawrence ¹⁰¹, M. Lazzaroni ^{71a,71b}, B. Le ¹⁰¹, E.M. Le Boulicaut ⁵¹,
 B. Leban ⁹³, A. Lebedev ⁸¹, M. LeBlanc ¹⁰¹, F. Ledroit-Guillon ⁶⁰, A.C.A. Lee ⁹⁶, S.C. Lee ¹⁴⁸,
 S. Lee ^{47a,47b}, T.F. Lee ⁹², L.L. Leeuw ^{33c}, H.P. Lefebvre ⁹⁵, M. Lefebvre ¹⁶⁵, C. Leggett ^{17a},
 G. Lehmann Miotto ³⁶, M. Leigh ⁵⁶, W.A. Leight ¹⁰³, W. Leinonen ¹¹³, A. Leisos ^{152,s},
 M.A.L. Leite ^{83c}, C.E. Leitgeb ⁴⁸, R. Leitner ¹³³, K.J.C. Leney ⁴⁴, T. Lenz ²⁴, S. Leone ^{74a},
 C. Leonidopoulos ⁵², A. Leopold ¹⁴⁴, C. Leroy ¹⁰⁸, R. Les ¹⁰⁷, C.G. Lester ³²,
 M. Levchenko ³⁷, J. Levêque ⁴, D. Levin ¹⁰⁶, L.J. Levinson ¹⁶⁹, M.P. Lewicki ⁸⁷, D.J. Lewis ⁴,
 A. Li ⁵, B. Li ^{62b}, C. Li ^{62a}, C-Q. Li ^{62c}, H. Li ^{62a}, H. Li ^{62b}, H. Li ^{14c}, H. Li ^{14b}, H. Li ^{62b},
 K. Li ¹³⁸, L. Li ^{62c}, M. Li ^{14a,14e}, Q.Y. Li ^{62a}, S. Li ^{14a,14e}, S. Li ^{62d,62c,d}, T. Li ⁵, X. Li ¹⁰⁴,
 Z. Li ¹²⁶, Z. Li ¹⁰⁴, Z. Li ⁹², Z. Li ^{14a,14e}, S. Liang ^{14a,14e}, Z. Liang ^{14a}, M. Liberatore ¹³⁵,
 B. Liberti ^{76a}, K. Lie ^{64c}, J. Lieber Marin ^{83b}, H. Lien ⁶⁸, K. Lin ¹⁰⁷, R.E. Lindley ⁷,
 J.H. Lindon ², E. Lipeles ¹²⁸, A. Lipniacka ¹⁶, A. Lister ¹⁶⁴, J.D. Little ⁴, B. Liu ^{14a},
 B.X. Liu ¹⁴², D. Liu ^{62d,62c}, J.B. Liu ^{62a}, J.K.K. Liu ³², K. Liu ^{62d,62c}, M. Liu ^{62a},

M.Y. Liu ^{62a}, P. Liu ^{14a}, Q. Liu ^{62d,138,62c}, X. Liu ^{62a}, Y. Liu ^{14d,14e}, Y.L. Liu ^{62b}, Y.W. Liu ^{62a},
J. Llorente Merino ¹⁴², S.L. Lloyd ⁹⁴, E.M. Lobodzinska ⁴⁸, P. Loch ⁷, S. Loffredo ^{76a,76b},
T. Lohse ¹⁸, K. Lohwasser ¹³⁹, E. Loiacono ⁴⁸, M. Lokajicek ^{131,*}, J.D. Lomas ²⁰,
J.D. Long ¹⁶², I. Longarini ¹⁶⁰, L. Longo ^{70a,70b}, R. Longo ¹⁶², I. Lopez Paz ⁶⁷,
A. Lopez Solis ⁴⁸, J. Lorenz ¹⁰⁹, N. Lorenzo Martinez ⁴, A.M. Lory ¹⁰⁹,
G. Löschke Centeno ¹⁴⁶, O. Loseva ³⁷, X. Lou ^{47a,47b}, X. Lou ^{14a,14e}, A. Lounis ⁶⁶, J. Love ⁶,
P.A. Love ⁹¹, G. Lu ^{14a,14e}, M. Lu ⁸⁰, S. Lu ¹²⁸, Y.J. Lu ⁶⁵, H.J. Lubatti ¹³⁸, C. Luci ^{75a,75b},
F.L. Lucio Alves ^{14c}, A. Lucotte ⁶⁰, F. Luehring ⁶⁸, I. Luise ¹⁴⁵, O. Lukianchuk ⁶⁶,
O. Lundberg ¹⁴⁴, B. Lund-Jensen ¹⁴⁴, N.A. Luongo ¹²³, M.S. Lutz ¹⁵¹, D. Lynn ²⁹, H. Lyons ⁹²,
R. Lysak ¹³¹, E. Lytken ⁹⁸, V. Lyubushkin ³⁸, T. Lyubushkina ³⁸, M.M. Lyukova ¹⁴⁵, H. Ma ²⁹,
K. Ma ^{62a}, L.L. Ma ^{62b}, Y. Ma ¹²¹, D.M. Mac Donell ¹⁶⁵, G. Maccarrone ⁵³,
J.C. MacDonald ¹⁰⁰, P.C. Machado De Abreu Farias ^{83b}, R. Madar ⁴⁰, W.F. Mader ⁵⁰,
T. Madula ⁹⁶, J. Maeda ⁸⁵, T. Maeno ²⁹, M. Maerker ⁵⁰, H. Maguire ¹³⁹, V. Maiboroda ¹³⁵,
A. Maio ^{130a,130b,130d}, K. Maj ^{86a}, O. Majersky ⁴⁸, S. Majewski ¹²³, N. Makovec ⁶⁶,
V. Maksimovic ¹⁵, B. Malaescu ¹²⁷, Pa. Malecki ⁸⁷, V.P. Maleev ³⁷, F. Malek ⁶⁰, M. Mali ⁹³,
D. Malito ⁹⁵, U. Mallik ⁸⁰, S. Maltezos ¹⁰, S. Malyukov ³⁸, J. Mamuzic ¹³, G. Mancini ⁵³,
G. Manco ^{73a,73b}, J.P. Mandalia ⁹⁴, I. Mandić ⁹³, L. Manhaes de Andrade Filho ^{83a},
I.M. Maniatis ¹⁶⁹, J. Manjarres Ramos ^{102,ab}, D.C. Mankad ¹⁶⁹, A. Mann ¹⁰⁹, B. Mansoulie ¹³⁵,
S. Manzoni ³⁶, A. Marantis ^{152,s}, G. Marchiori ⁵, M. Marcisovsky ¹³¹, C. Marcon ^{71a},
M. Marinescu ²⁰, M. Marjanovic ¹²⁰, E.J. Marshall ⁹¹, Z. Marshall ^{17a}, S. Marti-Garcia ¹⁶³,
T.A. Martin ¹⁶⁷, V.J. Martin ⁵², B. Martin dit Latour ¹⁶, L. Martinelli ^{75a,75b}, M. Martinez ^{13,t},
P. Martinez Agullo ¹⁶³, V.I. Martinez Outschoorn ¹⁰³, P. Martinez Suarez ¹³, S. Martin-Haugh ¹³⁴,
V.S. Martoiu ^{27b}, A.C. Martyniuk ⁹⁶, A. Marzin ³⁶, D. Mascione ^{78a,78b}, L. Masetti ¹⁰⁰,
T. Mashimo ¹⁵³, J. Masik ¹⁰¹, A.L. Maslennikov ³⁷, L. Massa ^{23b}, P. Massarotti ^{72a,72b},
P. Mastrandrea ^{74a,74b}, A. Mastroberardino ^{43b,43a}, T. Masubuchi ¹⁵³, T. Mathisen ¹⁶¹,
J. Matousek ¹³³, N. Matsuzawa ¹⁵³, J. Maurer ^{27b}, B. Maček ⁹³, D.A. Maximov ³⁷, R. Mazini ¹⁴⁸,
I. Maznas ¹⁵², M. Mazza ¹⁰⁷, S.M. Mazza ¹³⁶, E. Mazzeo ^{71a,71b}, C. Mc Ginn ²⁹,
J.P. Mc Gowan ¹⁰⁴, S.P. Mc Kee ¹⁰⁶, E.F. McDonald ¹⁰⁵, A.E. McDougall ¹¹⁴, J.A. Mcfayden ¹⁴⁶,
R.P. McGovern ¹²⁸, G. Mchedlidze ^{149b}, R.P. Mckenzie ^{33g}, T.C. Mclachlan ⁴⁸,
D.J. McLaughlin ⁹⁶, K.D. McLean ¹⁶⁵, S.J. McMahan ¹³⁴, P.C. McNamara ¹⁰⁵,
C.M. Mcpartland ⁹², R.A. McPherson ^{165,x}, S. Mehlhase ¹⁰⁹, A. Mehta ⁹², D. Melini ¹⁵⁰,
B.R. Mellado Garcia ^{33g}, A.H. Melo ⁵⁵, F. Meloni ⁴⁸, A.M. Mendes Jacques Da Costa ¹⁰¹,
H.Y. Meng ¹⁵⁵, L. Meng ⁹¹, S. Menke ¹¹⁰, M. Mentink ³⁶, E. Meoni ^{43b,43a}, C. Merlassino ¹²⁶,
L. Merola ^{72a,72b}, C. Meroni ^{71a,71b}, G. Merz ¹⁰⁶, O. Meshkov ³⁷, J. Metcalfe ⁶, A.S. Mete ⁶,
C. Meyer ⁶⁸, J-P. Meyer ¹³⁵, R.P. Middleton ¹³⁴, L. Mijović ⁵², G. Mikenberg ¹⁶⁹,
M. Míkestikova ¹³¹, M. Mikuž ⁹³, H. Mildner ¹⁰⁰, A. Milic ³⁶, C.D. Milke ⁴⁴, D.W. Miller ³⁹,
L.S. Miller ³⁴, A. Milov ¹⁶⁹, D.A. Milstead ^{47a,47b}, T. Min ^{14c}, A.A. Minaenko ³⁷,
I.A. Minashvili ^{149b}, L. Mince ⁵⁹, A.I. Mincer ¹¹⁷, B. Mindur ^{86a}, M. Mineev ³⁸, Y. Mino ⁸⁸,
L.M. Mir ¹³, M. Miralles Lopez ¹⁶³, M. Mironova ^{17a}, A. Mishima ¹⁵³, M.C. Missio ¹¹³,
A. Mitra ¹⁶⁷, V.A. Mitsou ¹⁶³, Y. Mitsumori ¹¹¹, O. Miu ¹⁵⁵, P.S. Miyagawa ⁹⁴,
T. Mkrtchyan ^{63a}, M. Mlinarevic ⁹⁶, T. Mlinarevic ⁹⁶, M. Mlynarikova ³⁶, S. Mobius ¹⁹,
P. Moder ⁴⁸, P. Mogg ¹⁰⁹, A.F. Mohammed ^{14a,14e}, S. Mohapatra ⁴¹, G. Mokgatitswane ^{33g},
L. Moleri ¹⁶⁹, B. Mondal ¹⁴¹, S. Mondal ¹³², K. Mönig ⁴⁸, E. Monnier ¹⁰²,
L. Monsonis Romero ¹⁶³, J. Montejo Berlingen ¹³, M. Montella ¹¹⁹, F. Montekali ^{77a,77b},
F. Monticelli ⁹⁰, S. Monzani ^{69a,69c}, N. Morange ⁶⁶, A.L. Moreira De Carvalho ^{130a},
M. Moreno Llácer ¹⁶³, C. Moreno Martinez ⁵⁶, P. Moretini ^{57b}, S. Morgenstern ³⁶, M. Morii ⁶¹,
M. Morinaga ¹⁵³, A.K. Morley ³⁶, F. Morodei ^{75a,75b}, L. Morvaj ³⁶, P. Moschovakos ³⁶,

B. Moser ³⁶, M. Mosidze ^{149b}, T. Moskalets ⁵⁴, P. Moskvitina ¹¹³, J. Moss ^{31,m},
 E.J.W. Moyse ¹⁰³, O. Mtintsilana ^{33g}, S. Muanza ¹⁰², J. Mueller ¹²⁹, D. Muenstermann ⁹¹,
 R. Müller ¹⁹, G.A. Mullier ¹⁶¹, A.J. Mullin³², J.J. Mullin¹²⁸, D.P. Mungo ¹⁵⁵, D. Munoz Perez ¹⁶³,
 F.J. Munoz Sanchez ¹⁰¹, M. Murin ¹⁰¹, W.J. Murray ^{167,134}, A. Murrone ^{71a,71b}, J.M. Muse ¹²⁰,
 M. Muškinja ^{17a}, C. Mwewa ²⁹, A.G. Myagkov ^{37,a}, A.J. Myers ⁸, A.A. Myers¹²⁹, G. Myers ⁶⁸,
 M. Myska ¹³², B.P. Nachman ^{17a}, O. Nackenhorst ⁴⁹, A. Nag ⁵⁰, K. Nagai ¹²⁶, K. Nagano ⁸⁴,
 J.L. Nagle ^{29,aj}, E. Nagy ¹⁰², A.M. Nairz ³⁶, Y. Nakahama ⁸⁴, K. Nakamura ⁸⁴, K. Nakkalil ⁵,
 H. Nanjo ¹²⁴, R. Narayan ⁴⁴, E.A. Narayanan ¹¹², I. Naryshkin ³⁷, M. Naseri ³⁴, S. Nasri ¹⁵⁹,
 C. Nass ²⁴, G. Navarro ^{22a}, J. Navarro-Gonzalez ¹⁶³, R. Nayak ¹⁵¹, A. Nayaz ¹⁸,
 P.Y. Nechaeva ³⁷, F. Nechansky ⁴⁸, L. Nedic ¹²⁶, T.J. Neep ²⁰, A. Negri ^{73a,73b}, M. Negrini ^{23b},
 C. Nellist ¹¹⁴, C. Nelson ¹⁰⁴, K. Nelson ¹⁰⁶, S. Nemecek ¹³¹, M. Nessi ^{36,h}, M.S. Neubauer ¹⁶²,
 F. Neuhaus ¹⁰⁰, J. Neundorf ⁴⁸, R. Newhouse ¹⁶⁴, P.R. Newman ²⁰, C.W. Ng ¹²⁹, Y.W.Y. Ng ⁴⁸,
 B. Ngair ^{35e}, H.D.N. Nguyen ¹⁰⁸, R.B. Nickerson ¹²⁶, R. Nicolaidou ¹³⁵, J. Nielsen ¹³⁶,
 M. Niemeyer ⁵⁵, J. Niermann ^{55,36}, N. Nikiforou ³⁶, V. Nikolaenko ^{37,a}, I. Nikolic-Audit ¹²⁷,
 K. Nikolopoulos ²⁰, P. Nilsson ²⁹, I. Ninca ⁴⁸, H.R. Nindhito ⁵⁶, G. Ninio ¹⁵¹, A. Nisati ^{75a},
 N. Nishu ², R. Nisius ¹¹⁰, J-E. Nitschke ⁵⁰, E.K. Nkadimeng ^{33g}, T. Nobe ¹⁵³, D.L. Noel ³²,
 T. Nommensen ¹⁴⁷, M.B. Norfolk ¹³⁹, R.R.B. Norisam ⁹⁶, B.J. Norman ³⁴, J. Novak ⁹³,
 T. Novak ⁴⁸, L. Novotny ¹³², R. Novotny ¹¹², L. Nozka ¹²², K. Ntekas ¹⁶⁰,
 N.M.J. Nunes De Moura Junior ^{83b}, E. Nurse⁹⁶, J. Ocariz ¹²⁷, A. Ochi ⁸⁵, I. Ochoa ^{130a},
 S. Oerdek ^{48,u}, J.T. Offermann ³⁹, A. Ogrodnik ¹³³, A. Oh ¹⁰¹, C.C. Ohm ¹⁴⁴, H. Oide ⁸⁴,
 R. Oishi ¹⁵³, M.L. Ojeda ⁴⁸, M.W. O'Keefe⁹², Y. Okumura ¹⁵³, L.F. Oleiro Seabra ^{130a},
 S.A. Olivares Pino ^{137d}, D. Oliveira Damazio ²⁹, D. Oliveira Goncalves ^{83a}, J.L. Oliver ¹⁶⁰,
 A. Olszewski ⁸⁷, Ö.O. Öncel ⁵⁴, A.P. O'Neill ¹⁹, A. Onofre ^{130a,130e}, P.U.E. Onyisi ¹¹,
 M.J. Oreglia ³⁹, G.E. Orellana ⁹⁰, D. Orestano ^{77a,77b}, N. Orlando ¹³, R.S. Orr ¹⁵⁵,
 V. O'Shea ⁵⁹, L.M. Osojnak ¹²⁸, R. Ospanov ^{62a}, G. Otero y Garzon ³⁰, H. Otono ⁸⁹,
 P.S. Ott ^{63a}, G.J. Ottino ^{17a}, M. Ouchrif ^{35d}, J. Ouellette ²⁹, F. Ould-Saada ¹²⁵, M. Owen ⁵⁹,
 R.E. Owen ¹³⁴, K.Y. Oyulmaz ^{21a}, V.E. Ozcan ^{21a}, N. Ozturk ⁸, S. Ozturk ⁸², H.A. Pacey ³²,
 A. Pacheco Pages ¹³, C. Padilla Aranda ¹³, G. Padovano ^{75a,75b}, S. Pagan Griso ^{17a},
 G. Palacino ⁶⁸, A. Palazzo ^{70a,70b}, S. Palestini ³⁶, J. Pan ¹⁷², T. Pan ^{64a}, D.K. Panchal ¹¹,
 C.E. Pandini ¹¹⁴, J.G. Panduro Vazquez ⁹⁵, H.D. Pandya ¹, H. Pang ^{14b}, P. Pani ⁴⁸,
 G. Panizzo ^{69a,69c}, L. Paolozzi ⁵⁶, C. Papadatos ¹⁰⁸, S. Parajuli ⁴⁴, A. Paramonov ⁶,
 C. Paraskevopoulos ¹⁰, D. Paredes Hernandez ^{64b}, T.H. Park ¹⁵⁵, M.A. Parker ³², F. Parodi ^{57b,57a},
 E.W. Parrish ¹¹⁵, V.A. Parrish ⁵², J.A. Parsons ⁴¹, U. Parzefall ⁵⁴, B. Pascual Dias ¹⁰⁸,
 L. Pascual Dominguez ¹⁵¹, E. Pasqualucci ^{75a}, S. Passaggio ^{57b}, F. Pastore ⁹⁵, P. Pasuwan ^{47a,47b},
 P. Patel ⁸⁷, U.M. Patel ⁵¹, J.R. Pater ¹⁰¹, T. Pauly ³⁶, J. Parkes ¹⁴³, M. Pedersen ¹²⁵,
 R. Pedro ^{130a}, S.V. Peleganchuk ³⁷, O. Penc ³⁶, E.A. Pender ⁵², H. Peng ^{62a}, K.E. Pensi ¹⁰⁹,
 M. Penzin ³⁷, B.S. Peralva ^{83d}, A.P. Pereira Peixoto ⁶⁰, L. Pereira Sanchez ^{47a,47b},
 D.V. Perepelitsa ^{29,aj}, E. Perez Codina ^{156a}, M. Perganti ¹⁰, L. Perini ^{71a,71b,*}, H. Pernegger ³⁶,
 O. Perrin ⁴⁰, K. Peters ⁴⁸, R.F.Y. Peters ¹⁰¹, B.A. Petersen ³⁶, T.C. Petersen ⁴², E. Petit ¹⁰²,
 V. Petousis ¹³², C. Petridou ^{152,e}, A. Petrukhin ¹⁴¹, M. Pettee ^{17a}, N.E. Pettersson ³⁶,
 A. Petukhov ³⁷, K. Petukhova ¹³³, R. Pezoa ^{137f}, L. Pezzotti ³⁶, G. Pezzullo ¹⁷², T.M. Pham ¹⁷⁰,
 T. Pham ¹⁰⁵, P.W. Phillips ¹³⁴, G. Piacquadio ¹⁴⁵, E. Pianori ^{17a}, F. Piazza ^{71a,71b}, R. Piegai ³⁰,
 D. Pietreanu ^{27b}, A.D. Pilkington ¹⁰¹, M. Pinamonti ^{69a,69c}, J.L. Pinfeld ²,
 B.C. Pinheiro Pereira ^{130a}, A.E. Pinto Pinoargote ^{100,135}, L. Pintucci ^{69a,69c}, K.M. Piper ¹⁴⁶,
 A. Pirttikoski ⁵⁶, D.A. Pizzi ³⁴, L. Pizzimento ^{64b}, A. Pizzini ¹¹⁴, M.-A. Pleier ²⁹, V. Plesanovs⁵⁴,
 V. Pleskot ¹³³, E. Plotnikova³⁸, G. Poddar ⁴, R. Poettgen ⁹⁸, L. Poggioli ¹²⁷, I. Pokharel ⁵⁵,
 S. Polacek ¹³³, G. Polesello ^{73a}, A. Poley ^{142,156a}, R. Polifka ¹³², A. Polini ^{23b}, C.S. Pollard ¹⁶⁷,

Z.B. Pollock [ID119](#), V. Polychronakos [ID29](#), E. Pompa Pacchi [ID75a,75b](#), D. Ponomarenko [ID113](#), L. Pontecorvo [ID36](#), S. Popa [ID27a](#), G.A. Popeneciu [ID27d](#), A. Poreba [ID36](#), D.M. Portillo Quintero [ID156a](#), S. Pospisil [ID132](#), M.A. Postill [ID139](#), P. Postolache [ID27c](#), K. Potamianos [ID167](#), P.A. Potepa [ID86a](#), I.N. Potrap [ID38](#), C.J. Potter [ID32](#), H. Potti [ID1](#), T. Poulsen [ID48](#), J. Poveda [ID163](#), M.E. Pozo Astigarraga [ID36](#), A. Prades Ibanez [ID163](#), J. Pretel [ID54](#), D. Price [ID101](#), M. Primavera [ID70a](#), M.A. Principe Martin [ID99](#), R. Privara [ID122](#), T. Procter [ID59](#), M.L. Proffitt [ID138](#), N. Proklova [ID128](#), K. Prokofiev [ID64c](#), G. Proto [ID110](#), S. Protopopescu [ID29](#), J. Proudfoot [ID6](#), M. Przybycien [ID86a](#), W.W. Przygoda [ID86b](#), J.E. Puddefoot [ID139](#), D. Pudzha [ID37](#), D. Pyatiizbyantseva [ID37](#), J. Qian [ID106](#), D. Qichen [ID101](#), Y. Qin [ID101](#), T. Qiu [ID52](#), A. Quadt [ID55](#), M. Queitsch-Maitland [ID101](#), G. Quetant [ID56](#), R.P. Quinn [ID164](#), G. Rabanal Bolanos [ID61](#), D. Rafanoharana [ID54](#), F. Ragusa [ID71a,71b](#), J.L. Rainbolt [ID39](#), J.A. Raine [ID56](#), S. Rajagopalan [ID29](#), E. Ramakoti [ID37](#), K. Ran [ID48,14e](#), N.P. Rapheeha [ID33g](#), H. Rasheed [ID27b](#), V. Raskina [ID127](#), D.F. Rassloff [ID63a](#), S. Rave [ID100](#), B. Ravina [ID55](#), I. Ravinovich [ID169](#), M. Raymond [ID36](#), A.L. Read [ID125](#), N.P. Readioff [ID139](#), D.M. Rebutzi [ID73a,73b](#), G. Redlinger [ID29](#), A.S. Reed [ID110](#), K. Reeves [ID26](#), J.A. Reidelsturz [ID171](#), D. Reikher [ID151](#), A. Rej [ID141](#), C. Rembser [ID36](#), A. Renardi [ID48](#), M. Renda [ID27b](#), M.B. Rendel [ID110](#), F. Renner [ID48](#), A.G. Rennie [ID160](#), A.L. Rescia [ID48](#), S. Resconi [ID71a](#), M. Ressegotti [ID57b,57a](#), S. Rettie [ID36](#), J.G. Reyes Rivera [ID107](#), E. Reynolds [ID17a](#), O.L. Rezanova [ID37](#), P. Reznicek [ID133](#), N. Ribaric [ID91](#), E. Ricci [ID78a,78b](#), R. Richter [ID110](#), S. Richter [ID47a,47b](#), E. Richter-Was [ID86b](#), M. Ridel [ID127](#), S. Ridouani [ID35d](#), P. Rieck [ID117](#), P. Riedler [ID36](#), M. Rijssenbeek [ID145](#), A. Rimoldi [ID73a,73b](#), M. Rimoldi [ID48](#), L. Rinaldi [ID23b,23a](#), T.T. Rinn [ID29](#), M.P. Rinnagel [ID109](#), G. Ripellino [ID161](#), I. Riu [ID13](#), P. Rivadeneira [ID48](#), J.C. Rivera Vergara [ID165](#), F. Rizatdinova [ID121](#), E. Rizvi [ID94](#), B.A. Roberts [ID167](#), B.R. Roberts [ID17a](#), S.H. Robertson [ID104,x](#), D. Robinson [ID32](#), C.M. Robles Gajardo [ID137f](#), M. Robles Manzano [ID100](#), A. Robson [ID59](#), A. Rocchi [ID76a,76b](#), C. Roda [ID74a,74b](#), S. Rodriguez Bosca [ID63a](#), Y. Rodriguez Garcia [ID22a](#), A. Rodriguez Rodriguez [ID54](#), A.M. Rodríguez Vera [ID156b](#), S. Roe [ID36](#), J.T. Roemer [ID160](#), A.R. Roepe-Gier [ID136](#), J. Roggel [ID171](#), O. Røhne [ID125](#), R.A. Rojas [ID103](#), C.P.A. Roland [ID68](#), J. Roloff [ID29](#), A. Romaniouk [ID37](#), E. Romano [ID73a,73b](#), M. Romano [ID23b](#), A.C. Romero Hernandez [ID162](#), N. Rompotis [ID92](#), L. Roos [ID127](#), S. Rosati [ID75a](#), B.J. Rosser [ID39](#), E. Rossi [ID126](#), E. Rossi [ID72a,72b](#), L.P. Rossi [ID57b](#), L. Rossini [ID54](#), R. Rosten [ID119](#), M. Rotaru [ID27b](#), B. Rottler [ID54](#), C. Rougier [ID102,ab](#), D. Rousseau [ID66](#), D. Rousso [ID32](#), A. Roy [ID162](#), S. Roy-Garand [ID155](#), A. Rozanov [ID102](#), Y. Rozen [ID150](#), X. Ruan [ID33g](#), A. Rubio Jimenez [ID163](#), A.J. Ruby [ID92](#), V.H. Ruelas Rivera [ID18](#), T.A. Ruggeri [ID1](#), A. Ruggiero [ID126](#), A. Ruiz-Martinez [ID163](#), A. Rummler [ID36](#), Z. Rurikova [ID54](#), N.A. Rusakovich [ID38](#), H.L. Russell [ID165](#), G. Russo [ID75a,75b](#), J.P. Rutherford [ID7](#), S. Rutherford Colmenares [ID32](#), K. Rybacki [ID91](#), M. Rybar [ID133](#), E.B. Rye [ID125](#), A. Ryzhov [ID44](#), J.A. Sabater Iglesias [ID56](#), P. Sabatini [ID163](#), L. Sabetta [ID75a,75b](#), H.F-W. Sadrozinski [ID136](#), F. Safai Tehrani [ID75a](#), B. Safarzadeh Samani [ID146](#), M. Safdari [ID143](#), S. Saha [ID165](#), M. Sahinsoy [ID110](#), M. Saimpert [ID135](#), M. Saito [ID153](#), T. Saito [ID153](#), D. Salamani [ID36](#), A. Salnikov [ID143](#), J. Salt [ID163](#), A. Salvador Salas [ID13](#), D. Salvatore [ID43b,43a](#), F. Salvatore [ID146](#), A. Salzburger [ID36](#), D. Sammel [ID54](#), D. Sampsonidis [ID152,e](#), D. Sampsonidou [ID123](#), J. Sánchez [ID163](#), A. Sanchez Pineda [ID4](#), V. Sanchez Sebastian [ID163](#), H. Sandaker [ID125](#), C.O. Sander [ID48](#), J.A. Sandesara [ID103](#), M. Sandhoff [ID171](#), C. Sandoval [ID22b](#), D.P.C. Sankey [ID134](#), T. Sano [ID88](#), A. Sansoni [ID53](#), L. Santi [ID75a,75b](#), C. Santoni [ID40](#), H. Santos [ID130a,130b](#), S.N. Santpur [ID17a](#), A. Santra [ID169](#), K.A. Saoucha [ID116b](#), J.G. Saraiva [ID130a,130d](#), J. Sardain [ID7](#), O. Sasaki [ID84](#), K. Sato [ID157](#), C. Sauer [ID63b](#), F. Sauerburger [ID54](#), E. Sauvan [ID4](#), P. Savard [ID155,ah](#), R. Sawada [ID153](#), C. Sawyer [ID134](#), L. Sawyer [ID97](#), I. Sayago Galvan [ID163](#), C. Sbarra [ID23b](#), A. Sbrizzi [ID23b,23a](#), T. Scanlon [ID96](#), J. Schaarschmidt [ID138](#), P. Schacht [ID110](#), D. Schaefer [ID39](#), U. Schäfer [ID100](#), A.C. Schaffer [ID66,44](#), D. Schaile [ID109](#), R.D. Schamberger [ID145](#), C. Scharf [ID18](#), M.M. Schefer [ID19](#), V.A. Schegelsky [ID37](#), D. Scheirich [ID133](#), F. Schenck [ID18](#), M. Schernau [ID160](#), C. Scheulen [ID55](#), C. Schiavi [ID57b,57a](#), E.J. Schioppa [ID70a,70b](#), M. Schioppa [ID43b,43a](#), B. Schlag [ID143,o](#), K.E. Schleicher [ID54](#), S. Schlenker [ID36](#), J. Schmeing [ID171](#),

M.A. Schmidt [ID171](#), K. Schmieden [ID100](#), C. Schmitt [ID100](#), S. Schmitt [ID48](#), L. Schoeffel [ID135](#),
A. Schoening [ID63b](#), P.G. Scholer [ID54](#), E. Schopf [ID126](#), M. Schott [ID100](#), J. Schovancova [ID36](#),
S. Schramm [ID56](#), F. Schroeder [ID171](#), T. Schroer [ID56](#), H-C. Schultz-Coulon [ID63a](#), M. Schumacher [ID54](#),
B.A. Schumm [ID136](#), Ph. Schune [ID135](#), A.J. Schuy [ID138](#), H.R. Schwartz [ID136](#), A. Schwartzman [ID143](#),
T.A. Schwarz [ID106](#), Ph. Schwemling [ID135](#), R. Schwienhorst [ID107](#), A. Sciandra [ID136](#), G. Sciolla [ID26](#),
F. Scuri [ID74a](#), C.D. Sebastiani [ID92](#), K. Sedlaczek [ID115](#), P. Seema [ID18](#), S.C. Seidel [ID112](#), A. Seiden [ID136](#),
B.D. Seidlitz [ID41](#), C. Seitz [ID48](#), J.M. Seixas [ID83b](#), G. Sekhniaidze [ID72a](#), S.J. Sekula [ID44](#), L. Selem [ID60](#),
N. Semprini-Cesari [ID23b,23a](#), D. Sengupta [ID56](#), V. Senthilkumar [ID163](#), L. Serin [ID66](#), L. Serkin [ID69a,69b](#),
M. Sessa [ID76a,76b](#), H. Severini [ID120](#), F. Sforza [ID57b,57a](#), A. Sfyrta [ID56](#), E. Shabalina [ID55](#), R. Shaheen [ID144](#),
J.D. Shahinian [ID128](#), D. Shaked Renous [ID169](#), L.Y. Shan [ID14a](#), M. Shapiro [ID17a](#), A. Sharma [ID36](#),
A.S. Sharma [ID164](#), P. Sharma [ID80](#), S. Sharma [ID48](#), P.B. Shatalov [ID37](#), K. Shaw [ID146](#), S.M. Shaw [ID101](#),
A. Shcherbakova [ID37](#), Q. Shen [ID62c,5](#), P. Sherwood [ID96](#), L. Shi [ID96](#), X. Shi [ID14a](#), C.O. Shimmin [ID172](#),
J.D. Shinner [ID95](#), I.P.J. Shipsey [ID126](#), S. Shirabe [ID56,h](#), M. Shiyakova [ID38,v](#), J. Shlomi [ID169](#),
M.J. Shochet [ID39](#), J. Shojaii [ID105](#), D.R. Shope [ID125](#), B. Shrestha [ID120](#), S. Shrestha [ID119,ak](#),
E.M. Shrif [ID33g](#), M.J. Shroff [ID165](#), P. Sicho [ID131](#), A.M. Sickles [ID162](#), E. Sideras Haddad [ID33g](#),
A. Sidoti [ID23b](#), F. Siegert [ID50](#), Dj. Sijacki [ID15](#), R. Sikora [ID86a](#), F. Sili [ID90](#), J.M. Silva [ID20](#),
M.V. Silva Oliveira [ID29](#), S.B. Silverstein [ID47a](#), S. Simion [ID66](#), R. Simoniello [ID36](#), E.L. Simpson [ID59](#),
H. Simpson [ID146](#), L.R. Simpson [ID106](#), N.D. Simpson [ID98](#), S. Simsek [ID82](#), S. Sindhu [ID55](#), P. Sinervo [ID155](#),
S. Singh [ID155](#), S. Sinha [ID48](#), S. Sinha [ID101](#), M. Sioli [ID23b,23a](#), I. Siral [ID36](#), E. Sitnikova [ID48](#),
S.Yu. Sivoklov [ID37,*](#), J. Sjölin [ID47a,47b](#), A. Skaf [ID55](#), E. Skorda [ID20](#), P. Skubic [ID120](#), M. Slawinska [ID87](#),
V. Smakhtin [ID169](#), B.H. Smart [ID134](#), J. Smiesko [ID36](#), S.Yu. Smirnov [ID37](#), Y. Smirnov [ID37](#),
L.N. Smirnova [ID37,a](#), O. Smirnova [ID98](#), A.C. Smith [ID41](#), E.A. Smith [ID39](#), H.A. Smith [ID126](#),
J.L. Smith [ID92](#), R. Smith [ID143](#), M. Smizanska [ID91](#), K. Smolek [ID132](#), A.A. Snesarev [ID37](#), S.R. Snider [ID155](#),
H.L. Snoek [ID114](#), S. Snyder [ID29](#), R. Sobie [ID165,x](#), A. Soffer [ID151](#), C.A. Solans Sanchez [ID36](#),
E.Yu. Soldatov [ID37](#), U. Soldevila [ID163](#), A.A. Solodkov [ID37](#), S. Solomon [ID26](#), A. Soloshenko [ID38](#),
K. Solovieva [ID54](#), O.V. Solovyanov [ID40](#), V. Solovyev [ID37](#), P. Sommer [ID36](#), A. Sonay [ID13](#),
W.Y. Song [ID156b](#), J.M. Sonneveld [ID114](#), A. Sopczak [ID132](#), A.L. Sopio [ID96](#), F. Sopkova [ID28b](#),
V. Sothilingam [ID63a](#), S. Sottocornola [ID68](#), R. Soualah [ID116b](#), Z. Soumami [ID35e](#), D. South [ID48](#),
N. Soybelman [ID169](#), S. Spagnolo [ID70a,70b](#), M. Spalla [ID110](#), D. Sperlich [ID54](#), G. Spigo [ID36](#), S. Spinali [ID91](#),
D.P. Spiteri [ID59](#), M. Spousta [ID133](#), E.J. Staats [ID34](#), A. Stabile [ID71a,71b](#), R. Stamen [ID63a](#), A. Stampekis [ID20](#),
M. Standke [ID24](#), E. Stanecka [ID87](#), M.V. Stange [ID50](#), B. Stanislaus [ID17a](#), M.M. Stanitzki [ID48](#), B. Stapf [ID48](#),
E.A. Starchenko [ID37](#), G.H. Stark [ID136](#), J. Stark [ID102,ab](#), D.M. Starko [ID156b](#), P. Staroba [ID131](#),
P. Starovoitov [ID63a](#), S. Stärz [ID104](#), R. Staszewski [ID87](#), G. Stavropoulos [ID46](#), J. Steentoft [ID161](#),
P. Steinberg [ID29](#), B. Stelzer [ID142,156a](#), H.J. Stelzer [ID129](#), O. Stelzer-Chilton [ID156a](#), H. Stenzel [ID58](#),
T.J. Stevenson [ID146](#), G.A. Stewart [ID36](#), J.R. Stewart [ID121](#), M.C. Stockton [ID36](#), G. Stoicea [ID27b](#),
M. Stolarski [ID130a](#), S. Stonjek [ID110](#), A. Straessner [ID50](#), J. Strandberg [ID144](#), S. Strandberg [ID47a,47b](#),
M. Stratmann [ID171](#), M. Strauss [ID120](#), T. Strebler [ID102](#), P. Strizenec [ID28b](#), R. Ströhmer [ID166](#),
D.M. Strom [ID123](#), L.R. Strom [ID48](#), R. Stroynowski [ID44](#), A. Strubig [ID47a,47b](#), S.A. Stucci [ID29](#),
B. Stugu [ID16](#), J. Stupak [ID120](#), N.A. Styles [ID48](#), D. Su [ID143](#), S. Su [ID62a](#), W. Su [ID62d](#), X. Su [ID62a,66](#),
K. Sugizaki [ID153](#), V.V. Sulin [ID37](#), M.J. Sullivan [ID92](#), D.M.S. Sultan [ID78a,78b](#), L. Sultanaliev [ID37](#),
S. Sultansoy [ID3b](#), T. Sumida [ID88](#), S. Sun [ID106](#), S. Sun [ID170](#), O. Sunneborn Gudnadottir [ID161](#), N. Sur [ID102](#),
M.R. Sutton [ID146](#), H. Suzuki [ID157](#), M. Svatos [ID131](#), M. Swiatlowski [ID156a](#), T. Swirski [ID166](#),
I. Sykora [ID28a](#), M. Sykora [ID133](#), T. Sykora [ID133](#), D. Ta [ID100](#), K. Tackmann [ID48,u](#), A. Taffard [ID160](#),
R. Tafirout [ID156a](#), J.S. Tafoya Vargas [ID66](#), E.P. Takeva [ID52](#), Y. Takubo [ID84](#), M. Talby [ID102](#),
A.A. Talyshev [ID37](#), K.C. Tam [ID64b](#), N.M. Tamir [ID151](#), A. Tanaka [ID153](#), J. Tanaka [ID153](#), R. Tanaka [ID66](#),
M. Tanasini [ID57b,57a](#), Z. Tao [ID164](#), S. Tapia Araya [ID137f](#), S. Tapprogge [ID100](#),
A. Tarek Abouelfadl Mohamed [ID107](#), S. Tarem [ID150](#), K. Tariq [ID14a](#), G. Tarna [ID102,27b](#), G.F. Tartarelli [ID71a](#),

P. Tas ¹³³, M. Tasevsky ¹³¹, E. Tassi ^{43b,43a}, A.C. Tate ¹⁶², G. Tateno ¹⁵³, Y. Tayalati ^{35e,w},
 G.N. Taylor ¹⁰⁵, W. Taylor ^{156b}, H. Teagle ⁹², A.S. Tee ¹⁷⁰, R. Teixeira De Lima ¹⁴³,
 P. Teixeira-Dias ⁹⁵, J.J. Teoh ¹⁵⁵, K. Terashi ¹⁵³, J. Terron ⁹⁹, S. Terzo ¹³, M. Testa ⁵³,
 R.J. Teuscher ^{155,x}, A. Thaler ⁷⁹, O. Theiner ⁵⁶, N. Themistokleous ⁵², T. Thevenaux-Pelzer ¹⁰²,
 O. Thielmann ¹⁷¹, D.W. Thomas ⁹⁵, J.P. Thomas ²⁰, E.A. Thompson ^{17a}, P.D. Thompson ²⁰,
 E. Thomson ¹²⁸, Y. Tian ⁵⁵, V. Tikhomirov ^{37,a}, Yu.A. Tikhonov ³⁷, S. Timoshenko ³⁷,
 D. Timoshyn ¹³³, E.X.L. Ting ¹, P. Tipton ¹⁷², S.H. Tlou ^{33g}, A. Tnourji ⁴⁰, K. Todome ¹⁵⁴,
 S. Todorova-Nova ¹³³, S. Todt ⁵⁰, M. Togawa ⁸⁴, J. Tojo ⁸⁹, S. Tokár ^{28a}, K. Tokushuku ⁸⁴,
 O. Toldaiev ⁶⁸, R. Tombs ³², M. Tomoto ^{84,111}, L. Tompkins ^{143,o}, K.W. Topolnicki ^{86b},
 E. Torrence ¹²³, H. Torres ^{102,ab}, E. Torró Pastor ¹⁶³, M. Toscani ³⁰, C. Tosciri ³⁹, M. Tost ¹¹,
 D.R. Tovey ¹³⁹, A. Traeet ¹⁶, I.S. Trandafir ^{27b}, T. Trefzger ¹⁶⁶, A. Tricoli ²⁹, I.M. Trigger ^{156a},
 S. Trincaz-Duvoid ¹²⁷, D.A. Trischuk ²⁶, B. Trocmé ⁶⁰, C. Troncon ^{71a}, L. Truong ^{33c},
 M. Trzebinski ⁸⁷, A. Trzupiek ⁸⁷, F. Tsai ¹⁴⁵, M. Tsai ¹⁰⁶, A. Tsiamis ^{152,e}, P.V. Tsiareshka ³⁷,
 S. Tsigaridas ^{156a}, A. Tsirigotis ^{152,s}, V. Tsiskaridze ¹⁵⁵, E.G. Tskhadadze ^{149a},
 M. Tsopoulou ^{152,e}, Y. Tsujikawa ⁸⁸, I.I. Tsukerman ³⁷, V. Tsulaia ^{17a}, S. Tsuno ⁸⁴, O. Tsur ¹⁵⁰,
 K. Tsuru ¹¹⁸, D. Tsybychev ¹⁴⁵, Y. Tu ^{64b}, A. Tudorache ^{27b}, V. Tudorache ^{27b}, A.N. Tuna ³⁶,
 S. Turchikhin ^{57b,57a}, I. Turk Cakir ^{3a}, R. Turra ^{71a}, T. Turtuvshin ^{38,y}, P.M. Tuts ⁴¹,
 S. Tzamarias ^{152,e}, P. Tzani ¹⁰, E. Tzovara ¹⁰⁰, F. Ukegawa ¹⁵⁷, P.A. Ulloa Poblete ^{137c,137b},
 E.N. Umaka ²⁹, G. Unal ³⁶, M. Unal ¹¹, A. Undrus ²⁹, G. Unel ¹⁶⁰, J. Urban ^{28b},
 P. Urquijo ¹⁰⁵, G. Usai ⁸, R. Ushioda ¹⁵⁴, M. Usman ¹⁰⁸, Z. Uysal ^{21b}, L. Vacavant ¹⁰²,
 V. Vacek ¹³², B. Vachon ¹⁰⁴, K.O.H. Vadla ¹²⁵, T. Vafeiadis ³⁶, A. Vaitkus ⁹⁶, C. Valderanis ¹⁰⁹,
 E. Valdes Santurio ^{47a,47b}, M. Valente ^{156a}, S. Valentinetti ^{23b,23a}, A. Valero ¹⁶³,
 E. Valiente Moreno ¹⁶³, A. Vallier ^{102,ab}, J.A. Valls Ferrer ¹⁶³, D.R. Van Arneeman ¹¹⁴,
 T.R. Van Daalen ¹³⁸, A. Van Der Graaf ⁴⁹, P. Van Gemmeren ⁶, M. Van Rijnbach ^{125,36},
 S. Van Stroud ⁹⁶, I. Van Vulpen ¹¹⁴, M. Vanadia ^{76a,76b}, W. Vandelli ³⁶, M. Vandenbroucke ¹³⁵,
 E.R. Vandewall ¹²¹, D. Vannicola ¹⁵¹, L. Vannoli ^{57b,57a}, R. Vari ^{75a}, E.W. Varnes ⁷,
 C. Varni ^{17b}, T. Varol ¹⁴⁸, D. Varouchas ⁶⁶, L. Varriale ¹⁶³, K.E. Varvell ¹⁴⁷, M.E. Vasile ^{27b},
 L. Vaslin ⁴⁰, G.A. Vasquez ¹⁶⁵, A. Vasyukov ³⁸, F. Vazeille ⁴⁰, T. Vazquez Schroeder ³⁶,
 J. Veatch ³¹, V. Vecchio ¹⁰¹, M.J. Veen ¹⁰³, I. Veliscek ¹²⁶, L.M. Veloce ¹⁵⁵, F. Veloso ^{130a,130c},
 S. Veneziano ^{75a}, A. Ventura ^{70a,70b}, S. Ventura Gonzalez ¹³⁵, A. Verbytskyi ¹¹⁰,
 M. Verducci ^{74a,74b}, C. Vergis ²⁴, M. Verissimo De Araujo ^{83b}, W. Verkerke ¹¹⁴,
 J.C. Vermeulen ¹¹⁴, C. Vernieri ¹⁴³, M. Vessella ¹⁰³, M.C. Vetterli ^{142,ah}, A. Vgenopoulos ^{152,e},
 N. Viaux Maira ^{137f}, T. Vickey ¹³⁹, O.E. Vickey Boeriu ¹³⁹, G.H.A. Viehhauser ¹²⁶, L. Vignani ^{63b},
 M. Villa ^{23b,23a}, M. Villaplana Perez ¹⁶³, E.M. Villhauer ⁵², E. Vilucchi ⁵³, M.G. Vincter ³⁴,
 G.S. Virdee ²⁰, A. Vishwakarma ⁵², A. Visibile ¹¹⁴, C. Vittori ³⁶, I. Vivarelli ¹⁴⁶, V. Vladimirov ¹⁶⁷,
 E. Voevodina ¹¹⁰, F. Vogel ¹⁰⁹, P. Vokac ¹³², Yu. Volkotrub ^{86a}, J. Von Ahnen ⁴⁸,
 E. Von Toerne ²⁴, B. Vormwald ³⁶, V. Vorobel ¹³³, K. Vorobev ³⁷, M. Vos ¹⁶³, K. Voss ¹⁴¹,
 J.H. Vossebeld ⁹², M. Vozak ¹¹⁴, L. Vozdecky ⁹⁴, N. Vranjes ¹⁵, M. Vranjes Milosavljevic ¹⁵,
 M. Vreeswijk ¹¹⁴, R. Vuillermet ³⁶, O. Vujanovic ¹⁰⁰, I. Vukotic ³⁹, S. Wada ¹⁵⁷, C. Wagner ¹⁰³,
 J.M. Wagner ^{17a}, W. Wagner ¹⁷¹, S. Wahdan ¹⁷¹, H. Wahlberg ⁹⁰, M. Wakida ¹¹¹, J. Walder ¹³⁴,
 R. Walker ¹⁰⁹, W. Walkowiak ¹⁴¹, A. Wall ¹²⁸, T. Wamorkar ⁶, A.Z. Wang ¹⁷⁰, C. Wang ¹⁰⁰,
 C. Wang ^{62c}, H. Wang ^{17a}, J. Wang ^{64a}, R.-J. Wang ¹⁰⁰, R. Wang ⁶¹, R. Wang ⁶,
 S.M. Wang ¹⁴⁸, S. Wang ^{62b}, T. Wang ^{62a}, W.T. Wang ⁸⁰, W. Wang ^{14a}, X. Wang ^{14c},
 X. Wang ¹⁶², X. Wang ^{62c}, Y. Wang ^{62d}, Y. Wang ^{14c}, Z. Wang ¹⁰⁶, Z. Wang ^{62d,51,62c},
 Z. Wang ¹⁰⁶, A. Warburton ¹⁰⁴, R.J. Ward ²⁰, N. Warrack ⁵⁹, A.T. Watson ²⁰, H. Watson ⁵⁹,
 M.F. Watson ²⁰, E. Watton ^{59,134}, G. Watts ¹³⁸, B.M. Waugh ⁹⁶, C. Weber ²⁹, H.A. Weber ¹⁸,
 M.S. Weber ¹⁹, S.M. Weber ^{63a}, C. Wei ^{62a}, Y. Wei ¹²⁶, A.R. Weidberg ¹²⁶, E.J. Weik ¹¹⁷,

J. Weingarten ⁴⁹, M. Weirich ¹⁰⁰, C. Weiser ⁵⁴, C.J. Wells ⁴⁸, T. Wenaus ²⁹, B. Wendland ⁴⁹, T. Wengler ³⁶, N.S. Wenke ¹¹⁰, N. Wermes ²⁴, M. Wessels ^{63a}, A.M. Wharton ⁹¹, A.S. White ⁶¹, A. White ⁸, M.J. White ¹, D. Whiteson ¹⁶⁰, L. Wickremasinghe ¹²⁴, W. Wiedenmann ¹⁷⁰, C. Wiel ⁵⁰, M. Wielers ¹³⁴, C. Wiglesworth ⁴², D.J. Wilbern ¹²⁰, H.G. Wilkens ³⁶, D.M. Williams ⁴¹, H.H. Williams ¹²⁸, S. Williams ³², S. Willocq ¹⁰³, B.J. Wilson ¹⁰¹, P.J. Windischhofer ³⁹, F.I. Winkel ³⁰, F. Winklmeier ¹²³, B.T. Winter ⁵⁴, J.K. Winter ¹⁰¹, M. Wittgen ¹⁴³, M. Wobisch ⁹⁷, Z. Wolfs ¹¹⁴, J. Wollrath ¹⁶⁰, M.W. Wolter ⁸⁷, H. Wolters ^{130a,130c}, A.F. Wongel ⁴⁸, S.D. Worm ⁴⁸, B.K. Wosiek ⁸⁷, K.W. Woźniak ⁸⁷, S. Wozniwski ⁵⁵, K. Wraight ⁵⁹, C. Wu ²⁰, J. Wu ^{14a,14e}, M. Wu ^{64a}, M. Wu ¹¹³, S.L. Wu ¹⁷⁰, X. Wu ⁵⁶, Y. Wu ^{62a}, Z. Wu ¹³⁵, J. Wuerzinger ^{110,af}, T.R. Wyatt ¹⁰¹, B.M. Wynne ⁵², S. Xella ⁴², L. Xia ^{14c}, M. Xia ^{14b}, J. Xiang ^{64c}, M. Xie ^{62a}, X. Xie ^{62a}, S. Xin ^{14a,14e}, J. Xiong ^{17a}, D. Xu ^{14a}, H. Xu ^{62a}, L. Xu ^{62a}, R. Xu ¹²⁸, T. Xu ¹⁰⁶, Y. Xu ^{14b}, Z. Xu ⁵², Z. Xu ^{14a}, B. Yabsley ¹⁴⁷, S. Yacoub ^{33a}, Y. Yamaguchi ¹⁵⁴, E. Yamashita ¹⁵³, H. Yamauchi ¹⁵⁷, T. Yamazaki ^{17a}, Y. Yamazaki ⁸⁵, J. Yan ^{62c}, S. Yan ¹²⁶, Z. Yan ²⁵, H.J. Yang ^{62c,62d}, H.T. Yang ^{62a}, S. Yang ^{62a}, T. Yang ^{64c}, X. Yang ^{62a}, X. Yang ^{14a}, Y. Yang ⁴⁴, Y. Yang ^{62a}, Z. Yang ^{62a}, W.-M. Yao ^{17a}, Y.C. Yap ⁴⁸, H. Ye ^{14c}, H. Ye ⁵⁵, J. Ye ^{14a}, S. Ye ²⁹, X. Ye ^{62a}, Y. Yeh ⁹⁶, I. Yeletsikh ³⁸, B.K. Yeo ^{17b}, M.R. Yexley ⁹⁶, P. Yin ⁴¹, K. Yorita ¹⁶⁸, S. Younas ^{27b}, C.J.S. Young ³⁶, C. Young ¹⁴³, C. Yu ^{14a,14e}, Y. Yu ^{62a}, M. Yuan ¹⁰⁶, R. Yuan ^{62b,k}, L. Yue ⁹⁶, M. Zaazoua ^{62a}, B. Zabinski ⁸⁷, E. Zaid ⁵², T. Zakareishvili ^{149b}, N. Zakharchuk ³⁴, S. Zambito ⁵⁶, J.A. Zamora Saa ^{137d,137b}, J. Zang ¹⁵³, D. Zanzi ⁵⁴, O. Zaplatilek ¹³², C. Zeitnitz ¹⁷¹, H. Zeng ^{14a}, J.C. Zeng ¹⁶², D.T. Zenger Jr ²⁶, O. Zenin ³⁷, T. Ženiš ^{28a}, S. Zenz ⁹⁴, S. Zerradi ^{35a}, D. Zerwas ⁶⁶, M. Zhai ^{14a,14e}, B. Zhang ^{14c}, D.F. Zhang ¹³⁹, J. Zhang ^{62b}, J. Zhang ⁶, K. Zhang ^{14a,14e}, L. Zhang ^{14c}, P. Zhang ^{14a,14e}, R. Zhang ¹⁷⁰, S. Zhang ¹⁰⁶, T. Zhang ¹⁵³, X. Zhang ^{62c}, X. Zhang ^{62b}, Y. Zhang ^{62c,5}, Y. Zhang ⁹⁶, Z. Zhang ^{17a}, Z. Zhang ⁶⁶, H. Zhao ¹³⁸, P. Zhao ⁵¹, T. Zhao ^{62b}, Y. Zhao ¹³⁶, Z. Zhao ^{62a}, A. Zhemchugov ³⁸, J. Zheng ^{14c}, K. Zheng ¹⁶², X. Zheng ^{62a}, Z. Zheng ¹⁴³, D. Zhong ¹⁶², B. Zhou ¹⁰⁶, H. Zhou ⁷, N. Zhou ^{62c}, Y. Zhou ⁷, C.G. Zhu ^{62b}, J. Zhu ¹⁰⁶, Y. Zhu ^{62c}, Y. Zhu ^{62a}, X. Zhuang ^{14a}, K. Zhukov ³⁷, V. Zhulanov ³⁷, N.I. Zimine ³⁸, J. Zinsser ^{63b}, M. Ziolkowski ¹⁴¹, L. Živković ¹⁵, A. Zoccoli ^{23b,23a}, K. Zoch ⁵⁶, T.G. Zorbas ¹³⁹, O. Zormpa ⁴⁶, W. Zou ⁴¹, L. Zwalinski ³⁶.

¹Department of Physics, University of Adelaide, Adelaide; Australia.

²Department of Physics, University of Alberta, Edmonton AB; Canada.

³(^a)Department of Physics, Ankara University, Ankara; (^b)Division of Physics, TOBB University of Economics and Technology, Ankara; Türkiye.

⁴LAPP, Université Savoie Mont Blanc, CNRS/IN2P3, Annecy; France.

⁵APC, Université Paris Cité, CNRS/IN2P3, Paris; France.

⁶High Energy Physics Division, Argonne National Laboratory, Argonne IL; United States of America.

⁷Department of Physics, University of Arizona, Tucson AZ; United States of America.

⁸Department of Physics, University of Texas at Arlington, Arlington TX; United States of America.

⁹Physics Department, National and Kapodistrian University of Athens, Athens; Greece.

¹⁰Physics Department, National Technical University of Athens, Zografou; Greece.

¹¹Department of Physics, University of Texas at Austin, Austin TX; United States of America.

¹²Institute of Physics, Azerbaijan Academy of Sciences, Baku; Azerbaijan.

¹³Institut de Física d'Altes Energies (IFAE), Barcelona Institute of Science and Technology, Barcelona; Spain.

¹⁴(^a)Institute of High Energy Physics, Chinese Academy of Sciences, Beijing; (^b)Physics Department,

Tsinghua University, Beijing;^(c)Department of Physics, Nanjing University, Nanjing;^(d)School of Science, Shenzhen Campus of Sun Yat-sen University;^(e)University of Chinese Academy of Science (UCAS), Beijing; China.

¹⁵Institute of Physics, University of Belgrade, Belgrade; Serbia.

¹⁶Department for Physics and Technology, University of Bergen, Bergen; Norway.

¹⁷(^a)Physics Division, Lawrence Berkeley National Laboratory, Berkeley CA;^(b)University of California, Berkeley CA; United States of America.

¹⁸Institut für Physik, Humboldt Universität zu Berlin, Berlin; Germany.

¹⁹Albert Einstein Center for Fundamental Physics and Laboratory for High Energy Physics, University of Bern, Bern; Switzerland.

²⁰School of Physics and Astronomy, University of Birmingham, Birmingham; United Kingdom.

²¹(^a)Department of Physics, Bogazici University, Istanbul;^(b)Department of Physics Engineering, Gaziantep University, Gaziantep;^(c)Department of Physics, Istanbul University, Istanbul; Türkiye.

²²(^a)Facultad de Ciencias y Centro de Investigaciones, Universidad Antonio Nariño,

Bogotá;^(b)Departamento de Física, Universidad Nacional de Colombia, Bogotá; Colombia.

²³(^a)Dipartimento di Fisica e Astronomia A. Righi, Università di Bologna, Bologna;^(b)INFN Sezione di Bologna; Italy.

²⁴Physikalisches Institut, Universität Bonn, Bonn; Germany.

²⁵Department of Physics, Boston University, Boston MA; United States of America.

²⁶Department of Physics, Brandeis University, Waltham MA; United States of America.

²⁷(^a)Transilvania University of Brasov, Brasov;^(b)Horia Hulubei National Institute of Physics and Nuclear Engineering, Bucharest;^(c)Department of Physics, Alexandru Ioan Cuza University of Iasi, Iasi;^(d)National Institute for Research and Development of Isotopic and Molecular Technologies, Physics Department, Cluj-Napoca;^(e)National University of Science and Technology Politehnica, Bucharest;^(f)West University in Timisoara, Timisoara;^(g)Faculty of Physics, University of Bucharest, Bucharest; Romania.

²⁸(^a)Faculty of Mathematics, Physics and Informatics, Comenius University, Bratislava;^(b)Department of Subnuclear Physics, Institute of Experimental Physics of the Slovak Academy of Sciences, Kosice; Slovak Republic.

²⁹Physics Department, Brookhaven National Laboratory, Upton NY; United States of America.

³⁰Universidad de Buenos Aires, Facultad de Ciencias Exactas y Naturales, Departamento de Física, y CONICET, Instituto de Física de Buenos Aires (IFIBA), Buenos Aires; Argentina.

³¹California State University, CA; United States of America.

³²Cavendish Laboratory, University of Cambridge, Cambridge; United Kingdom.

³³(^a)Department of Physics, University of Cape Town, Cape Town;^(b)iThemba Labs, Western

Cape;^(c)Department of Mechanical Engineering Science, University of Johannesburg,

Johannesburg;^(d)National Institute of Physics, University of the Philippines Diliman

(Philippines);^(e)University of South Africa, Department of Physics, Pretoria;^(f)University of Zululand,

KwaDlangezwa;^(g)School of Physics, University of the Witwatersrand, Johannesburg; South Africa.

³⁴Department of Physics, Carleton University, Ottawa ON; Canada.

³⁵(^a)Faculté des Sciences Ain Chock, Réseau Universitaire de Physique des Hautes Energies - Université Hassan II, Casablanca;^(b)Faculté des Sciences, Université Ibn-Tofail, Kénitra;^(c)Faculté des Sciences Semlalia, Université Cadi Ayyad, LPHEA-Marrakech;^(d)LPMR, Faculté des Sciences, Université Mohamed Premier, Oujda;^(e)Faculté des sciences, Université Mohammed V, Rabat;^(f)Institute of Applied Physics, Mohammed VI Polytechnic University, Ben Guerir; Morocco.

³⁶CERN, Geneva; Switzerland.

³⁷Affiliated with an institute covered by a cooperation agreement with CERN.

³⁸Affiliated with an international laboratory covered by a cooperation agreement with CERN.

- ³⁹Enrico Fermi Institute, University of Chicago, Chicago IL; United States of America.
- ⁴⁰LPC, Université Clermont Auvergne, CNRS/IN2P3, Clermont-Ferrand; France.
- ⁴¹Nevis Laboratory, Columbia University, Irvington NY; United States of America.
- ⁴²Niels Bohr Institute, University of Copenhagen, Copenhagen; Denmark.
- ⁴³(^a)Dipartimento di Fisica, Università della Calabria, Rende; (^b)INFN Gruppo Collegato di Cosenza, Laboratori Nazionali di Frascati; Italy.
- ⁴⁴Physics Department, Southern Methodist University, Dallas TX; United States of America.
- ⁴⁵Physics Department, University of Texas at Dallas, Richardson TX; United States of America.
- ⁴⁶National Centre for Scientific Research "Demokritos", Agia Paraskevi; Greece.
- ⁴⁷(^a)Department of Physics, Stockholm University; (^b)Oskar Klein Centre, Stockholm; Sweden.
- ⁴⁸Deutsches Elektronen-Synchrotron DESY, Hamburg and Zeuthen; Germany.
- ⁴⁹Fakultät Physik , Technische Universität Dortmund, Dortmund; Germany.
- ⁵⁰Institut für Kern- und Teilchenphysik, Technische Universität Dresden, Dresden; Germany.
- ⁵¹Department of Physics, Duke University, Durham NC; United States of America.
- ⁵²SUPA - School of Physics and Astronomy, University of Edinburgh, Edinburgh; United Kingdom.
- ⁵³INFN e Laboratori Nazionali di Frascati, Frascati; Italy.
- ⁵⁴Physikalisches Institut, Albert-Ludwigs-Universität Freiburg, Freiburg; Germany.
- ⁵⁵II. Physikalisches Institut, Georg-August-Universität Göttingen, Göttingen; Germany.
- ⁵⁶Département de Physique Nucléaire et Corpusculaire, Université de Genève, Genève; Switzerland.
- ⁵⁷(^a)Dipartimento di Fisica, Università di Genova, Genova; (^b)INFN Sezione di Genova; Italy.
- ⁵⁸II. Physikalisches Institut, Justus-Liebig-Universität Giessen, Giessen; Germany.
- ⁵⁹SUPA - School of Physics and Astronomy, University of Glasgow, Glasgow; United Kingdom.
- ⁶⁰LPSC, Université Grenoble Alpes, CNRS/IN2P3, Grenoble INP, Grenoble; France.
- ⁶¹Laboratory for Particle Physics and Cosmology, Harvard University, Cambridge MA; United States of America.
- ⁶²(^a)Department of Modern Physics and State Key Laboratory of Particle Detection and Electronics, University of Science and Technology of China, Hefei; (^b)Institute of Frontier and Interdisciplinary Science and Key Laboratory of Particle Physics and Particle Irradiation (MOE), Shandong University, Qingdao; (^c)School of Physics and Astronomy, Shanghai Jiao Tong University, Key Laboratory for Particle Astrophysics and Cosmology (MOE), SKLPPC, Shanghai; (^d)Tsung-Dao Lee Institute, Shanghai; China.
- ⁶³(^a)Kirchhoff-Institut für Physik, Ruprecht-Karls-Universität Heidelberg, Heidelberg; (^b)Physikalisches Institut, Ruprecht-Karls-Universität Heidelberg, Heidelberg; Germany.
- ⁶⁴(^a)Department of Physics, Chinese University of Hong Kong, Shatin, N.T., Hong Kong; (^b)Department of Physics, University of Hong Kong, Hong Kong; (^c)Department of Physics and Institute for Advanced Study, Hong Kong University of Science and Technology, Clear Water Bay, Kowloon, Hong Kong; China.
- ⁶⁵Department of Physics, National Tsing Hua University, Hsinchu; Taiwan.
- ⁶⁶IJCLab, Université Paris-Saclay, CNRS/IN2P3, 91405, Orsay; France.
- ⁶⁷Centro Nacional de Microelectrónica (IMB-CNM-CSIC), Barcelona; Spain.
- ⁶⁸Department of Physics, Indiana University, Bloomington IN; United States of America.
- ⁶⁹(^a)INFN Gruppo Collegato di Udine, Sezione di Trieste, Udine; (^b)ICTP, Trieste; (^c)Dipartimento Politecnico di Ingegneria e Architettura, Università di Udine, Udine; Italy.
- ⁷⁰(^a)INFN Sezione di Lecce; (^b)Dipartimento di Matematica e Fisica, Università del Salento, Lecce; Italy.
- ⁷¹(^a)INFN Sezione di Milano; (^b)Dipartimento di Fisica, Università di Milano, Milano; Italy.
- ⁷²(^a)INFN Sezione di Napoli; (^b)Dipartimento di Fisica, Università di Napoli, Napoli; Italy.
- ⁷³(^a)INFN Sezione di Pavia; (^b)Dipartimento di Fisica, Università di Pavia, Pavia; Italy.
- ⁷⁴(^a)INFN Sezione di Pisa; (^b)Dipartimento di Fisica E. Fermi, Università di Pisa, Pisa; Italy.
- ⁷⁵(^a)INFN Sezione di Roma; (^b)Dipartimento di Fisica, Sapienza Università di Roma, Roma; Italy.

- ^{76(a)}INFN Sezione di Roma Tor Vergata;^(b)Dipartimento di Fisica, Università di Roma Tor Vergata, Roma; Italy.
- ^{77(a)}INFN Sezione di Roma Tre;^(b)Dipartimento di Matematica e Fisica, Università Roma Tre, Roma; Italy.
- ^{78(a)}INFN-TIFPA;^(b)Università degli Studi di Trento, Trento; Italy.
- ⁷⁹Universität Innsbruck, Department of Astro and Particle Physics, Innsbruck; Austria.
- ⁸⁰University of Iowa, Iowa City IA; United States of America.
- ⁸¹Department of Physics and Astronomy, Iowa State University, Ames IA; United States of America.
- ⁸²Istinye University, Sariyer, Istanbul; Türkiye.
- ^{83(a)}Departamento de Engenharia Elétrica, Universidade Federal de Juiz de Fora (UFJF), Juiz de Fora;^(b)Universidade Federal do Rio De Janeiro COPPE/EE/IF, Rio de Janeiro;^(c)Instituto de Física, Universidade de São Paulo, São Paulo;^(d)Rio de Janeiro State University, Rio de Janeiro; Brazil.
- ⁸⁴KEK, High Energy Accelerator Research Organization, Tsukuba; Japan.
- ⁸⁵Graduate School of Science, Kobe University, Kobe; Japan.
- ^{86(a)}AGH University of Krakow, Faculty of Physics and Applied Computer Science, Krakow;^(b)Marian Smoluchowski Institute of Physics, Jagiellonian University, Krakow; Poland.
- ⁸⁷Institute of Nuclear Physics Polish Academy of Sciences, Krakow; Poland.
- ⁸⁸Faculty of Science, Kyoto University, Kyoto; Japan.
- ⁸⁹Research Center for Advanced Particle Physics and Department of Physics, Kyushu University, Fukuoka ; Japan.
- ⁹⁰Instituto de Física La Plata, Universidad Nacional de La Plata and CONICET, La Plata; Argentina.
- ⁹¹Physics Department, Lancaster University, Lancaster; United Kingdom.
- ⁹²Oliver Lodge Laboratory, University of Liverpool, Liverpool; United Kingdom.
- ⁹³Department of Experimental Particle Physics, Jožef Stefan Institute and Department of Physics, University of Ljubljana, Ljubljana; Slovenia.
- ⁹⁴School of Physics and Astronomy, Queen Mary University of London, London; United Kingdom.
- ⁹⁵Department of Physics, Royal Holloway University of London, Egham; United Kingdom.
- ⁹⁶Department of Physics and Astronomy, University College London, London; United Kingdom.
- ⁹⁷Louisiana Tech University, Ruston LA; United States of America.
- ⁹⁸Fysiska institutionen, Lunds universitet, Lund; Sweden.
- ⁹⁹Departamento de Física Teórica C-15 and CIAFF, Universidad Autónoma de Madrid, Madrid; Spain.
- ¹⁰⁰Institut für Physik, Universität Mainz, Mainz; Germany.
- ¹⁰¹School of Physics and Astronomy, University of Manchester, Manchester; United Kingdom.
- ¹⁰²CPPM, Aix-Marseille Université, CNRS/IN2P3, Marseille; France.
- ¹⁰³Department of Physics, University of Massachusetts, Amherst MA; United States of America.
- ¹⁰⁴Department of Physics, McGill University, Montreal QC; Canada.
- ¹⁰⁵School of Physics, University of Melbourne, Victoria; Australia.
- ¹⁰⁶Department of Physics, University of Michigan, Ann Arbor MI; United States of America.
- ¹⁰⁷Department of Physics and Astronomy, Michigan State University, East Lansing MI; United States of America.
- ¹⁰⁸Group of Particle Physics, University of Montreal, Montreal QC; Canada.
- ¹⁰⁹Fakultät für Physik, Ludwig-Maximilians-Universität München, München; Germany.
- ¹¹⁰Max-Planck-Institut für Physik (Werner-Heisenberg-Institut), München; Germany.
- ¹¹¹Graduate School of Science and Kobayashi-Maskawa Institute, Nagoya University, Nagoya; Japan.
- ¹¹²Department of Physics and Astronomy, University of New Mexico, Albuquerque NM; United States of America.
- ¹¹³Institute for Mathematics, Astrophysics and Particle Physics, Radboud University/Nikhef, Nijmegen;

Netherlands.

¹¹⁴Nikhef National Institute for Subatomic Physics and University of Amsterdam, Amsterdam; Netherlands.

¹¹⁵Department of Physics, Northern Illinois University, DeKalb IL; United States of America.

¹¹⁶(^a)New York University Abu Dhabi, Abu Dhabi;(^b)University of Sharjah, Sharjah; United Arab Emirates.

¹¹⁷Department of Physics, New York University, New York NY; United States of America.

¹¹⁸Ochanomizu University, Otsuka, Bunkyo-ku, Tokyo; Japan.

¹¹⁹Ohio State University, Columbus OH; United States of America.

¹²⁰Homer L. Dodge Department of Physics and Astronomy, University of Oklahoma, Norman OK; United States of America.

¹²¹Department of Physics, Oklahoma State University, Stillwater OK; United States of America.

¹²²Palacký University, Joint Laboratory of Optics, Olomouc; Czech Republic.

¹²³Institute for Fundamental Science, University of Oregon, Eugene, OR; United States of America.

¹²⁴Graduate School of Science, Osaka University, Osaka; Japan.

¹²⁵Department of Physics, University of Oslo, Oslo; Norway.

¹²⁶Department of Physics, Oxford University, Oxford; United Kingdom.

¹²⁷LPNHE, Sorbonne Université, Université Paris Cité, CNRS/IN2P3, Paris; France.

¹²⁸Department of Physics, University of Pennsylvania, Philadelphia PA; United States of America.

¹²⁹Department of Physics and Astronomy, University of Pittsburgh, Pittsburgh PA; United States of America.

¹³⁰(^a)Laboratório de Instrumentação e Física Experimental de Partículas - LIP, Lisboa;(^b)Departamento de Física, Faculdade de Ciências, Universidade de Lisboa, Lisboa;(^c)Departamento de Física, Universidade de Coimbra, Coimbra;(^d)Centro de Física Nuclear da Universidade de Lisboa, Lisboa;(^e)Departamento de Física, Universidade do Minho, Braga;(^f)Departamento de Física Teórica y del Cosmos, Universidad de Granada, Granada (Spain);(^g)Departamento de Física, Instituto Superior Técnico, Universidade de Lisboa, Lisboa; Portugal.

¹³¹Institute of Physics of the Czech Academy of Sciences, Prague; Czech Republic.

¹³²Czech Technical University in Prague, Prague; Czech Republic.

¹³³Charles University, Faculty of Mathematics and Physics, Prague; Czech Republic.

¹³⁴Particle Physics Department, Rutherford Appleton Laboratory, Didcot; United Kingdom.

¹³⁵IRFU, CEA, Université Paris-Saclay, Gif-sur-Yvette; France.

¹³⁶Santa Cruz Institute for Particle Physics, University of California Santa Cruz, Santa Cruz CA; United States of America.

¹³⁷(^a)Departamento de Física, Pontificia Universidad Católica de Chile, Santiago;(^b)Millennium Institute for Subatomic physics at high energy frontier (SAPHIR), Santiago;(^c)Instituto de Investigación Multidisciplinario en Ciencia y Tecnología, y Departamento de Física, Universidad de La Serena;(^d)Universidad Andres Bello, Department of Physics, Santiago;(^e)Instituto de Alta Investigación, Universidad de Tarapacá, Arica;(^f)Departamento de Física, Universidad Técnica Federico Santa María, Valparaíso; Chile.

¹³⁸Department of Physics, University of Washington, Seattle WA; United States of America.

¹³⁹Department of Physics and Astronomy, University of Sheffield, Sheffield; United Kingdom.

¹⁴⁰Department of Physics, Shinshu University, Nagano; Japan.

¹⁴¹Department Physik, Universität Siegen, Siegen; Germany.

¹⁴²Department of Physics, Simon Fraser University, Burnaby BC; Canada.

¹⁴³SLAC National Accelerator Laboratory, Stanford CA; United States of America.

¹⁴⁴Department of Physics, Royal Institute of Technology, Stockholm; Sweden.

- ¹⁴⁵Departments of Physics and Astronomy, Stony Brook University, Stony Brook NY; United States of America.
- ¹⁴⁶Department of Physics and Astronomy, University of Sussex, Brighton; United Kingdom.
- ¹⁴⁷School of Physics, University of Sydney, Sydney; Australia.
- ¹⁴⁸Institute of Physics, Academia Sinica, Taipei; Taiwan.
- ¹⁴⁹^(a)E. Andronikashvili Institute of Physics, Iv. Javakhishvili Tbilisi State University, Tbilisi;^(b)High Energy Physics Institute, Tbilisi State University, Tbilisi;^(c)University of Georgia, Tbilisi; Georgia.
- ¹⁵⁰Department of Physics, Technion, Israel Institute of Technology, Haifa; Israel.
- ¹⁵¹Raymond and Beverly Sackler School of Physics and Astronomy, Tel Aviv University, Tel Aviv; Israel.
- ¹⁵²Department of Physics, Aristotle University of Thessaloniki, Thessaloniki; Greece.
- ¹⁵³International Center for Elementary Particle Physics and Department of Physics, University of Tokyo, Tokyo; Japan.
- ¹⁵⁴Department of Physics, Tokyo Institute of Technology, Tokyo; Japan.
- ¹⁵⁵Department of Physics, University of Toronto, Toronto ON; Canada.
- ¹⁵⁶^(a)TRIUMF, Vancouver BC;^(b)Department of Physics and Astronomy, York University, Toronto ON; Canada.
- ¹⁵⁷Division of Physics and Tomonaga Center for the History of the Universe, Faculty of Pure and Applied Sciences, University of Tsukuba, Tsukuba; Japan.
- ¹⁵⁸Department of Physics and Astronomy, Tufts University, Medford MA; United States of America.
- ¹⁵⁹United Arab Emirates University, Al Ain; United Arab Emirates.
- ¹⁶⁰Department of Physics and Astronomy, University of California Irvine, Irvine CA; United States of America.
- ¹⁶¹Department of Physics and Astronomy, University of Uppsala, Uppsala; Sweden.
- ¹⁶²Department of Physics, University of Illinois, Urbana IL; United States of America.
- ¹⁶³Instituto de Física Corpuscular (IFIC), Centro Mixto Universidad de Valencia - CSIC, Valencia; Spain.
- ¹⁶⁴Department of Physics, University of British Columbia, Vancouver BC; Canada.
- ¹⁶⁵Department of Physics and Astronomy, University of Victoria, Victoria BC; Canada.
- ¹⁶⁶Fakultät für Physik und Astronomie, Julius-Maximilians-Universität Würzburg, Würzburg; Germany.
- ¹⁶⁷Department of Physics, University of Warwick, Coventry; United Kingdom.
- ¹⁶⁸Waseda University, Tokyo; Japan.
- ¹⁶⁹Department of Particle Physics and Astrophysics, Weizmann Institute of Science, Rehovot; Israel.
- ¹⁷⁰Department of Physics, University of Wisconsin, Madison WI; United States of America.
- ¹⁷¹Fakultät für Mathematik und Naturwissenschaften, Fachgruppe Physik, Bergische Universität Wuppertal, Wuppertal; Germany.
- ¹⁷²Department of Physics, Yale University, New Haven CT; United States of America.
- ^a Also Affiliated with an institute covered by a cooperation agreement with CERN.
- ^b Also at An-Najah National University, Nablus; Palestine.
- ^c Also at Borough of Manhattan Community College, City University of New York, New York NY; United States of America.
- ^d Also at Center for High Energy Physics, Peking University; China.
- ^e Also at Center for Interdisciplinary Research and Innovation (CIRI-AUTH), Thessaloniki; Greece.
- ^f Also at Centro Studi e Ricerche Enrico Fermi; Italy.
- ^g Also at CERN, Geneva; Switzerland.
- ^h Also at Département de Physique Nucléaire et Corpusculaire, Université de Genève, Genève; Switzerland.
- ⁱ Also at Departament de Física de la Universitat Autònoma de Barcelona, Barcelona; Spain.
- ^j Also at Department of Financial and Management Engineering, University of the Aegean, Chios; Greece.

- k* Also at Department of Physics and Astronomy, Michigan State University, East Lansing MI; United States of America.
- l* Also at Department of Physics, Ben Gurion University of the Negev, Beer Sheva; Israel.
- m* Also at Department of Physics, California State University, Sacramento; United States of America.
- n* Also at Department of Physics, King's College London, London; United Kingdom.
- o* Also at Department of Physics, Stanford University, Stanford CA; United States of America.
- p* Also at Department of Physics, University of Fribourg, Fribourg; Switzerland.
- q* Also at Department of Physics, University of Thessaly; Greece.
- r* Also at Department of Physics, Westmont College, Santa Barbara; United States of America.
- s* Also at Hellenic Open University, Patras; Greece.
- t* Also at Institutio Catalana de Recerca i Estudis Avancats, ICREA, Barcelona; Spain.
- u* Also at Institut für Experimentalphysik, Universität Hamburg, Hamburg; Germany.
- v* Also at Institute for Nuclear Research and Nuclear Energy (INRNE) of the Bulgarian Academy of Sciences, Sofia; Bulgaria.
- w* Also at Institute of Applied Physics, Mohammed VI Polytechnic University, Ben Guerir; Morocco.
- x* Also at Institute of Particle Physics (IPP); Canada.
- y* Also at Institute of Physics and Technology, Mongolian Academy of Sciences, Ulaanbaatar; Mongolia.
- z* Also at Institute of Physics, Azerbaijan Academy of Sciences, Baku; Azerbaijan.
- aa* Also at Institute of Theoretical Physics, Ilia State University, Tbilisi; Georgia.
- ab* Also at L2IT, Université de Toulouse, CNRS/IN2P3, UPS, Toulouse; France.
- ac* Also at Lawrence Livermore National Laboratory, Livermore; United States of America.
- ad* Also at National Institute of Physics, University of the Philippines Diliman (Philippines); Philippines.
- ae* Also at Ochanomizu University, Otsuka, Bunkyo-ku, Tokyo; Japan.
- af* Also at Technical University of Munich, Munich; Germany.
- ag* Also at The Collaborative Innovation Center of Quantum Matter (CICQM), Beijing; China.
- ah* Also at TRIUMF, Vancouver BC; Canada.
- ai* Also at Università di Napoli Parthenope, Napoli; Italy.
- aj* Also at University of Colorado Boulder, Department of Physics, Colorado; United States of America.
- ak* Also at Washington College, Chestertown, MD; United States of America.
- al* Also at Yeditepe University, Physics Department, Istanbul; Türkiye.
- * Deceased